# Antihypertensive effect of brain-targeted mechanical intervention with passive head motion

**Authors:**

**Shuhei Murase[1,2,22], Naoyoshi Sakitani[1,3,22], Takahiro Maekawa[1], Daisuke Yoshino[4], Kouji Takano[5], Ayumu Konno[6], Hirokazu Hirai[6], Taku Saito[2], Sakae Tanaka[2], Keisuke Shinohara[7], Takuya Kishi[8], Yuki Yoshikawa[9], Takamasa Sakai[9], Makoto Ayaori[10], Hirohiko Inanami[11], Koji Tomiyasu[12], Atsushi Takashima[13], Toru Ogata[1,14], Hirotsugu Tsuchimochi[15], Shinya Sato[16], Shigeyoshi Saito[17], Kohzoh Yoshino[18], Yuiko Matsuura[19], Kenichi Funamoto[20], Hiroki Ochi[1], Masahiro Shinohara[1], Motoshi Nagao[1] and Yasuhiro Sawada[1,2,3,4,21]*

**Affiliations:**

[1]Department of Rehabilitation for Motor Functions, National Rehabilitation Center for Persons with Disabilities, Tokorozawa, Japan. [2]Department of Orthopaedic Surgery, Graduate School of Medicine, The University of Tokyo, Tokyo, Japan. [3]Department of Cell Biology, National Cerebral and Cardiovascular Center, Suita, Japan. [4]Division of Advanced Applied Physics, Institute of Engineering, Tokyo University of Agriculture and Technology, Koganei, Japan. [5]Department of Rehabilitation for Brain Functions, National Rehabilitation Center for Persons with Disabilities, Tokorozawa, Japan. [6]Department of Neurophysiology & Neural

22 Repair, Gunma University Graduate School of Medicine, Maebashi, Japan. [7]Department of
23 Cardiovascular Medicine, Kyushu University Graduate School of Medical Sciences, Fukuoka,
24 Japan. [8]Department of Cardiology, Graduate School of Medicine, International University of
25 Health and Welfare, Okawa, Japan. [9]Department of Bioengineering, Graduate School of
26 Engineering, The University of Tokyo, Tokyo, Japan. [10]Tokorozawa Heart Center, Tokorozawa,
27 Japan. [11]Inanami Spine & Joint Hospital/Iwai Orthopaedic Medical Hospital, Iwai Medical
28 Foundation, Tokyo, Japan. [12]Center of Sports Science and Health Promotion, [13]Department of
29 Assistive Technology, National Rehabilitation Center for Persons with Disabilities,
30 Tokorozawa, Japan. [14]Department of Rehabilitation Medicine, Graduate School of Medicine,
31 The University of Tokyo, Tokyo, Japan. [15]Department of Cardiac Physiology, [16]Department of
32 Advanced Medical Technologies, National Cerebral and Cardiovascular Center, Suita, Japan.
33 [17]Department of Medical Physics and Engineering, Division of Health Sciences, Osaka
34 University Graduate School of Medicine, Suita, Japan. [18]School of Biological and
35 Environmental Sciences, Kwansei Gakuin University, Sanda, Japan. [19]Department of Health and
36 Sports, Niigata University of Health and Welfare, Niigata, Japan. [20]Institute of Fluid Science,
37 Tohoku University, Sendai, Japan. [21]Department of Clinical Research, National Rehabilitation
38 Center for Persons with Disabilities, Tokorozawa, Japan.
39 [22]These authors contributed equally: Shuhei Murase, Naoyoshi Sakitani.
40 *Correspondence to Yasuhiro Sawada, Department of Clinical Research, National Rehabilitation

Center for Persons with Disabilities, 4-1 Namiki, Tokorozawa, Saitama 359-8555, Japan, Tel: +81-4-2995-3100, Fax: +81-4-2995-0355, Email: ys454-ind@umin.ac.jp

**Abstract**

**Physical exercise is known to be beneficial for various brain functions. However, the mechanisms behind the positive effects of exercise on the brain remain to be elucidated. Here we show that passive head motion in hypertensive rats, which reproduces the mechanical accelerations generated in their heads during moderate-velocity treadmill running, decreases the expression of angiotensin II type 1 receptor (AT1R) in astrocytes in the rostral ventrolateral medulla (RVLM), thereby lowering blood pressure. Passive head motion generates interstitial fluid movement that is estimated to exert shear stress with an average magnitude of <1 Pa on the cells in the rat medulla. Fluid shear stress of a sub-Pa magnitude decreases AT1R expression in cultured astrocytes. In hypertensive rats, inhibition of interstitial fluid movement following hydrogel introduction to the RVLM eliminates the antihypertensive effects of passive head motion and treadmill running. Furthermore, vertically oscillating chair riding by hypertensive adult humans, which reproduces the mechanical accelerations generated in their heads during light jogging or fast walking, lowers their blood pressure. Our findings indicate that moderate mechanical intervention can have antihypertensive effects by modulating the function of RVLM**

**astrocytes through interstitial fluid shear stress. We anticipate that mechanical regulation is responsible for a variety of the positive effects of physical exercise on human health, particularly those related to brain functions.**

## Introduction

Exercise is known to be effective as a therapeutic/preventative measure for numerous physical disorders and diseases including hypertension[1,2], which is a major cause of stroke and cardiovascular diseases making the biggest risk factor for death worldwide[3]. However, the mechanisms underlying the antihypertensive effect of exercise remain to be elucidated.

Whereas the majority (>90%) of human hypertension comprises essential hypertension, the cause of which is unidentifiable[4], long-term regulation of blood pressure (BP) has been recognized to be largely dependent on sodium excretion adjusting systems mainly involving kidney functions[5]. Elevated activity of the sympathetic nervous system also importantly contributes to the development of hypertension[6-8]. Rostral ventrolateral medulla (RVLM), which is located in the brainstem, plays a critical role in determining the basal activity of the sympathetic nervous system, and its functional integrity is essential for the maintenance of basal vasomotor tone and regulation of BP[6,9]. Angiotensin II (Ang II) is the major bioactive peptide of the renin-angiotensin system (RAS), and is known to regulate BP as well as other biological processes such as cell growth/apoptosis/migration, inflammation, and fibrosis[10]. The biological effects of Ang II are mediated by its interaction with two distinct high-affinity G protein-coupled

80 receptors, Ang II type 1 receptor (AT1R) and type 2 receptor. Of these receptors, AT1R is
81 responsible for most of the known physiological and pathophysiological processes related to
82 Ang II. Whereas RAS is involved in the functional regulation of various "peripheral" organs and
83 tissues such as kidney and vessels, it also regulates brain functions within the blood-brain
84 barrier, including the control and maintenance of sympathetic nerve activity and cognitive
85 ability[11]. In particular, the role of AT1R signaling in the RVLM in cardiovascular regulation has
86 been extensively studied and demonstrated. For example, the pressor and depressor responses to
87 Ang II and Ang II antagonists, respectively, injected into the RVLM have been reported to be
88 enhanced in spontaneously hypertensive rats (SHRs)[12,13]. We have previously demonstrated that
89 treadmill running at moderate velocities alleviates the sympathetic nerve activity, involving
90 attenuation of AT1R signaling in the RVLM of stroke-prone spontaneously hypertensive rats
91 (SHRSPs)[14], a substrain of SHRs that exhibit severer hypertension as compared with SHRs[15].
92 However, the details about the changes in AT1R signaling in the RVLM of these hypertensive
93 rats have yet to be elucidated. It remains unclear what type(s) of cells (e.g., neurons or
94 astrocytes) are primarily responsible for the altered AT1R signaling in the RVLM of SHRs or
95 SHRSPs. Furthermore, the causal relationship between the increased AT1R signal activity in the
96 RVLM and high BP in SHRs or SHRSPs in their steady state (i.e., apart from their responses to
97 pharmacological interventions) is left unrevealed.
98 AT1R has also been shown to play a vital role in regulating a variety of physiological or

99 pathological processes, including cellular responses to mechanical perturbations[16,17]. For
100 example, mechanical stretching of cardiac myocytes activates AT1R signaling[18], and fluid shear
101 stress (FSS) of average 1.5 Pa lowers AT1R expression in human vein endothelial cells[19].
102 Although intervening the Ang II-AT1R system through pharmacological approaches, such as
103 administration of angiotensin-converting enzyme inhibitor or selective AT1R blocker, has been
104 established as an effective therapeutic strategy for hypertension[20], mechano-responsive
105 attenuation of AT1R signaling has not been clinically utilized as an antihypertensive measure.
106 Many of physical workouts, particularly aerobic exercises, involve vertical body
107 motions, which generate mechanical accelerations in the head at the time of foot contact with
108 the ground (i.e., landing). The importance of mechanical loads is well established in the
109 physiological regulation of bones, the stiffest organ that only allows tiny deformation[21].
110 Osteocytes, the mechanosensory cells embedded in bones[22], are assumed to undergo minimal
111 deformations under physiological conditions. We have reported that FSS on osteocytes derived
112 from interstitial fluid flow induced upon physical activity plays an important role in maintaining
113 bone homeostasis[23]. Given that the brain is not a rigid organ, minimally deforming forces or
114 stress distribution changes in the brain during exercise or even activity of daily living (e.g.,
115 walking) may produce beneficial effects. We have previously shown that in the prefrontal cortex
116 (PFC) of rodents, moderate mechanical intervention-induced FSS modulates serotonin signaling
117 in the neurons in situ[24]. Based on these previous findings together with the distribution of

118 interstitial fluid throughout the whole brain, we hypothesized that moderate mechanical
119 intervention might have antihypertensive effects involving FSS-mediated modulation of AT1R
120 signaling in the RVLM.
121
122 **Results**
123 **Application of cyclical mechanical intervention to the head by passive motion lowers the**
124 **BP in SHRSPs.** To determine the effects of a mechanical intervention of a moderate intensity on
125 BP, we first sought to develop an experimental system that reproduces the acceleration
126 generated in the head during rats' treadmill running at a modest velocity (20 m/min), a typical
127 experimental intervention to test the effects of physical exercise on rats[25,26]. In a recent study, we
128 observed that treadmill running of rats (20 m/min) generated 5-mm vertical oscillation of their
129 heads with ~1.0 × *g* peak accelerations and 2-Hz frequency; therefore, we developed a "passive
130 head motion" (PHM) system to produce 2-Hz 5-mm vertical oscillation exerting 1.0 × *g*
131 acceleration peaks in the heads of rats[24]. In the current study, we examined the effects of
132 mechanical intervention on BP in SHRSPs, using the PHM system. Similar to the
133 antihypertensive effect of treadmill running on SHRs or SHRSPs that we and others reported
134 previously[15,25,27], application of PHM (30 min/day, 28 consecutive days; see Fig. 1a)
135 significantly lowered their BP as compared to their controls (Fig. 1b,c), whereas heart rate (HR)
136 was not significantly affected by PHM (Fig. 1d). Anesthesia alone (daily 30 min) did not

137 significantly alter the BP in SHRSPs (Extended Data Fig. 1a), indicating that the

138 antihypertensive effect resulted specifically from PHM. The anti-cardiac hypertrophy effect of

139 PHM on SHRSPs (Fig. 1e) as well as the lack of these PHM effects on control normotensive

140 rats (Wistar-Kyoto: WKY) (Fig. 1b,c,e) were also consistent with previous reports describing

141 treadmill running as an antihypertensive intervention for SHRs[27]. As was observed in our

142 treadmill running experiments[14], PHM decreased 24-h urinary norepinephrine excretion of

143 SHRSPs (Fig. 1f). This suggests that PHM mitigates the sympathetic hyperactivity[28].

144 Collectively, these results support our hypothesis that cyclical application of moderate

145 mechanical intervention to the head has an antihypertensive effect. Notably, ≥4-week PHM

146 significantly decreased or delayed the stroke incidence in the SHRSPs (Extended Data Fig.

147 1b−d).

148 Next, we characterized PHM as an antihypertensive intervention by testing for various

149 directions, frequencies, and amplitudes (peak magnitudes of acceleration). PHM that generated

150 acceleration peaks of 1.0 × *g* in the rostral-caudal direction, but not in the left-right direction,

151 had antihypertensive effects on SHRSPs (Extended Data Fig. 2a–c), suggestive of the

152 directional selectivity. Regarding frequency, vertical PHM (peak magnitude of 1.0 × *g*) of 0.5

153 Hz, but not of 0.2 Hz, lowered the BP in SHRSPs to the approximately same extent as 2-Hz

154 PHM did (Extended Data Fig. 3a–c). Furthermore, PHM generating a peak magnitude of 0.5 ×

155 *g*, but not 0.2 × *g*, was approximately as antihypertensive as 1.0-×-*g* PHM (Extended Data Fig.

156 3a,d,e). These results suggest the existence of a threshold and a plateau phase of frequency and

157 amplitude (magnitude) of PHM in terms of its antihypertensive effects.

158

159 **PHM down-regulates AT1R expression in RVLM astrocytes of SHRSPs.** We then looked

160 into the mechanism of how PHM alleviated the development of hypertension in SHRSPs. We

161 previously reported that down-regulation of the AT1R signaling in the RVLM is responsible for

162 the treadmill running-induced sympathoinhibition in SHRSPs[14]. Given the mechanical

163 regulation of AT1R expression in endothelial cells[19], we examined whether PHM modulated the

164 AT1R expression in RVLM neurons and astrocytes of SHRSPs. In our histochemical analysis,

165 we defined neuronal nuclei (NeuN)-positive cells as neurons[29] and glial fibrillary acidic protein

166 (GFAP)-positive cells as astrocytes[30]. PHM (30 min/day, 28 days) did not significantly change

167 the relative population of AT1R-expressing neurons and astrocytes in the RVLM of WKY rats

168 (Fig. 1g). In contrast, 4-week PHM significantly decreased the expression of AT1R in the

169 astrocytes, but not in the neurons, of SHRSPs' RVLM (Fig. 1h). Notably, the AT1R expression

170 in the RVLM neurons was comparable between WKY rats and SHRSPs, either with or without

171 PHM (Fig. 1i). In contrast, the AT1R expression was significantly higher in the RVLM

172 astrocytes of SHRSPs without PHM (Fig. 1j, columns 1 and 3). PHM lowered the AT1R

173 expression in the RVLM astrocytes of SHRSPs to the level equivalent to that of WKY rats (Fig.

174 1j, columns 1, 2, and 4). Taken together, the AT1R expression in RVLM astrocytes appeared to

175 be correlated with the antihypertensive effect of PHM on SHRSPs. In line with this observation,
176 4-week treadmill running of SHRSPs also decreased the AT1R expression in their RVLM
177 astrocytes, but not neurons (Extended Data Fig. 4a−c).
178
179 **PHM alleviates the sensitivity of the RVLM in SHRSPs to Ang II or Ang II antagonist.** We
180 next sought to examine whether the PHM-induced decrease in AT1R expression in the RVLM
181 astrocytes of SHRSPs (Fig. 1j, columns 3 and 4) was functionally relevant to the suppression of
182 AT1R signaling. To this end, we analyzed the pressor responses to Ang II injected into the
183 unilateral RVLM of WKY rats and SHRSPs, either subjected to 4-week PHM or left sedentary
184 under anesthesia (30 min/day, 28 days) (Fig. 2a). As we previously reported[14], SHRSPs without
185 PHM exhibited significantly greater pressor response to Ang II administered to the RVLM than
186 WKY rats (Fig. 2b, compare between top and bottom of left panels; Fig. 2c, compare columns 1
187 and 3). Four-week PHM alleviated the pressor response to Ang II injected into the RVLM of
188 SHRSPs, but not of WKY rats (Fig. 2b, compare left and right; Fig. 2c, compare columns 1 vs. 2
189 and 3 vs. 4). Furthermore, the depressor response to Ang II antagonist injected into the unilateral
190 RVLM[13] was also mitigated by 4-week PHM in SHRSPs, but not in WKY rats (Fig. 2d,e). These
191 results support the functional relevance of the PHM-induced decrease in the AT1R expression in
192 the RVLM astrocytes of SHRSPs (Fig. 1j).
193 To examine whether the increased AT1R expression in the RVLM astrocytes of

194 SHRSPs was associated with their development of hypertension, we manipulated the AT1R
195 signaling by introducing exogenous expression of AT1R-associated protein (AGTRAP), which
196 interacts with AT1R and tempers the Ang II-mediated signals by promoting AT1R
197 internalization[31]. To this end, we used an adeno-associated virus (AAV)-mediated gene delivery
198 system[32]. AAV serotype 9 (AAV9) vectors were injected locally to transduce the RVLM cells
199 (Fig. 3a and Extended Data Fig. 5a). To achieve astrocyte- and neuron-specific gene expression,
200 we used the AAV9 vectors that harbored mouse GFAP promoter (AAV-GFAP) and rat neuron-
201 specific enolase (NSE) promoter (AAV-NSE), respectively (Fig. 3a). Because these vectors
202 contained a region encoding GFP and 2A sequence of porcine teschovirus-1 (P2A; self-cleaving
203 peptides[33]) (Fig. 3a), observation of the green fluorescence allowed us to identify the cells in
204 which transgene was expressed (Fig. 3b,c and Extended Data Fig. 5a−e). The AAV-mediated
205 expression of AGTRAP in astrocytes (Fig. 3b) but not in neurons (Fig. 3c) of the bilateral
206 RVLMs in SHRSPs significantly lowered the BP as compared with their control SHRSPs in
207 which only GFP was virally expressed in the RVLM astrocytes or neurons (Fig. 3d,e).
208 Furthermore, the AAV-mediated expression of AGTRAP in astrocytes, but not neurons, of
209 SHRSPs' bilateral RVLMs decreased the 24-h urinary norepinephrine excretion (Fig. 3f).
210 Injection of the control AAV vector (GFAP-control or NSE-control) did not significantly affect
211 the BP of SHRSPs (Extended Data Fig. 5f). These results support the importance of AT1R signal
212 intensity in the RVLM astrocytes for SHRSPs' development of hypertension and sympathetic

213 hyperactivity, as well as the physiological relevance of the PHM-induced decrease in the AT1R

214 expression we observed in the RVLM astrocytes of SHRSPs (Fig. 1j).

215

216 **PHM generates low-amplitude pressure waves and induces interstitial fluid movement in**

217 **rat RVLM.** We then sought to determine the physical effects that PHM produced in the rat

218 RVLM. To do so, we analyzed local pressure changes using a telemetry pressure sensor (Fig. 4a)

219 as we described previously[24]. PHM generated pressure waves (changes) with ~1.2 mm Hg peak

220 amplitude (Fig. 4b−d). Because the frequency of these PHM-induced pressure changes was

221 equivalent to that of PHM (2 Hz), they were likely due to the local cyclical microdeformation

222 generated upon the PHM. We then postulated an analogy to bone, an organ that only yields to

223 minimal deformation. Because the function of bone is known to be modulated by interstitial

224 fluid flow-derived shear stress on osteocytes[23], we speculated that the interstitial fluid movement

225 generated by the microdeformation-induced stress distribution changes in the brain might result

226 in the shear stress-mediated regulation of nervous cell functions[24].

227 To analyze the PHM-induced interstitial fluid movement in the RVLM, we injected an

228 iodine-based contrast agent (Isovist®) into the RVLM of anesthetized rats, and tracked its

229 distribution with sequential micro-computed tomography (μCT) (Fig. 4e) as we previously did

230 to analyze the movement of intramuscular interstitial fluid[34]. We found that PHM significantly

231 promoted Isovist spreading in the rostral-caudal and dorsal-ventral (*y*- and *z*-axes, Fig. 4f)

directions (Fig. 4g,h). In contrast, PHM did not significantly affect the left-right spreading (*x*-axis, Fig. 4f) of Isovist (Fig. 4g,h). From the extent of PHM-induced increase in Isovist spread, we estimated that the velocity of interstitial fluid movement in the rat RVLM was increased by approximately two- to three-times during PHM; however, precise evaluation was difficult because of differences in size and time scales between our μCT analysis (100-μm order, >30-min interval) and PHM effects at a cellular level (μm order, ~0.5-s interval).

Our analyses using a multiphoton microscope (Extended Data Fig. 6a−c) and magnetic resonance (MR) imaging (MRI) (Extended Data Fig. 6d) indicated that the interstitial space of the rat RVLM is not randomly structured but oriented approximately along the centroidal line of this part of the brain as shown in Extended Data Fig. 6e. Furthermore, the cross-sectional area of the interstitial space was estimated to be 0.0083−0.18 $\mu m^2$ (Extended Data Fig. 7a−d). We assume that PHM generates cyclical microdeformation in the rat RVLM (Extended Data Fig. 7e), thereby promoting interstitial fluid movement.

Integrating these findings with previous reports on the property[35], flow velocity[36-38], and occupancy[39] of interstitial fluid in the brain, we calculated the average magnitude of interstitial fluid flow-derived shear stress exerted on rat RVLM cells during PHM (0.076−0.53 Pa; Supplementary Table 1).

**FSS on astrocytes decreases AT1R expression in vitro.** We then sought to determine what

251 type of mechanical force was responsible for the PHM-induced decrease in the AT1R expression
252 in RVLM astrocytes (Fig. 1h,j) by in vitro experiments using cultured cells. Taking the
253 approximate nature of our FSS calculation (Supplementary Table 1) into account, we
254 extensively examined whether application of FSS or hydrostatic pressure change (HPC), another
255 type of mechanical intervention, modulated AT1R expression. Based on our calculation
256 (Supplementary Table 1), we applied pulsatile FSS with an average magnitude of 0.05−0.7 Pa to
257 cultured primary astrocytes, which were prepared from the astrocyte-GFP mice[40] (Extended
258 Data Fig. 8a), using a system we previously reported[23,24,34]. Quantitative polymerase chain
259 reaction (qPCR) analysis revealed that application of FSS with ≥0.3-Pa magnitude (0.5 Hz, 30
260 min) significantly decreased the AT1R expression in astrocytes for at least 24 h in an apparently
261 magnitude-dependent manner (Fig. 5a and Extended Data Fig. 8b). In contrast, cyclical
262 application of HPC, ranging from 1 to 40 mm Hg, nonsignificantly altered (≤10 mm Hg) or
263 significantly increased (≥20 mm Hg) the AT1R expression in cultured astrocytes (Fig. 5b).
264 Consistently, immunostaining (Fig. 5c,d) and fluorescently labeled ligand (Ang II) binding (Fig.
265 5e,f) analyses of cultured astrocytes indicated that the AT1R expression was significantly
266 decreased by exposure to 30-min 0.7-Pa FSS. Collectively, FSS at magnitudes <1 Pa, but not
267 HPC, on astrocytes decreases the AT1R expression in vitro. Notably, FSS application to
268 Neuro2A cells, which exhibit neuronal phenotypes and morphology[41,42], did not decrease the
269 AT1R expression (Extended Data Fig. 8c−e).

270 The duration (>24 h) of FSS effects on the AT1R expression in astrocytes (Fig. 5) poses
271 a possibility of cumulative effects of FSS applied repeatedly at 24-h intervals. Nevertheless, 2-
272 day PHM (30 min/day) alleviated the pressor and depressor responses to Ang II and AT1R
273 blocker, respectively, injected into the RVLM in SHRSPs (Extended Data Fig. 9a−e), supporting
274 the relevance of the relatively quick decrease in AT1R expression in our FSS experiments to our
275 in vivo observations. Taken together, our in vitro findings are consistent with the notion that the
276 FSS-mediated persistent reduction of the AT1R expression is involved in the effects of daily
277 PHM application on BP (Fig. 1b,c) and AT1R expression in the RVLM astrocytes (Fig. 1h,j) in
278 SHRSPs. In contrast to PHM (Fig. 1b) and treadmill running[25], both of which required >2 weeks
279 to decrease the BP in hypertensive rats, daily AT1R blocker administration has been reported to
280 decrease the BP of hypertensive rats in less than one week[43,44]. The decrease in the AT1R
281 signaling in RVLM astrocytes may take considerably longer time to elicit its consequences on
282 cardiovascular variables as compared with the systemic RAS blockade[45]. Relatedly, 4-week
283 PHM in SHRSPs initiated in the plateau phase of their hypertension development (age of 21
284 weeks) did not significantly alter BP (Extended Data Fig. 10a−c), although it did decrease the
285 AT1R expression in RVLM astrocytes, but not neurons (Extended Data Fig. 10d−f). These
286 findings imply the existence of a complex mechanism that links AT1R signaling in RVLM
287 astrocytes with BP regulation, which can be irreversibly modified depending on various factors.
288 For example, both vascular and renal functions in SHRSPs have been reported to be impaired in

289 association with aging (≥16 weeks) and severity of hypertension (mean arterial pressure [MAP]

290 ≥200 mm Hg)[46-49].

291

292 **Hindrance of interstitial fluid movement by hydrogel introduction in the RVLM eliminates**

293 **the ability of PHM to decrease the AT1R expression in RVLM astrocytes and the BP in**

294 **SHRSPs.** To examine whether the interstitial fluid movement in the RVLM mediated the effects

295 of PHM on the BP and AT1R expression in the RVLM astrocytes of SHRSPs, we modulated the

296 local interstitial fluid dynamics. Following the procedure we used to restrict the interstitial fluid

297 movement in the mouse PFC[24], we hindered the interstitial fluid movement in situ by

298 microinjecting mutually reactive polyethylene glycol (PEG) gel-precursor (pre-gel) solutions

299 into the rat RVLM (Fig. 6a). Injected pre-gel solution spread over the rat RVLM, leading to

300 hydrogel formation in the interstitial space in situ (Extended Data Fig. 11a). We previously

301 showed that hydrogel introduction only hinders the fluid movement but does not restrict the

302 diffusion of small molecules inside the gel[24,50]. Consistent with this, hydrogel introduction did

303 not delay or attenuate the pressor and depressor responses to Ang II and Ang II antagonist,

304 respectively, injected into the RVLM (Extended Data Fig. 11b−f), indicating rapid solute

305 diffusivity through the hydrogel.

306 Hydrogel introduction in the bilateral RVLMs eliminated the ability of PHM to

307 decrease the BP (Fig. 6b, black and orange lines; Fig. 6c, columns 2 and 3), urinary

308 norepinephrine excretion (Fig. 6d, columns 2 and 3), and AT1R expression in the RVLM
309 astrocytes (Fig. 6e, rows 2 and 3; Fig. 6f, columns 2 and 3) in SHRSPs. In contrast, hydrogel
310 introduction increased the BP (Fig. 6b, blue and orange lines; Fig. 6c, columns 1 and 3),
311 norepinephrine excretion (Fig. 6d, columns 1 and 3), and AT1R expression in the RVLM
312 astrocytes (Fig. 6e, rows 1 and 3; Fig. 6f, columns 1 and 3) of SHRSPs subjected to PHM. The
313 AT1R expression in the RVLM neurons of SHRSPs remained unaltered irrespective of the
314 combination of PHM and hydrogel introduction (Fig. 6e,g). These results suggest that hydrogel
315 introduction in the RVLM disrupts the mechanism mediating the PHM-induced decrease in BP,
316 norepinephrine excretion, and AT1R expression in the RVLM astrocytes of SHRSPs. In line
317 with this, the antihypertensive effect of daily treadmill running in SHRSPs was eliminated by
318 hydrogel introduction in the RVLM (Extended Data Fig. 12a−c), supporting our hypothesis
319 about the mechanism underlying the antihypertensive effects of exercise.
320 As was the case with the mouse PFC[24], hydrogel introduction (Extended Data Fig. 13a)
321 did not affect the overall cell number or apoptosis (Extended Data Fig. 13b,c), survival or
322 apoptosis of the RVLM astrocytes (Extended Data Fig. 13d,e) and neurons (Extended Data Fig.
323 13f,g), and the expression of pro-inflammatory cytokines (TNF-α and IL-1β) (Extended Data
324 Fig. 13h) in the RVLM. Furthermore, hydrogel introduction in the rat RVLM did not
325 significantly alter the intramedullary pressure (Extended Data Fig. 13i). Collectively, the loss of
326 the PHM effects by hydrogel introduction in the bilateral RVLMs of SHRSPs (Fig. 6b−f) is

327 likely to result from the hydrogel-mediated alteration in interstitial fluid dynamics, rather than
328 the decreased cell viability and/or enhanced inflammatory responses caused by the impaired
329 nutrient supply, removal of metabolic wastes, or persistent PEG existence/contact.

330 Consistent with these results supporting the importance of interstitial fluid movement
331 (flow) in the RVLM of SHRSPs, both their BP and HR remained unchanged during the
332 transition from before to after the initiation of PHM (Extended Data Fig. 14), precluding the
333 response of baroreceptors, either carotid or aortic, to PHM. Furthermore, the activity of the
334 aortic depressor nerve, which transmits afferent signals from baroreceptors and chemoreceptors
335 located in the aortic arch[51], also remained unaltered from before to after PHM initiation
336 (Extended Data Fig. 14). Therefore, the baroreceptor response does not appear to be responsible
337 for the antihypertensive effects of PHM on SHRSPs.

338

339 **Vertically oscillating chair riding (VOCR) lowers BP in hypertensive adult humans.** The
340 results from our animal experiments reveal the antihypertensive effect of the mechanical
341 accelerations generated in the head during treadmill running at a moderate velocity. This
342 prompted us to test whether application of mechanical intervention to the head lowered BP in
343 hypertensive humans. We observed light jogging or fast walking (locomotion at the velocity of 7
344 km/h) typically produce ~2-Hz vertical acceleration waves with an amplitude of ~1.0 × *g* in the
345 person's head (Extended Data Fig. 15a, top). It seemed difficult to apply vertical forces only to

346 the heads of human subjects safely without leading to considerable discomfort and distress.
347 Therefore, we constructed a chair that could vertically oscillate at a frequency of 2 Hz
348 (Extended Data Fig. 15b) and produce ~1.0 × *g* acceleration waves in the head of the occupant
349 (Extended Data Fig. 15a, bottom), although the other body parts were also subjected to cyclical
350 vertical movements in this system. The waveform of the vertical acceleration (Extended Data
351 Fig. 15a, bottom) was also determined considering the subject's comfort in addition to technical
352 issues.

353 Given that previous reports regarding antihypertensive effects of aerobic exercise
354 typically recommend ≥3−4 days per week (frequency) and ≥30 min per session or day
355 (duration)[2], we set our regimen of VOCR as 3 days/week (Monday, Wednesday, and Friday
356 unless needed to assign otherwise for particular reasons such as public holidays) and 30
357 min/day. Our pilot study following protocol 1, in which we simply compared the subjects' BP
358 and HR before and after 4-week (12 times) VOCR (Extended Data Fig. 15c), showed that
359 VOCR decreased the BP in hypertensive humans (Extended Data Fig. 15d).

360 We then conducted a human study of protocol 2, in which we followed the changes in
361 subjects' BP and HR more minutely (Extended Data Fig. 16a). Encouraged by the positive
362 results from the study of protocol 1, we adopted the same VOCR regimen as to its frequency (3
363 days/week) and duration (30 min/day). To detect the trends of the BP and HR changes more
364 reliably by reducing the influences from their interday variabilities, we followed and analyzed

365 “value of the week”s (see Methods). Participants were subjected to serial blood sampling to
366 measure the plasma catecholamines (epinephrine, norepinephrine, and dopamine) and renin
367 activity, and serum aldosterone and C-reactive protein (CRP) before and after the intervention
368 period (Extended Data Fig. 16a). To conduct the second blood sampling on the next day of the
369 last bout of VOCR, the intervention period was extended from four weeks (total 12 times,
370 typically 26 days) to 4.5 weeks (total 14 times, 30−31 days) because blood sampling could not
371 be done during weekends at our hospital. Systolic BP (SBP), diastolic BP (DBP), and MAP
372 (“value of the week”s) immediately after the intervention period significantly decreased as
373 compared with those immediately before the intervention period (Fig. 7a). Notably, the post-
374 intervention follow-up showed that the BP-lowering effect apparently persisted for four weeks,
375 but not five weeks, after the last bout of VOCR (Fig. 7b). Similar to our animal study, we did
376 not observe significant changes in the HR by the VOCR intervention (Fig. 7a,b and Extended
377 Data Fig. 15d). Significant differences were not detected in the blood levels of catecholamines,
378 aldosterone, renin activity, and CRP between before and after the VOCR intervention (Extended
379 Data Fig. 16b).

380 The antihypertensive effect of VOCR observed in the participants of protocols 1 and 2
381 (Supplementary Table 2) prompted us to proceed to protocol 3 in which we examined whether
382 non-oscillating chair riding (NOCR), a control for VOCR, affected the BP of hypertensive adult
383 humans (Extended Data Fig. 17a). We asked the participants in protocol 3 for their agreement to

384 the continuous beat-by-beat BP and inter-beat (R−R) interval (RRI) recording. In those who
385 agreed to these measurements, we analyzed the SBP and RRI variabilities (see Methods).
386 Whereas 4.5-week NOCR did not significantly affect participants' BP (Fig. 8a, top), VOCR
387 significantly lowered it (Fig. 8a, bottom), as in the studies following protocols 1 and 2. NOCR
388 did not significantly alter the low-frequency (LF) power in SBP variability (Fig. 8b) or the ratio
389 of LF/high frequency (HF) power (LF/HF ratio) in RRI variability (Fig. 8c). In contrast, VOCR
390 significantly decreased the former (Fig. 8b) and elicited a decreasing tendency in the latter (Fig.
391 8c). These findings indicate that VOCR decreases the vascular sympathetic nerve activity[52,53]
392 and its dominance over the cardiac parasympathetic activity[52,54]; nevertheless, there remains
393 some controversy regarding the use of the LF/HF ratio in RRI variability as an appropriate
394 relevant indicator[55,56].
395 Collectively, our human studies suggest that VOCR, which reproduces mechanical
396 accelerations in the head during light jogging or fast walking, has an antihypertensive and
397 sympathoinhibitory effect in hypertensive humans. Although our animal studies were only
398 conducted in male rats, VOCR had antihypertensive effects in both male and female humans
399 (Extended Data Fig 17b). Importantly, in none of 33 VOCR subjects (Supplementary Table 2
400 and 3), apparent adverse events, including motion sickness and low back pain, were observed or
401 manifested in relation to the VOCR intervention.
402

403 **Discussion**

404 The antihypertensive effect of physical exercise has been shown to involve normalization of
405 sympathetic hyperactivity in the brain[57]. However, it is still unclear whether exercise directly
406 modulates the brain function. In this study, PHM, which reproduced mechanical accelerations
407 generated in the head during treadmill running, allowed us to dissect bodily activity-derived
408 physical effects.

409 Whereas AT1R signaling in both neurons and astrocytes in the RVLM have been
410 reported to be involved in regulating BP[58,59], we observed that the AT1R expression in RVLM
411 astrocytes was increased in SHRSPs as compared to that in WKY rats (Fig. 1j). In contrast, the
412 AT1R expression in RVLM neurons was comparable between WKY rats and SHRSPs (Fig. 1i),
413 although the AT1R expression in RVLM neurons has been shown to play an important role in
414 other animal model(s) of hypertension[58]. Together with the decreases in the BP and urinary
415 epinephrine excretion of SHRSPs in which RVLM astrocytes were transduced with the
416 AGTRAP gene (Fig. 3d−f), the intensity of AT1R signaling in RVLM astrocytes appears to be
417 critically involved in the pathogenesis of hypertension and sympathetic hyperactivity in
418 SHRSPs.

419 Four-week PHM decreased the urinary norepinephrine excretion and AT1R expression
420 in RVLM astrocytes of SHRSPs to the levels almost equivalent to those of WKY rats (Fig. 1f,j).
421 However, PHM only partially alleviated the development of hypertension in SHRSPs (Fig. 1b,c)

422 to the extent similar to the antihypertensive effects of treadmill running previously reported[25,60]
423 or observed in this study (Extended Data Fig. 12b). Therefore, it is evident that factors other
424 than the AT1R signaling in RVLM astrocytes also contribute to the pathogenesis of essential
425 hypertension.

426 AT1R expression in the cultured astrocytes decreased upon FSS application (Fig.
427 5a,c−f). This was consistent with our findings that PHM and treadmill running decreased the
428 AT1R expression in the RVLM astrocytes of SHRSPs (Fig. 1j and Extended Data Fig. 4c).
429 However, the AT1R expression level in the RVLM astrocytes was low in WKY rats even
430 without PHM (Fig. 1j), and this may raise a concern regarding the physiological relevance of
431 our in vitro FSS experiments using cultured astrocytes. Still, it has been reported that cultured
432 astrocytes typically exhibit increased "reactivity", and do not fully recapitulate the physiological
433 astrocytes in vivo[61]. We suggest that the FSS-induced decrease in the AT1R expression in
434 cultured astrocytes we observed represents the physiological functions of astrocytes, despite that
435 their increased basal AT1R expression may relate to the unphysiological aspects of two-
436 dimensional (2-D) culture on stiff substrates (culture plastics). Cells in static culture are exposed
437 to a complete absence of FSS, which may not be physiologically realized in vivo. Previous
438 reports describe increased extracellular fluid in the brains of hypertensive humans[62] and altered
439 dynamics of the intracerebral interstitial fluid of SHRs[63]. Aberrant regulation of RVLM
440 astrocytes' function that relates to altered interstitial fluid movement-derived FSS may underlie

441 the pathogenesis of essential hypertension.

442 PHM did not significantly alter the AT1R expression in SHRSPs' RVLM neurons (Fig.
443 1i), and FSS did not decrease the AT1R expression in cultured Neuro2A cells (Extended Data
444 Fig. 8c−e). However, we do not suspect that these results represent the absence of sensitivity of
445 neurons to FSS or other type(s) of mechanical stimulation, particularly because we observed the
446 PHM- and FSS-induced internalization of 5-$HT_{2A}$ receptor expressed in mouse PFC neurons and
447 Neuro2A cells, respectively[24]. Alternatively, we speculate that PHM and FSS may mitigate the
448 hyperexpression of AT1R related to aforementioned pathological status of SHRSPs' RVLM
449 astrocytes or unphysiological nature of cultured astrocytes. In line with this notion, PHM did not
450 significantly affect the AT1R expression in RVLM astrocytes in normotensive WKY rats (Fig.
451 1j).

452 Consistent with the lack of strict cell specificity in many of cellular responses to
453 mechanical forces[64], the FSS-induced decrease in AT1R expression, which was reported in
454 vascular cells[19], was also observed in cultured astrocytes. We speculate that there may be
455 common homeostasis-regulatory mechanisms at the cellular level that involve fluid flow-derived
456 shearing forces.

457 Based on our hypothesis concerning the similarity in the pathogenesis of high BP
458 between human essential hypertension and SHRSPs, we conducted human studies in which we
459 intended to reproduce the mechanical accelerations in the head that lowered the BP in SHRSPs.

460 Although the mechanism behind the apparent antihypertensive effect of VOCR remains to be
461 determined, the significant role of interstitial fluid dynamics in the RVLM, which we
462 demonstrated by our animal experiments, might be shared between humans and rats or other
463 animals (Extended Data Fig. 18). Whereas the plasma catecholamine levels were not
464 significantly changed by the VOCR intervention in the human study of protocol 2 (Extended
465 Data Fig. 16b), it is possible that the urinary epinephrine measures collected over 24 h in our rat
466 PHM experiments (Fig. 1f, 3f, and 6d) enhanced our ability to capture the sympathetic nerve
467 activity under "everyday-life" ambulatory conditions[65]. The findings from the study of protocol
468 3 suggest a sympathoinhibitory effect of VOCR (Fig. 8b,c).

469 Physical exercise is broadly useful to maintain the human health. Many of aerobic
470 exercises, including walking and running, involve impact-generating bodily actions creating
471 sharp accelerations in the head upon foot contacting with the ground. Furthermore, the
472 antihypertensive effects of PHM in the rostral-caudal direction (Extended Data Fig. 2) or with a
473 less peak magnitude (0.5 × *g*) or frequency (0.5 Hz) (Extended Data Fig. 3) may be relevant to
474 the decrease in BP caused by other forms of exercise such as swimming and bicycle riding[66,67].
475 We speculate that the beneficial effects of various types of exercises on a variety of brain
476 function-related diseases and health disorders may rely at least partly on the modest changes in
477 mechanical stress distribution in the brain, which may prompt optimal FSS on intracerebral
478 nervous cells. To the contrary, alterations in interstitial fluid movement-derived shear stress may

479 underlie the pathogenesis of various brain disorders, particularly those related to physical
480 inactivity or aging.

481 **Limitation of study.** There are several limitations of this study. We used SHRSP as an animal
482 model of essential hypertension. There are several differences between SHRSP and human
483 essential hypertension. SHRSPs develop hypertension in young adulthood, but not in middle age
484 as in humans. Furthermore, SHRSPs cannot model environmental influences that trigger human
485 hypertension, including increased salt intake, obesity, and physical inactivity. Nevertheless,
486 SHRSP allows us to obtain a chronic stable hypertensive condition with minimal inter-
487 individual variation, but without difficult or life-threatening technical interventions. We used
488 only male rats for our animal studies, although sex is an important variable for nearly all
489 diseases, including hypertension. This was because we intended to preclude or minimize the
490 potential influence of estrogen and progesterone, both of which basically act protectively on
491 cardiovascular systems, including the heart and endothelium. Perhaps for the same reason, in
492 many or even most of animal experiments in previous studies investigating the pathogenesis of
493 cardiovascular diseases, male animals have been used unless there is particular reason to analyze
494 female animals. In particular, we intended to be consistent with previous studies in which the
495 antihypertensive effects of treadmill running in male SHRs or SHRSPs were demonstrated[25,60].
496 However, as we did not aim to investigate only male-specific matters, we included human
497 participants of both sexes. Given that VOCR had antihypertensive effects in both male and

498 female humans (Extended Data Fig. 17b), we anticipate that the mechanical regulation of
499 RVLM astrocytes demonstrated in this study is not specific to males.

500 2-D cell culture experiments are non-physiologic particularly in light of 3-D
501 microenvironments in vivo, and do not entirely recapitulate physiological conditions.
502 Furthermore, our calculation of the FSS magnitude in vivo (Supplementary Table 1) is
503 approximate. However, our extensive in vitro studies by testing FSS and HPC with various
504 magnitudes/amplitudes (Fig. 5) supports the notion that FSS is responsible for the PHM-induced
505 decrease in AT1R expression in rat RVLM astrocytes. Because of the easy detachment of mouse
506 cerebral cortex- or hippocampus-derived primary neurons from the substrates by FSS, we tested
507 Neuro2A cells, an alternative of cultured neuronal cells, which stably adhered to the substrates
508 through FSS of magnitudes up to ~1 Pa[24].

509 We did not comprehensively analyze the effects of PHM on the brain functions, but
510 focused on the study of RVLM. PHM may modulate the AT1R signaling in other brain regions
511 that participate in the regulation of sympathetic nerve activity, including the anteroventral third
512 ventricle, paraventricular nucleus of the hypothalamus, and nucleus tractus solitarii[6,9]. It is
513 technically difficult to specifically interfere solely with the interstitial flow in the brain or other
514 tissues/organs in living animals. Nonetheless, hydrogel introduction in SHRSPs' RVLM
515 eliminated the decreasing effects of PHM on the BP and urinary norepinephrine excretion (Fig.
516 6b−d) as well as the antihypertensive effect of treadmill running (Extended Data Fig. 12),

517 supporting the critical role for the RVLM. Because hydrogel may exert yet unknown effects,
518 experiments of hydrogel introduction may not entirely prove the contribution of interstitial fluid
519 movement. For example, hydrogel introduction may alter the stiffness and elasticity of
520 extracellular matrix, which are known to affect the neurological physiology, pathology, and
521 development[68]. Regardless, from the unaltered cell survival/apoptosis, pro-inflammatory protein
522 expression, and pressure in the hydrogel-introduced RVLM of SHRSPs (Extended Data Fig. 13),
523 massive detrimental or favorable processes are unlikely to be responsible. Given the
524 involvement of reactive oxygen species (ROS) in hypertension in SHRSPs[69] and the unaltered
525 BP in hydrogel-introduced SHRSPs (Extended Data Fig. 12b), the immediate reduction of ROS
526 by PEG itself[70] also appears not to be responsible. Whereas further studies are required to
527 strictly determine the specific role of interstitial fluid dynamics in the RVLM, our findings
528 conform to the notion of its significance in BP control.

529 We conducted microinjection into the rat RVLM at a rate of 0.03−0.2 μL/min (see
530 Methods), ~4−20 times faster than that reportedly associated with excellent preservation of
531 central nervous tissue[71]. Although microinjection of 0.1–0.2 μL/min has been successfully
532 employed in animal (rat) brain research[72-75], our approach may have compromised the brain
533 region to some extent.

534 Unlike the case of PHM in rats, VOCR of humans generates vertical accelerations at
535 various body parts in addition to the head. Therefore, we cannot preclude the possibility that the

536 effects of VOCR also involves mechanical regulation of tissues and organs other than the brain.
537 For example, the antihypertensive effect of human VOCR became significant in ~2 weeks,
538 approximately as quickly as or even a little more quickly than that of rat PHM (compare the
539 MAP between SHRSPs in Fig. 1b and humans in Fig. 7b), despite the lower frequency of VOCR
540 (PHM: 7 days/week; VOCR: 3 days/week). This could be attributed to some additional influence
541 of cyclical vertical motion of body parts other than the head.

542 Our clinical studies are based on a small number of subjects (Supplementary Table 2
543 and 3) with a fixed condition (frequency of 2 Hz, peak acceleration of ~1.0 × *g*, 30 min/day, 3
544 days/week, 12−14 rides), and need further analysis with a much larger sample size and varying
545 conditions to determine the optimal VOCR.

546 The antihypertensive outcome of isometric exercise[76] cannot be explained by direct
547 mechanical effects on the brain; it is evidently mediated otherwise. Nevertheless, application of
548 moderate exercise-mimicking mechanical intervention is expected to be highly safe with
549 minimal possibility of adverse effects, providing a novel therapeutic/preventative strategy for
550 physical disorders including those resistant to conventional treatments such as drug
551 administration. Our approach utilizing mechanical interventions may bring considerable benefits
552 to those who cannot receive benefits from exercise because of physical disabilities.

553

554 **Data availability**

All data are included in this article and its supplementary information files. Raw data are available from the corresponding author upon reasonable request.

**Acknowledgements**

We thank K. Nakanishi, K. Hamamoto, and N. Kume for their consistent support. This work was in part supported by Intramural Research Fund from the Japanese Ministry of Health, Labour and Welfare; Grants-in-Aid for Scientific Research from the Japan Society for the Promotion of Science (KAKENHI 15H01820, 15H04966, 18H04088, 20K21778, 21H04866 to Y.S.; 20K19367 to N.S.; 17H02127 and 18H03138 to T.O.; 19K06899 to A.K.); Brain Mapping by Integrated Neurotechnologies for Disease Studies (Brain/MINDS, JP20dm0207057 to H.H.) and Research and Development Grants for Comprehensive Research for Persons with Disabilities (21dk0310116j0201 to Y.S. and D.Y.) from the Japan Agency for Medical Research and Development (AMED); the JST MIRAI Project (to Y.S. and D.Y.); the Naito Science & Engineering Foundation (to Y.S.); the Uehara Memorial Foundation (to Y.S.).

**Author contributions**

S.M. and N.S. conducted most of the animal/cell experiments. Y.S. and N.S. pursued the human studies. Y.S. conceived the research, designed the study, and led the project. K.S. and T.K. provided technical advice for the experiments involving measurement of cardiovascular

variables. N.S., K.T., M.S. and Y.S. wrote the manuscript. T.M. and A.T. contributed to the design and construction of the machine for PHM. D.Y. helped the in vitro FSS experiments. D.Y. and K.F. carried out calculation of in vivo FSS. T.S. and Y.Y. developed and provided the PEG hydrogel system. A.K. and H.H. prepared and provided the AAV vectors. S.Sat. and S.Sai. conducted the multiphoton microscopy and MRI experiments, respectively, and K.T. analyzed the images. K.Y. analyzed the data from human continuous BP and RRI measurements. K.T., T.K., M.A., H.I., Y.M., and T.O. supported Y.S. in the human studies. K.S., T.S., S.T. M.S., T.O., H.O., and M.N. provided technical, advisory and financial support.

## Competing interests

The authors declare no competing interest. S.M., T.M., T.O., A.T., and Y.S. joined the application of a patent for the vertically oscillating chair, which has been awarded in Japan, the US, the EU, and China (JP6592834; US16/616,935; EP18806753.2; CN201880033284.0) and under review in India (IN201927048891).

## References


1. Hagberg, J.M., Park, J.J. & Brown, M.D. The role of exercise training in the treatment of hypertension: an update. *Sports Med* **30**, 193-206 (2000).
2. Pescatello, L.S., MacDonald, H.V., Lamberti, L. & Johnson, B.T. Exercise for hypertension: A prescription update integrating existing recommendations with emerging research. *Curr Hypertens Rep* **17**, 87 (2015).

595 3. Lim, S.S., *et al.* A comparative risk assessment of burden of disease and injury
596 attributable to 67 risk factors and risk factor clusters in 21 regions, 1990-2010: a
597 systematic analysis for the Global Burden of Disease Study 2010. *Lancet* **380**, 2224-
598 2260 (2012).
599 4. Carretero, O.A. & Oparil, S. Essential hypertension. Part I: definition and etiology.
600 *Circulation* **101**, 329-335 (2000).
601 5. Guyton, A.C. Abnormal renal function and autoregulation in essential hypertension.
602 *Hypertension* **18**, III49-53 (1991).
603 6. Guyenet, P.G. The sympathetic control of blood pressure. *Nat Rev Neurosci* **7**, 335-346
604 (2006).
605 7. Grassi, G., Mark, A. & Esler, M. The sympathetic nervous system alterations in human
606 hypertension. *Circ Res* **116**, 976-990 (2015).
607 8. Malpas, S.C. Sympathetic nervous system overactivity and its role in the development of
608 cardiovascular disease. *Physiol Rev* **90**, 513-557 (2010).
609 9. Dampney, R.A. Functional organization of central pathways regulating the
610 cardiovascular system. *Physiol Rev* **74**, 323-364 (1994).
611 10. Fyhrquist, F. & Saijonmaa, O. Renin-angiotensin system revisited. *J Intern Med* **264**,
612 224-236 (2008).
613 11. Forrester, S.J., *et al.* Angiotensin II signal transduction: An update on mechanisms of
614 physiology and pathophysiology. *Physiol Rev* **98**, 1627-1738 (2018).
615 12. Ito, S., Komatsu, K., Tsukamoto, K., Kanmatsuse, K. & Sved, A.F. Ventrolateral medulla
616 AT1 receptors support blood pressure in hypertensive rats. *Hypertension* **40**, 552-559
617 (2002).
618 13. Muratani, H., Ferrario, C.M. & Averill, D.B. Ventrolateral medulla in spontaneously
619 hypertensive rats: role of angiotensin II. *Am J Physiol* **264**, R388-395 (1993).
620 14. Kishi, T. & Sunagawa, K. Exercise training plus calorie restriction causes synergistic
621 protection against cognitive decline via up-regulation of BDNF in hippocampus of
622 stroke-prone hypertensive rats. *Conf Proc IEEE Eng Med Biol Soc* **2012**, 6764-6767
623 (2012).
624 15. Nabika, T., Ohara, H., Kato, N. & Isomura, M. The stroke-prone spontaneously
625 hypertensive rat: still a useful model for post-GWAS genetic studies? *Hypertens Res* **35**,
626 477-484 (2012).
627 16. Lu, X., *et al.* Effects of local mechanical stimulation on coronary artery endothelial
628 function and angiotensin II type 1 receptor in pressure or flow-overload. *J Hypertens* **31**,
629 720-729 (2013).
630 17. Galie, P.A., Russell, M.W., Westfall, M.V. & Stegemann, J.P. Interstitial fluid flow and
631 cyclic strain differentially regulate cardiac fibroblast activation via AT1R and TGF-β1.
632 *Exp Cell Res* **318**, 75-84 (2012).

633 18. Zou, Y., *et al.* Mechanical stress activates angiotensin II type 1 receptor without the
634 involvement of angiotensin II. *Nat Cell Biol* **6**, 499-506 (2004).
635 19. Ramkhelawon, B., *et al.* Shear stress regulates angiotensin type 1 receptor expression in
636 endothelial cells. *Circ Res* **105**, 869-875 (2009).
637 20. Li, E.C., Heran, B.S. & Wright, J.M. Angiotensin converting enzyme (ACE) inhibitors
638 versus angiotensin receptor blockers for primary hypertension. *Cochrane Database Syst*
639 *Rev*, CD009096 (2014).
640 21. Weinbaum, S., Cowin, S.C. & Zeng, Y. A model for the excitation of osteocytes by
641 mechanical loading-induced bone fluid shear stresses. *J Biomech* **27**, 339-360 (1994).
642 22. Tatsumi, S., *et al.* Targeted ablation of osteocytes induces osteoporosis with defective
643 mechanotransduction. *Cell Metab* **5**, 464-475 (2007).
644 23. Miyazaki, T., *et al.* Mechanical regulation of bone homeostasis through p130Cas-
645 mediated alleviation of NF-κB activity. *Sci Adv* **5**, eaau7802 (2019).
646 24. Ryu, Y., *et al.* Mechanical regulation underlies effects of exercise on serotonin-induced
647 signaling in the prefrontal cortex neurons. *iScience* **23**, 100874 (2020).
648 25. Minami, N., *et al.* Effects of exercise and β-blocker on blood pressure and baroreflexes
649 in spontaneously hypertensive rats. *Am J Hypertens* **16**, 966-972 (2003).
650 26. Kim, S.E., *et al.* Treadmill exercise prevents aging-induced failure of memory through
651 an increase in neurogenesis and suppression of apoptosis in rat hippocampus. *Exp*
652 *Gerontol* **45**, 357-365 (2010).
653 27. Bertagnolli, M., *et al.* Exercise training reduces sympathetic modulation on
654 cardiovascular system and cardiac oxidative stress in spontaneously hypertensive rats.
655 *Am J Hypertens* **21**, 1188-1193 (2008).
656 28. Chidsey, C.A., Braunwald, E. & Morrow, A.G. Catecholamine excretion and cardiac
657 stores of norepinephrine in congestive heart failure. *Am J Med* **39**, 442-451 (1965).
658 29. Mullen, R.J., Buck, C.R. & Smith, A.M. NeuN, a neuronal specific nuclear protein in
659 vertebrates. *Development* **116**, 201-211 (1992).
660 30. Freeman, M.R. Specification and morphogenesis of astrocytes. *Science* **330**, 774-778
661 (2010).
662 31. Tamura, K., *et al.* The physiology and pathophysiology of a novel angiotensin receptor-
663 binding protein ATRAP/Agtrap. *Curr Pharm Des* **19**, 3043-3048 (2013).
664 32. Huda, F., *et al.* Distinct transduction profiles in the CNS via three injection routes of
665 AAV9 and the application to generation of a neurodegenerative mouse model. *Mol Ther*
666 *Methods Clin Dev* **1**, 14032 (2014).
667 33. Tang, X., *et al.* "Self-cleaving" 2A peptide from porcine teschovirus-1 mediates cleavage
668 of dual fluorescent proteins in transgenic Eimeria tenella. *Vet Res* **47**, 68 (2016).

669 34. Saitou, K., *et al.* Local cyclical compression modulates macrophage function in situ and
670 alleviates immobilization-induced muscle atrophy. *Clin Sci (Lond)* **132**, 2147-2161
671 (2018).
672 35. Cserr, H.F. & Patlak, C.S. Secretion and bulk flow of interstitial fluid. in *Physiology and*
673 *Pharmacology of the Blood-Brain Barrier*. ed. Bradbury, M.W.B. 245-261. Springer
674 Berlin Heidelberg, Berlin, Heidelberg (1992).
675 36. Chatterjee, K., Carman-Esparza, C.M. & Munson, J.M. Methods to measure, model and
676 manipulate fluid flow in brain. *J Neurosci Methods* **333**, 108541 (2020).
677 37. Geer, C.P. & Grossman, S.A. Interstitial fluid flow along white matter tracts: a
678 potentially important mechanism for the dissemination of primary brain tumors. *J*
679 *Neurooncol* **32**, 193-201 (1997).
680 38. Kingsmore, K.M., *et al.* MRI analysis to map interstitial flow in the brain tumor
681 microenvironment. *APL Bioeng* **2** (2018).
682 39. Hrabetova, S. & Nicholson, C. Biophysical Properties of Brain Extracellular Space
683 Explored with Ion-Selective Microelectrodes, Integrative Optical Imaging and Related
684 Techniques. in *Electrochemical Methods for Neuroscience*. eds. Michael, A.C. &
685 Borland, L.M. (2007).
686 40. Gong, S., *et al.* A gene expression atlas of the central nervous system based on bacterial
687 artificial chromosomes. *Nature* **425**, 917-925 (2003).
688 41. Goshima, Y., Ohsako, S. & Yamauchi, T. Overexpression of $Ca^{2+}$/calmodulin-dependent
689 protein kinase II in Neuro2A and NG108-15 neuroblastoma cell lines promotes neurite
690 outgrowth and growth cone motility. *J Neurosci* **13**, 559-567 (1993).
691 42. Yun, J., *et al.* Neuronal Per Arnt Sim (PAS) domain protein 4 (NPAS4) regulates neurite
692 outgrowth and phosphorylation of synapsin I. *J Biol Chem* **288**, 2655-2664 (2013).
693 43. Hamaguchi, R., Takemori, K., Inoue, T., Masuno, K. & Ito, H. Short-term treatment of
694 stroke-prone spontaneously hypertensive rats with an AT1 receptor blocker protects
695 against hypertensive end-organ damage by prolonged inhibition of the renin-angiotensin
696 system. *Clin Exp Pharmacol Physiol* **35**, 1151-1155 (2008).
697 44. Oddie, C.J., Dilley, R.J. & Bobik, A. Long-term angiotensin II antagonism in
698 spontaneously hypertensive rats: effects on blood pressure and cardiovascular amplifiers.
699 *Clin Exp Pharmacol Physiol* **19**, 392-395 (1992).
700 45. Rezacova, L., *et al.* Role of angiotensin II in chronic blood pressure control of
701 heterozygous Ren-2 transgenic rats: Peripheral vasoconstriction versus central
702 sympathoexcitation. *Biomed Pharmacother* **116**, 108996 (2019).
703 46. Husken, B.C., Hendriks, M.G., Pfaffendorf, M. & Van Zwieten, P.A. Effects of aging and
704 hypertension on the reactivity of isolated conduit and resistance vessels. *Microvasc Res*
705 **48**, 303-315 (1994).

706 47. Sepehrdad, R., *et al.* Amiloride reduces stroke and renalinjury in stroke-prone
707 hypertensive rats. *Am J Hypertens* **16**, 312-318 (2003).
708 48. Pirici, D., *et al.* Common impact of chronic kidney disease and brain microhemorrhages
709 on cerebral Aβ pathology in SHRSP. *Brain Pathol* **27**, 169-180 (2017).
710 49. Smeda, J.S. Renal function in stroke-prone rats fed a high-K+ diet. *Can J Physiol*
711 *Pharmacol* **75**, 796-806 (1997).
712 50. Fujiyabu, T., Toni, F., Li, X., Chung, U.I. & Sakai, T. Three cooperative diffusion
713 coefficients describing dynamics of polymer gels. *Chem Commun (Camb)* **54**, 6784-
714 6787 (2018).
715 51. Min, S., *et al.* Arterial baroreceptors sense blood pressure through decorated aortic
716 claws. *Cell Rep* **29**, 2192-2201 e2193 (2019).
717 52. Furlan, R., *et al.* Oscillatory patterns in sympathetic neural discharge and cardiovascular
718 variables during orthostatic stimulus. *Circulation* **101**, 886-892 (2000).
719 53. Milutinovic, S., Murphy, D. & Japundzic-Zigon, N. Central cholinergic modulation of
720 blood pressure short-term variability. *Neuropharmacology* **50**, 874-883 (2006).
721 54. Pagani, M., *et al.* Power spectral analysis of heart rate and arterial pressure variabilities
722 as a marker of sympatho-vagal interaction in man and conscious dog. *Circ Res* **59**, 178-
723 193 (1986).
724 55. Billman, G.E. The LF/HF ratio does not accurately measure cardiac sympatho-vagal
725 balance. *Front Physiol* **4**, 26 (2013).
726 56. Reyes del Paso, G.A., Langewitz, W., Mulder, L.J., van Roon, A. & Duschek, S. The
727 utility of low frequency heart rate variability as an index of sympathetic cardiac tone: a
728 review with emphasis on a reanalysis of previous studies. *Psychophysiology* **50**, 477-487
729 (2013).
730 57. Joyner, M.J. & Green, D.J. Exercise protects the cardiovascular system: effects beyond
731 traditional risk factors. *J Physiol* **587**, 5551-5558 (2009).
732 58. Jancovski, N., *et al.* Angiotensin type 1A receptor expression in C1 neurons of the rostral
733 ventrolateral medulla contributes to the development of angiotensin-dependent
734 hypertension. *Exp Physiol* **99**, 1597-1610 (2014).
735 59. Guo, F., *et al.* Astroglia are a possible cellular substrate of angiotensin(1-7) effects in the
736 rostral ventrolateral medulla. *Cardiovasc Res* **87**, 578-584 (2010).
737 60. Kishi, T., *et al.* Exercise training causes sympathoinhibition through antioxidant effect in
738 the rostral ventrolateral medulla of hypertensive rats. *Clin Exp Hypertens* **34**, 278-283
739 (2012).
740 61. Liddelow, S.A. & Barres, B.A. Reactive Astrocytes: Production, Function, and
741 Therapeutic Potential. *Immunity* **46**, 957-967 (2017).
742 62. Maclullich, A.M., *et al.* Higher systolic blood pressure is associated with increased water
743 diffusivity in normal-appearing white matter. *Stroke* **40**, 3869-3871 (2009).

63. Bedussi, B., *et al.* Enhanced interstitial fluid drainage in the hippocampus of spontaneously hypertensive rats. *Sci Rep* **7**, 744 (2017).
64. Iskratsch, T., Wolfenson, H. & Sheetz, M.P. Appreciating force and shape-the rise of mechanotransduction in cell biology. *Nat Rev Mol Cell Biol* **15**, 825-833 (2014).
65. Hughes, J.W., Watkins, L., Blumenthal, J.A., Kuhn, C. & Sherwood, A. Depression and anxiety symptoms are related to increased 24-hour urinary norepinephrine excretion among healthy middle-aged women. *J Psychosom Res* **57**, 353-358 (2004).
66. Tanaka, H., *et al.* Swimming training lowers the resting blood pressure in individuals with hypertension. *J Hypertens* **15**, 651-657 (1997).
67. Matsusaki, M., *et al.* Influence of workload on the antihypertensive effect of exercise. *Clin Exp Pharmacol Physiol* **19**, 471-479 (1992).
68. Li, S.C., *et al.* Tissue elasticity bridges cancer stem cells to the tumor microenvironment through microRNAs: Implications for a "watch-and-wait" approach to cancer. *Curr Stem Cell Res Ther* **12**, 455-470 (2017).
69. Kishi, T., *et al.* Increased reactive oxygen species in rostral ventrolateral medulla contribute to neural mechanisms of hypertension in stroke-prone spontaneously hypertensive rats. *Circulation* **109**, 2357-2362 (2004).
70. Luo, J., Borgens, R. & Shi, R. Polyethylene glycol improves function and reduces oxidative stress in synaptosomal preparations following spinal cord injury. *J Neurotrauma* **21**, 994-1007 (2004).
71. Guest, J., Benavides, F., Padgett, K., Mendez, E. & Tovar, D. Technical aspects of spinal cord injections for cell transplantation. Clinical and translational considerations. *Brain Res Bull* **84**, 267-279 (2011).
72. Peterson, S.L. & Armstrong, J.J. Muscarinic receptors mediate carbachol-induced inhibition of maximal electroshock seizures in the nucleus reticularis pontis oralis. *Epilepsia* **40**, 20-25 (1999).
73. Faingold, C.L., *et al.* GABA in the inferior colliculus plays a critical role in control of audiogenic seizures. *Brain Res* **640**, 40-47 (1994).
74. Shi, C., *et al.* Transportation in the interstitial space of the brain can be regulated by neuronal excitation. *Sci Rep* **5**, 17673 (2015).
75. Li, G.Q., *et al.* Role of cannabinoid receptor type 1 in rostral ventrolateral medulla in high-fat diet-induced hypertension in rats. *J Hypertens* **36**, 801-808 (2018).
76. Carlson, D.J., Dieberg, G., Hess, N.C., Millar, P.J. & Smart, N.A. Isometric exercise training for blood pressure management: a systematic review and meta-analysis. *Mayo Clin Proc* **89**, 327-334 (2014).
77. Limpert, E., Stahel, W.A. & Abbt, M. Log-normal distributions across the sciences: Keys and clues: On the charms of statistics, and how mechanical models resembling gambling machines offer a link to a handy way to characterize log-normal distributions, which can

provide deeper insight into variability and probability—normal or log-normal: That is the question. *BioScience* **51**, 341-352 (2001).

78. Byun, S., Hecht, V.C. & Manalis, S.R. Characterizing cellular biophysical responses to stress by relating density, deformability, and size. *Biophys J* **109**, 1565-1573 (2015).

79. ISO TS 21362:2018(E). Nanotechnologies – Analysis of nano-objects using asymmetrical-flow and centrifugal field flow fractionation (2018)

80. Carman, P.C. Fluid flow through granular beds. *Chemical Engineering Research and Design* **75**, S32-S48 (1997).

81. Xu, P. & Yu, B. Developing a new form of permeability and Kozeny–Carman constant for homogeneous porous media by means of fractal geometry. *Advances in Water Resources* **31**, 74-81 (2008).

82. Pedersen, J.A., Boschetti, F. & Swartz, M.A. Effects of extracellular fiber architecture on cell membrane shear stress in a 3D fibrous matrix. *J Biomech* **40**, 1484-1492 (2007).

83. Yetkin, F.*, et al.* Cerebrospinal fluid viscosity: a novel diagnostic measure for acute meningitis. *South Med J* **103**, 892-895 (2010).

84. Bloomfield, I.G., Johnston, I.H. & Bilston, L.E. Effects of proteins, blood cells and glucose on the viscosity of cerebrospinal fluid. *Pediatr Neurosurg* **28**, 246-251 (1998).

85. Tarbell, J.M. & Shi, Z.-D. Effect of the glycocalyx layer on transmission of interstitial flow shear stress to embedded cells. *Biomech Model Mechanobiol* **12**, 111-121 (2013).

86. Sakai, K.*, et al.* Overexpression of eNOS in NTS causes hypotension and bradycardia in vivo. *Hypertension* **36**, 1023-1028 (2000).

87. Kishi, T.*, et al.* Overexpression of eNOS in the RVLM causes hypotension and bradycardia via GABA release. *Hypertension* **38**, 896-901 (2001).

88. Paxinos, G. & Watson, C. *The rat brain in stereotaxic coordinates*, (Academic Press, 1998).

89. Hirooka, Y., Polson, J.W. & Dampney, R.A. Pressor and sympathoexcitatory effects of nitric oxide in the rostral ventrolateral medulla. *J Hypertens* **14**, 1317-1324 (1996).

90. Shinohara, Y.*, et al.* Effects of neutralizing antibody production on AAV-PHP.B-mediated transduction of the mouse central nervous system. *Mol Neurobiol* **56**, 4203-4214 (2019).

91. Shinohara, Y., Ohtani, T., Konno, A. & Hirai, H. Viral vector-based evaluation of regulatory regions in the neuron-specific enolase (NSE) promoter in mouse cerebellum in vivo. *Cerebellum* **16**, 913-922 (2017).

92. Konno, A.*, et al.* Mutant ataxin-3 with an abnormally expanded polyglutamine chain disrupts dendritic development and metabotropic glutamate receptor signaling in mouse cerebellar Purkinje cells. *Cerebellum* **13**, 29-41 (2014).

93. Matsuzaki, Y.*, et al.* Neurotropic Properties of AAV-PHP.B are shared among diverse inbred strains of mice. *Mol Ther* **27**, 700-704 (2019).

819 94. Sakitani, N., *et al.* Application of consistent massage-kike perturbations on mouse calves
820 and monitoring the resulting intramuscular pressure changes. *J Vis Exp* (2019).
821 95. Diaspro, A., *et al.* Multi-photon excitation microscopy. *Biomed Eng Online* **5**, 36 (2006).
822 96. Lei, Y., Han, H., Yuan, F., Javeed, A. & Zhao, Y. The brain interstitial system: Anatomy,
823 modeling, in vivo measurement, and applications. *Prog Neurobiol* **157**, 230-246 (2017).
824 97. Goerzen, D., *et al.* An MRI-derived neuroanatomical atlas of the Fischer 344 rat brain.
825 *Sci Rep* **10**, 6952 (2020).
826 98. Liu, C., De Luca, A., Rosso, A. & Talon, L. Darcy's law for yield stress fluids. *Phys Rev*
827 *Lett* **122**, 245502 (2019).
828 99. Johnson, A.K., Yarin, A.L. & Mashayek, F. Packing density and the Kozeny-Carman
829 equation. *Neurosurgery* **71**, E1064-1065; author reply E1065-1066 (2012).
830 100. de Vellis, J. & Cole, R. Preparation of mixed glial cultures from postnatal rat brain.
831 *Methods Mol Biol* **814**, 49-59 (2012).
832 101. Nagao, M., *et al.* Coordinated control of self-renewal and differentiation of neural stem
833 cells by Myc and the p19ARF-p53 pathway. *J Cell Biol* **183**, 1243-1257 (2008).
834 102. Sato, T., *et al.* New simple methods for isolating baroreceptor regions of carotid sinus
835 and aortic depressor nerves in rats. *Am J Physiol* **276**, H326-332 (1999).
836 103. Umemura, S., *et al.* The Japanese Society of Hypertension guidelines for the
837 management of hypertension (JSH 2019). *Hypertens Res* **42**, 1235-1481 (2019).
838 104. Oppenheim, A.V., Schafer, R.W., Buck, J.R., Buck, J.R. & Schafer, R.W. *Discrete-time*
839 *signal processing*, (Prentice Hall, Upper Saddle River, N.J, 1999).
840 105. King, C.E., *et al.* Postoperative continuous non-invasive cardiac output monitoring on
841 the ward: a feasibility study. *J Clin Monit Comput* **35**, 1349-1356 (2021).
842 106. Ogata, H., Kayaba, M., Kaneko, M., Ogawa, K. & Kiyono, K. Evaluation of sleep
843 quality in a disaster evacuee environment. *Int J Environ Res Public Health* **17**(2020).

844

845 **Figures and figure legends**

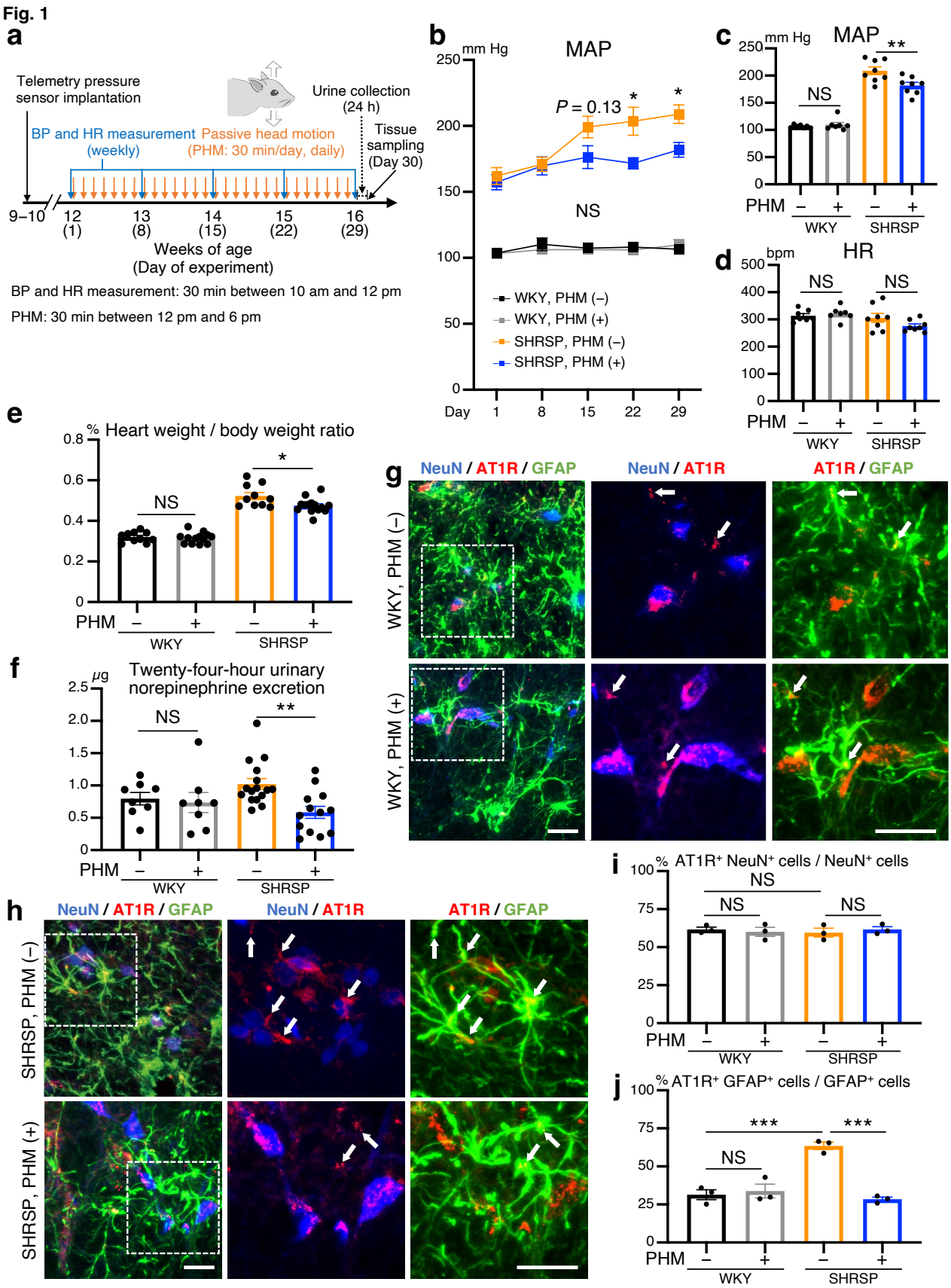


**Fig. 1 | Application of cyclical mechanical intervention to the head by passive motion**

848 **lowers the BP in SHRSPs, and AT1R expression in their RVLM astrocytes. a,** Schematic

849 representation of the experimental protocol to analyze the effects of PHM on the BP in rats. **b,c,**

850 Time courses **(b)** and values on Day 29 **(c)** of the MAP in WKY rats and SHRSPs, subjected to

851 either daily PHM or anesthesia only [**b**, SHRSP PHM (–) vs. (+): $P = 0.1344$ for Day15, $P =$

852 $0.0110$ for Day 22, $P = 0.0463$ for Day 29; WKY PHM (–) vs. (+): $P > 0.9999$ for Day 15, Day

853 22, and Day 29. **c**, $P = 0.9739$ for column 1 vs. 2, $P = 0.0046$ for column 3 vs. 4. $n = 7$ rats for

854 each group of WKY; $n = 8$ rats for each group of SHRSP]. **d,** HR values on Day 29 ($P = 0.9650$

855 for column 1 vs. 2, $P = 0.2362$ for column 3 vs. 4. $n = 7$ rats for each group of WKY; $n = 8$ rats

856 for each group of SHRSP). **e,** Relative heart weight (heart weight / whole body weight)

857 measured on Day 30 [$P = 0.9866$ for column 1 vs. 2, $P = 0.0152$ for column 3 vs. 4. $n = 10$ rats

858 for WKY, PHM (−); $n = 13$ rats for WKY, PHM (+); $n = 10$ rats for SHRSP, PHM (−); $n = 14$

859 rats for SHRSP, PHM (+)]. **f,** Twenty-four-hour (Day 29 to Day 30) urinary norepinephrine

860 excretion [$P = 0.9854$ for column 1 vs. 2, $P = 0.0085$ for column 3 vs. 4. $n = 8$ rats for each

861 group of WKY; $n = 16$ rats for SHRSP, PHM (−); $n = 13$ rats for SHRSP, PHM (+)]. **g,h,**

862 Micrographic images of anti-NeuN (blue), anti-GFAP (green) and anti-AT1R (red)

863 immunostaining of the RVLM of WKY rats **(g)** and SHRSPs **(h)**, either left sedentary (top) or

864 subjected to PHM (bottom) under anesthesia (30 min/day, 28 days). Higher magnification

865 images (center and right) refer to the areas indicated by dotted rectangles in low magnification

866 images (left). Arrows point to anti-AT1R immunosignals that overlap with anti-GFAP, but not

867 anti-NeuN, immunosignals in merged images. Scale bars, 50 μm. Images are representative of

868 three rats. **i,j,** Quantification of AT1R-positive neurons **(i)** and astrocytes **(j)** in the RVLM of

869 WKY rats and SHRSPs, either left sedentary or subjected to PHM. Fifty NeuN-positive ($NeuN^+$)

870 cells and 100 GFAP-positive ($GFAP^+$) cells were analyzed for each rat (**i**: $P = 0.9602$ for column

871 1 vs. 2, $P = 0.9215$ for column 1 vs. 3, $P = 0.9313$ for column 3 vs. 4. **j**: $P = 0.9455$ for column

872 1 vs. 2, $P = 0.0004$ for column 1 vs. 3, $P = 0.0002$ for column 3 vs. 4. $n = 3$ rats for each group).

873 Data are presented as mean ± s.e.m. *$P < 0.05$; **$P < 0.01$; ***$P < 0.001$; NS, not significant;

874 two-way repeated measures ANOVA with Bonferroni's post hoc multiple comparisons test **(b)**

875 or one-way ANOVA with Tukey's post hoc multiple comparisons test **(c−f,i,j)**.

**Extended Data Fig. 1**

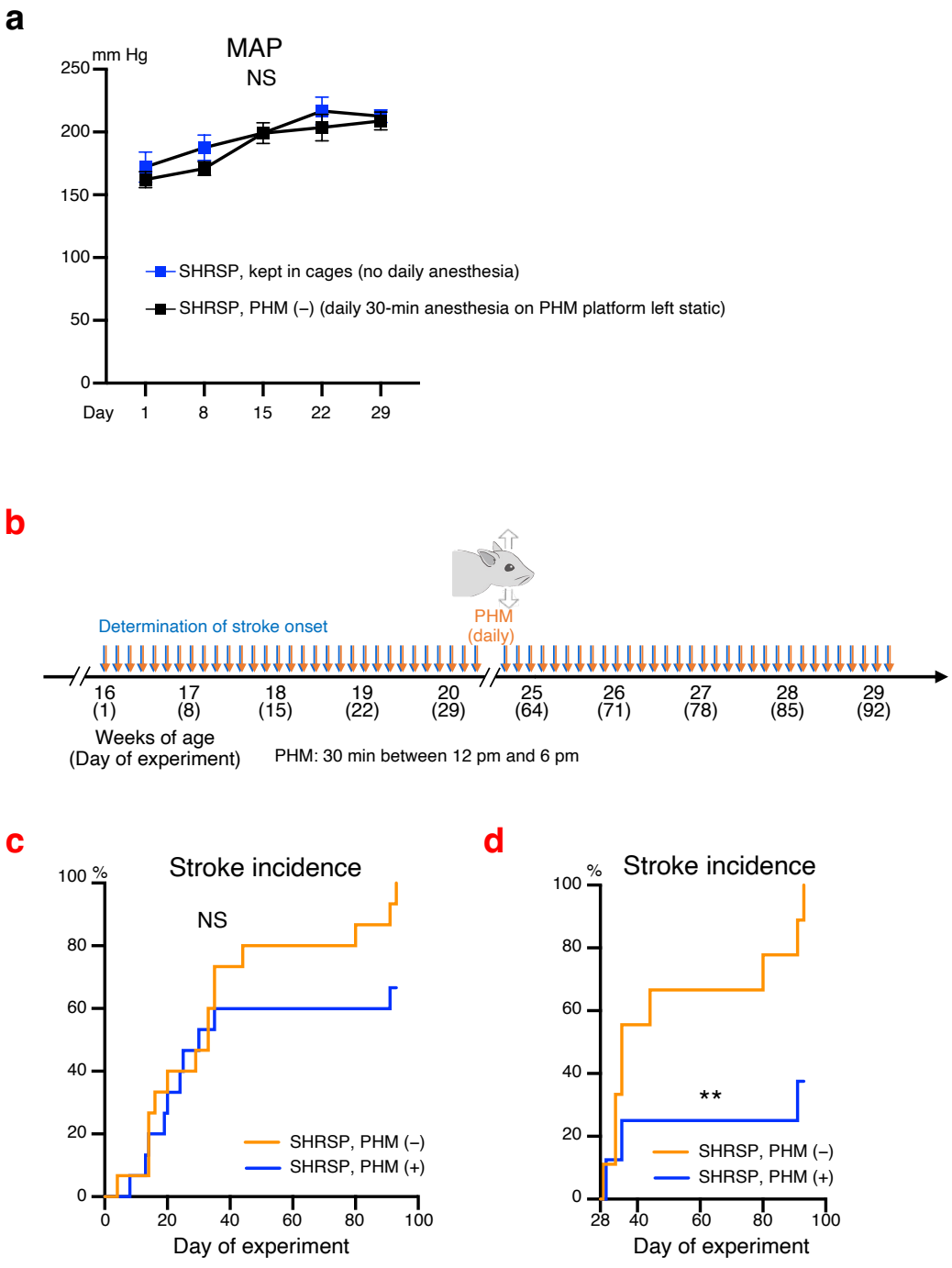


**Extended Data Fig. 1 | Daily anesthesia alone does not affect BP, and ≥4 weeks of daily PHM decreases or delays the stroke incidence in SHRSPs. a,** Time courses of the MAP of SHRSPs either routinely kept in cages (no anesthesia) or subjected to daily anesthesia on the platform of PHM machine without turning on its switch [PHM (−)] [$P > 0.9999$ for Day 15, Day

881 22, and Day 29. $n$ = 6 rats for no daily anesthesia; $n$ = 8 rats for PHM (−)]. **b,** Schematic

882 representation of the experimental protocol to analyze the effects of PHM on the stroke

883 incidence in SHRSPs. **c,d,** Kaplan-Meier curve of the stroke incidence in SHRSPs with and

884 without PHM represented as PHM (+) and PHM (−), respectively. Data from SHRSPs that did

885 not have a stroke during the first four weeks after the initiation of intervention (daily PHM or

886 anesthesia alone) is shown in **(d)** [**c**: $P$ = 0.1179. $n$ = 15 rats for PHM (−); $n$ = 15 rats for PHM

887 (+). **d**: $P$ = 0.0093. $n$ = 9 rats for PHM (−); $n$ = 8 rats for PHM (+)]. **$P$ < 0.01; NS, not

888 significant; two-way repeated measures ANOVA with Bonferroni's post hoc multiple

889 comparisons test **(a)** or long-rank test **(c,d)**.

**Extended Data Fig. 2**

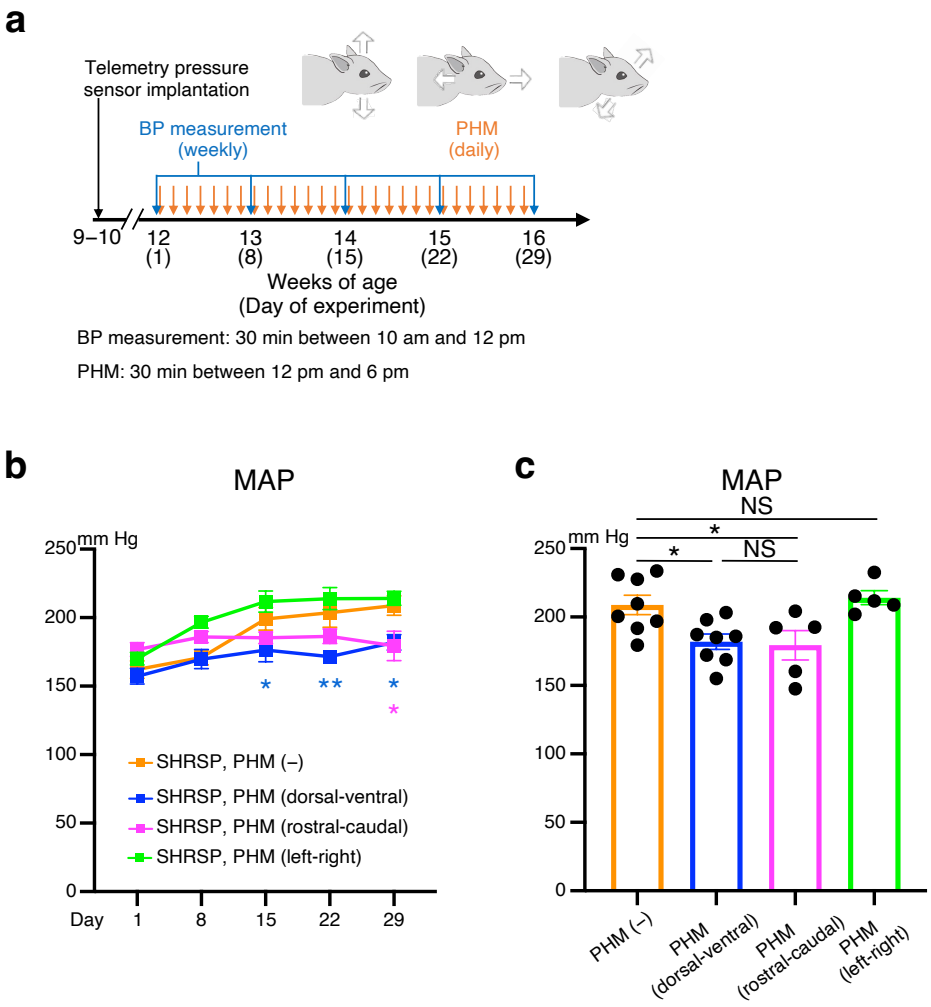


**Extended Data Fig. 2 | PHM in the rostral-caudal, but not left-right, direction lowers the BP in SHRSPs. a,** Schematic representation of the experimental protocol to analyze the effects of PHM on the BP in rats. **b,c,** Time courses **(b)** and values on Day 29 **(c)** of MAP in SHRSPs, subjected to either daily PHM or anesthesia only [**b**, orange vs. blue: $P = 0.0376$ for Day 15, $P = 0.0018$ for Day 22, $P = 0.0105$ for Day 29; orange vs. magenta: $P = 0.4131$ for Day 15, $P = 0.2448$ for Day 22, $P = 0.0148$ for Day 29; orange vs. green: $P = 0.4869$ for Day 15, $P = 0.6439$ for Day 22, $P = 0.9273$ for Day 29. **c**: $P = 0.0363$ for column 1 vs. 2, $P = 0.0465$ for column 1 vs. 3, $P = 0.9576$ for column 1 vs. 4, $P = 0.9948$ for column 2 vs. 3. $n = 8$ rats for PHM (−) and

899 PHM (dorsal-ventral); n = 5 rats for PHM (rostral-caudal) and PHM (left-right)]. The data for

900 columns 1 and 2 in **(c)** are respectively identical to those for columns 3 and 4 in Fig. 1c. Data

901 are presented as mean ± s.e.m. *$P < 0.05$; **$P < 0.01$; NS, not significant; two-way repeated

902 measures ANOVA with Dunnett's post hoc multiple comparisons test **(b)** or one-way ANOVA

903 with Tukey's post hoc multiple comparisons test **(c)**.

**Extended Data Fig. 3**

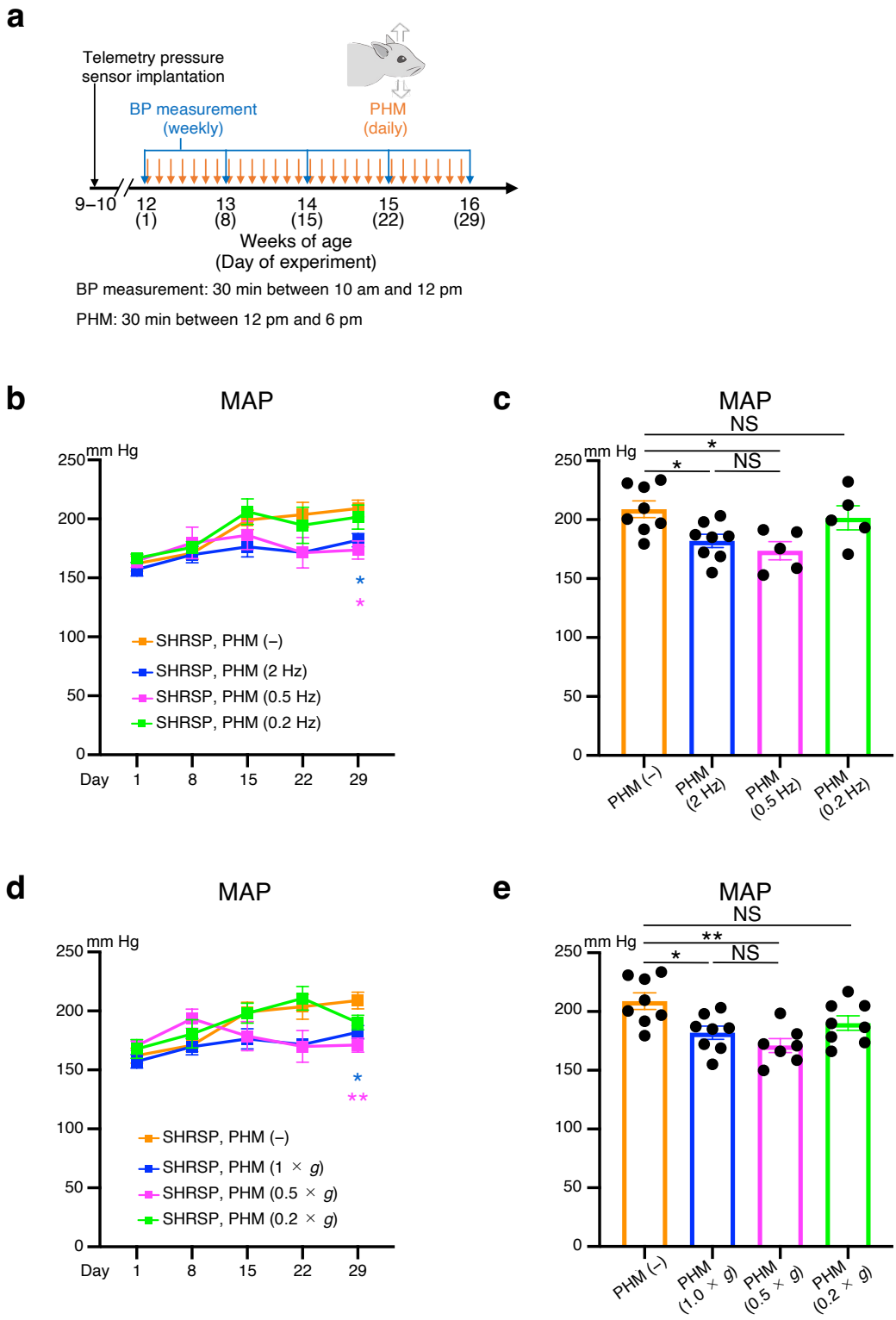


**Extended Data Fig. 3 | Antihypertensive effects of PHM with different frequencies or magnitudes. a,** Schematic representation of the experimental protocol to analyze the effects of PHM on the BP in SHRSPs. **b–e,** Time courses **(b,d)** and values on Day 29 **(c,e)** of MAP of

908 SHRSPs, subjected to daily PHM with either different frequencies **(b,c)** or peak accelerations

909 **(d,e)** [**b**, orange vs. blue: $P = 0.1871$ for Day 15, $P = 0.0519$ for Day 22, $P = 0.0282$ for Day 29;

910 orange vs. magenta: $P = 0.7252$ for Day 15, $P = 0.2053$ for Day 22, $P = 0.0208$ for Day 29;

911 orange vs. green: $P = 0.9212$ for Day 15, $P = 0.9356$ for Day 22, $P = 0.8950$ for Day 29. **c**: $P =$

912 0.0435 for column 1 vs. 2, $P = 0.0174$ for column1 vs. 3, $P = 0.9068$ for column 1 vs. 4, $P =$

913 0.8682 for column 2 vs. 3. $n = 8$ rats for PHM (−) and PHM (2 Hz); n = 5 rats for PHM (0.5 Hz)

914 and PHM (0.2 Hz). **d**, orange vs. blue: $P = 0.1812$ for Day 15, $P = 0.0504$ for Day 22, $P =$

915 0.0274 for Day 29; orange vs. magenta: $P = 0.4146$ for Day 15, $P = 0.1740$ for Day 22, $P =$

916 0.0036 for Day 29; orange vs. green: $P = 0.9996$ for Day 15, $P = 0.9267$ for Day 22, $P = 0.1618$

917 for Day 29. **e**: $P = 0.0227$ for column 1 vs. 2, $P = 0.0014$ for column 1 vs. 3, $P = 0.1664$ for

918 column 1 vs. 4, $P = 0.6283$ for column 2 vs. 3. $n = 8$ rats for PHM (−), PHM (1 × *g*), and PHM

919 (0.2 × *g*); n = 7 rats for PHM (0.5 × *g*)]. The data for columns 1 and 2 in **(c,e)** are respectively

920 identical to those for columns 3 and 4 in Fig. 1c. Data are presented as mean ± s.e.m. *$P < 0.05$;

921 **$P < 0.01$; NS, not significant; two-way repeated measures ANOVA with Dunnett's post hoc

922 multiple comparisons test **(b,d)** or one-way ANOVA with Tukey's post hoc multiple

923 comparisons test **(c,e)**.

924

**Extended Data Fig. 4**

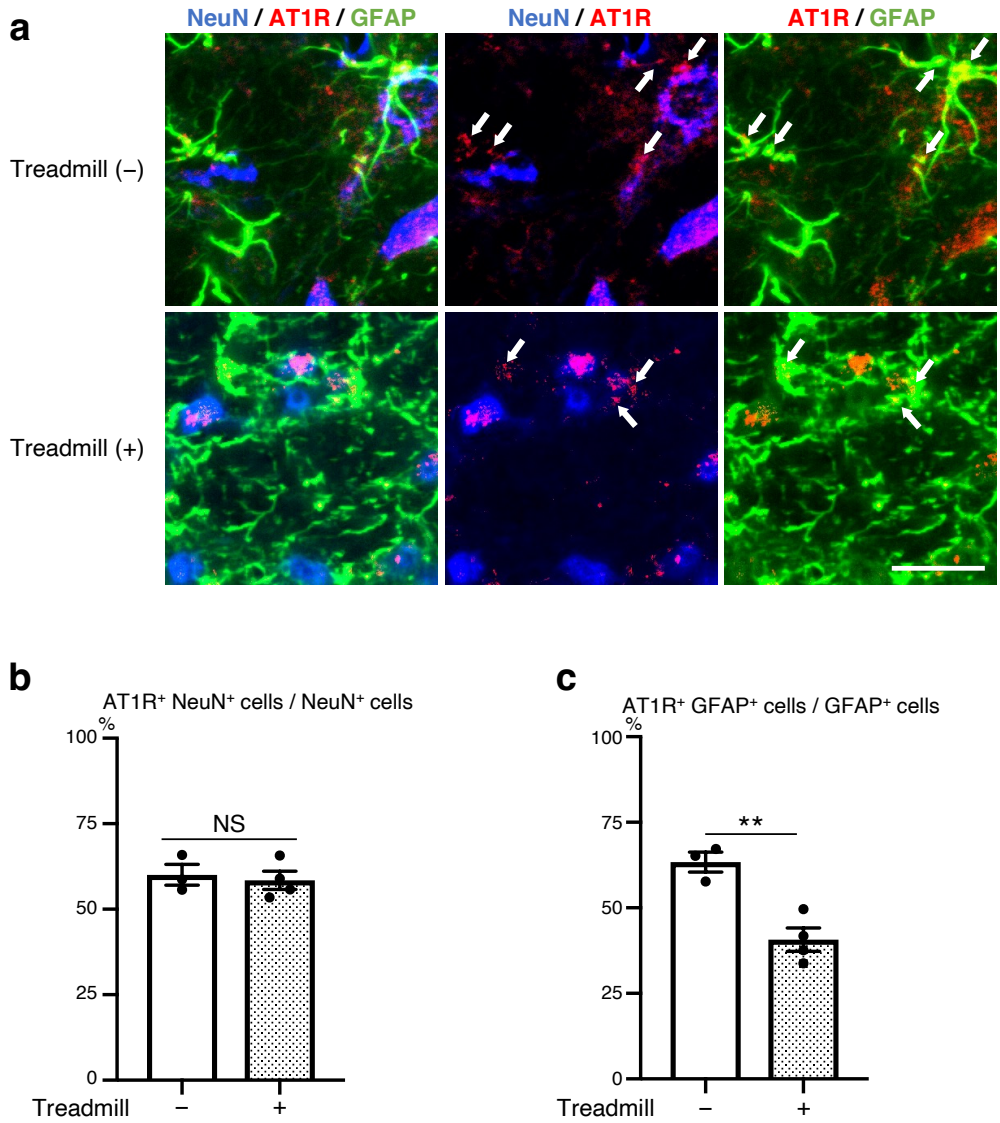


**Extended Data Fig. 4 | Treadmill running decreases AT1R expression in the RVLM astrocytes in SHRSPs. a,** Micrographic images anti-NeuN (blue), anti-GFAP (green) and anti-AT1R (red) immunostaining of the RVLM of SHRSPs, either placed in the static treadmill machine or subjected to treadmill running at the velocity of 20 m/min (30 min/day, 28 days). Arrows point to anti-AT1R immunosignals that overlap with anti-GFAP, but not anti-NeuN, immunosignals in merged images. Scale bar, 50 μm. Images are representative of three or four rats. **b,c,** Quantification of AT1R-positive neurons **(b)** and astrocytes **(c)** in the RVLM of

933 SHRSPs with or without 4-week treadmill running. Fifty $NeuN^+$ cells and 100 $GFAP^+$ cells were

934 analyzed for each rat [**b**: $P = 0.7056$. **c**: $P = 0.0048$. $n = 3$ rats for treadmill (−); $n = 4$ rats for

935 treadmill (+)]. Data are presented as mean ± s.e.m. **$P < 0.01$; NS, not significant, unpaired

936 two-tailed Student's *t*-test.

Fig. 2

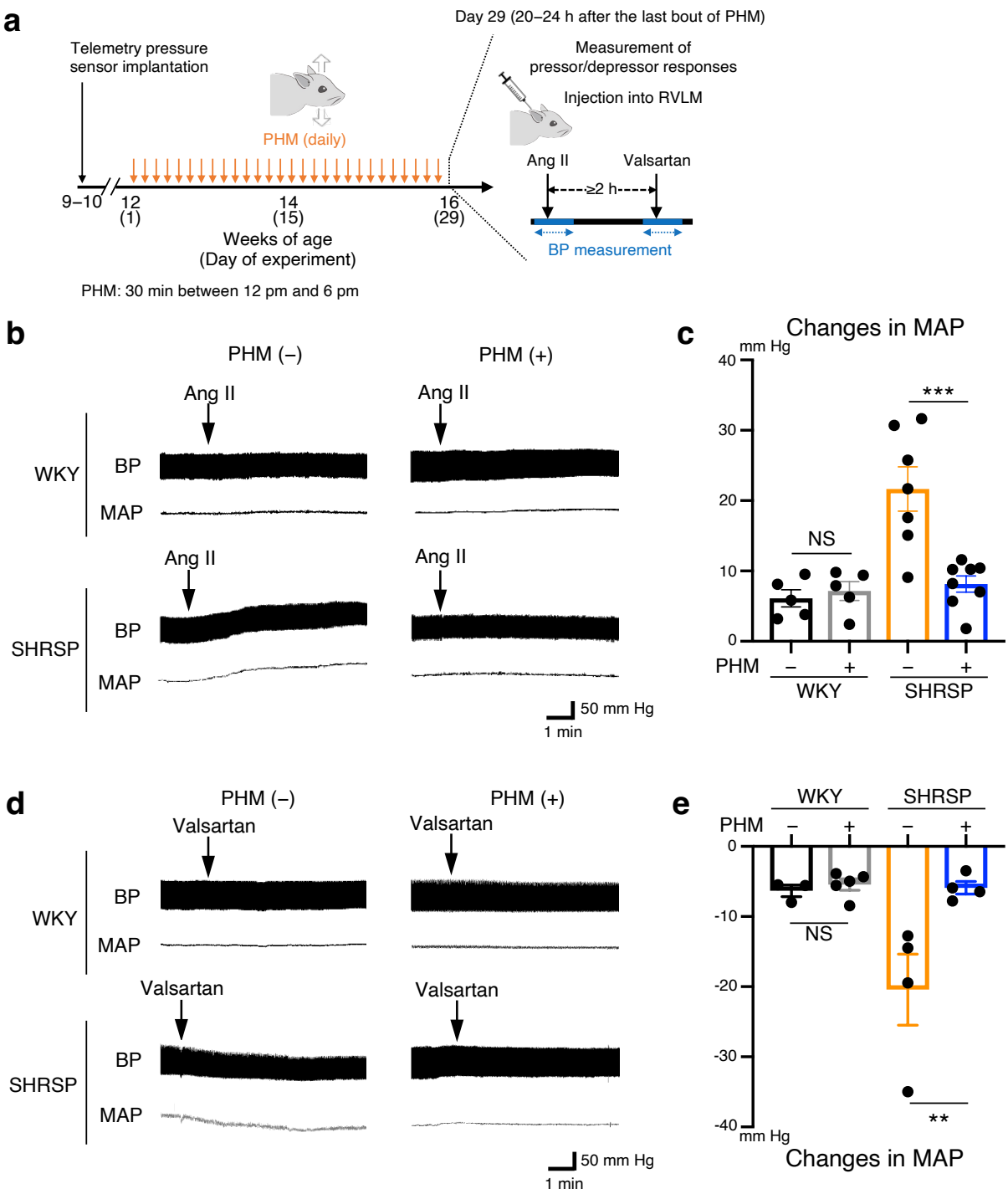


**Fig. 2 | PHM alleviates the sensitivity of RVLM in SHRSPs to Ang II or valsartan. a,** Schematic representation of the experimental protocol to analyze the effects of PHM on the sensitivity to Ang II or valsartan injected into the unilateral RVLM. Ang II (100 pmol) was injected into the unilateral RVLM of WKY rats and SHRSPs, either left sedentary (daily

942 anesthesia) or subjected to PHM (30 min/day, 28 days), with their BP monitored under urethane

943 anesthesia. Injection of valsartan (100 pmol) into the RVLM was conducted at least 2 h after the

944 injection of Ang II. **b,** Representative trajectories of BP (top in each panel) and MAP (bottom in

945 each panel). Arrows point to the time of the initiation of RVLM injection of Ang II. Right-

946 angled scale bar, 1 min / 50 mm Hg. **c,** Quantification of MAP change caused by Ang II

947 injection [$P = 0.9876$ for column 1 vs. 2, $P = 0.0003$ for column 3 vs. 4. $n = 5$ rats for each

948 group of WKY; $n = 7$ rats for SHRSP, PHM (−); $n = 8$ rats for SHRSP, PHM (+)]. **d,e,** Effects of

949 the RVLM injection of valsartan (100 pmol) examined as in **(b,c)** [**e**: $P = 0.9953$ for column 1

950 vs. 2, $P = 0.0099$ for column 3 vs. 4. $n = 3$ rats for WKY, PHM (−); $n = 5$ rats for WKY, PHM

951 (+); $n = 4$ rats for each group of SHRSP]. Data are presented as mean ± s.e.m. $^{**}P < 0.01$; $^{***}P$

952 $< 0.001$; NS, not significant; one-way ANOVA with Tukey's post hoc multiple comparisons test.

Fig. 3

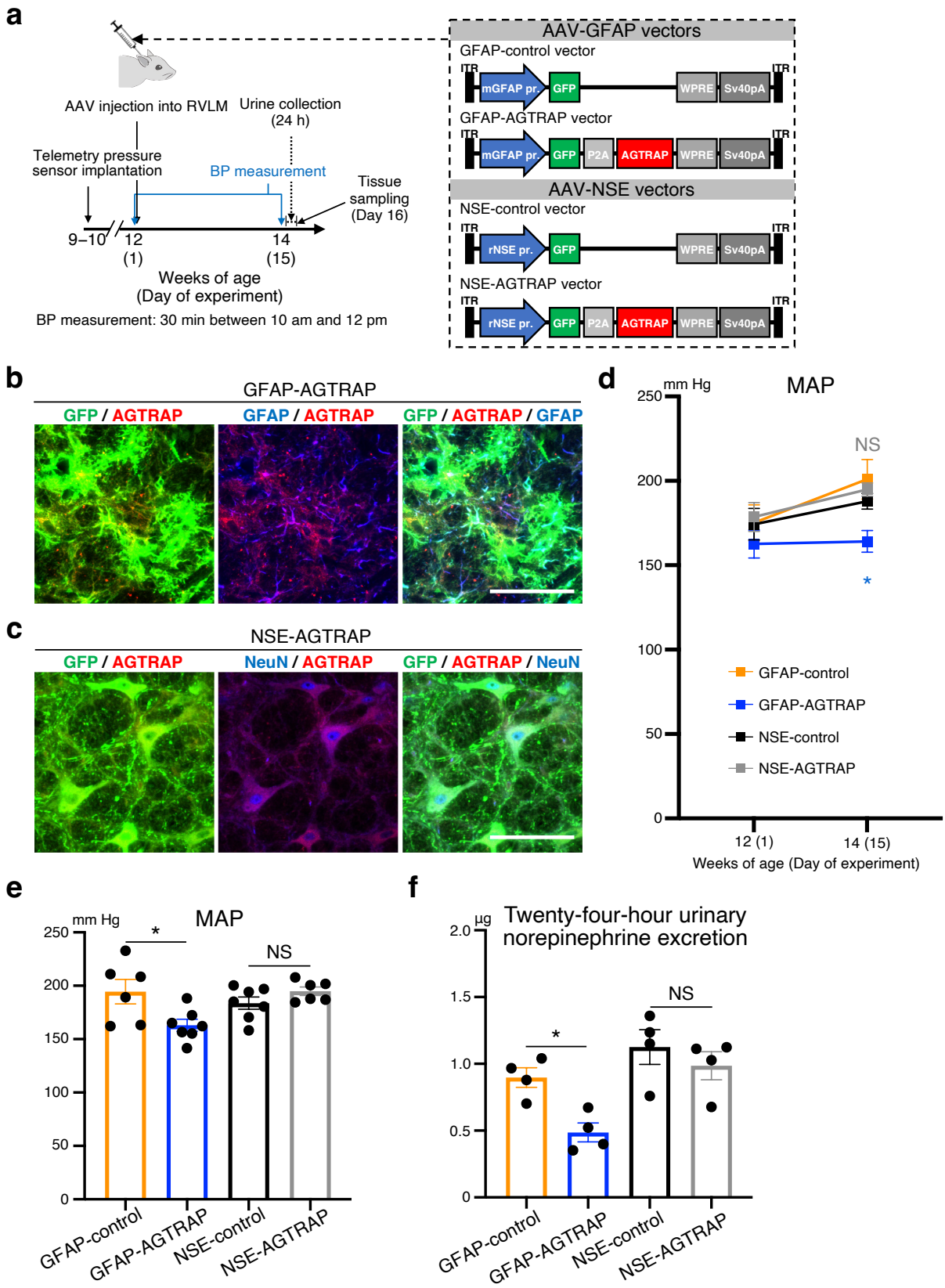


953

954 **Fig. 3 | AAV-mediated expression of AGTRAP in RVLM astrocytes, but not neurons,**

**lowers the BP in SHRSPs. a,** Schematic representation of the experimental protocol to analyze the effects of AAV-mediated transduction of RVLM astrocytes or neurons with the AGTRAP gene. ITR; inverted terminal repeat. **b,c,** Astrocyte- **(b)** and neuron- **(c)** specific transgene expression by the RVLM injection of AAV9 vectors. Micrographic images of GFP (green) and anti-GFAP **(b)** or anti-NeuN **(c)** immunostaining (blue) of RVLM of SHRSPs 15 days after the injection of AAV9 vectors indicated at the top of each panel. Scale bars, 50 μm. Images are representative of three rats. **d−f,** Values just before (Day 1) and 2 weeks after (Day 15) the AAV injection into the RVLM **(d)**, and values on Day 15 **(e)** of MAP (**d**: $P = 0.0222$ for GFAP-control vs. GFAP-AGTRAP and $P > 0.9999$ for NSE-control vs. NSE-AGTRAP. **e**: $P = 0.0229$ for column 1 vs. 2, $P = 0.6864$ for column 3 vs. 4. $n = 6$ rats for GFAP-control; $n = 7$ rats for GFAP-AGTRAP; $n = 7$ rats for NSE-control; $n = 6$ rats for NSE-AGTRAP) and 24-h urinary norepinephrine excretion **(f)** ($P = 0.0497$ for column 1 vs. 2, $P = 0.7455$ for column 3 vs. 4. $n = 4$ rats for each group) of SHRSPs subjected to the RVLM injection of AAV9 vectors. Data are presented as mean ± s.e.m. *$P < 0.05$; NS, not significant, two-way repeated measures ANOVA with Bonferroni's post hoc multiple comparisons test **(d)** or one-way ANOVA with Tukey's post hoc multiple comparisons test **(e,f)**.

**Extended Data Fig. 5**

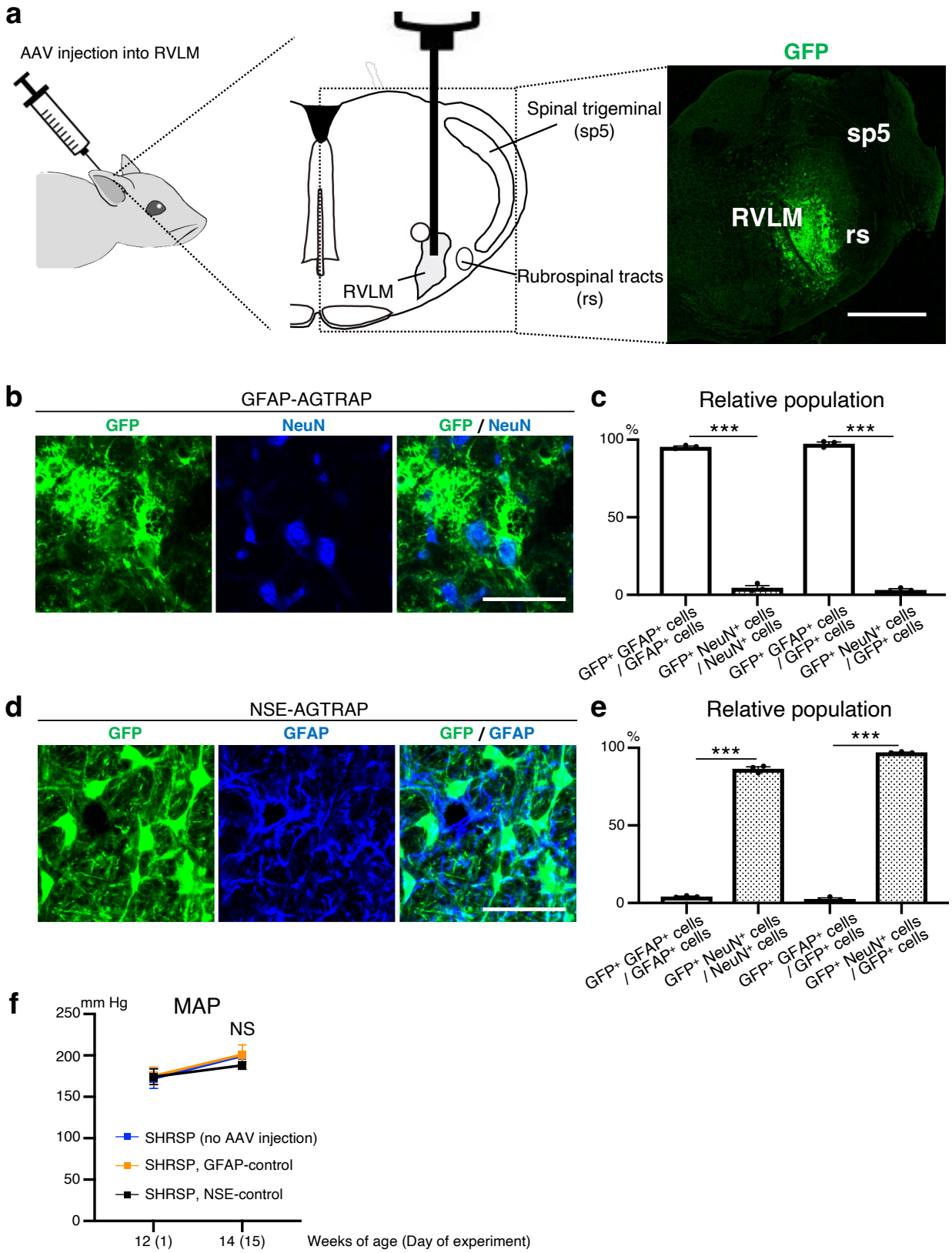


**Extended Data Fig. 5 | AAV-mediated transduction of RVLM astrocytes or neurons in**

973 **SHRSPs. a,** Schematic representation of the injection of AAV9 vectors to the RVLM.
974 Micrographic image is representative of three rats analyzed in Fig. 3b (two weeks after the
975 RVLM injection of GFAP-AGTRAP vector). GFP-derived fluorescence indicates cells
976 expressing the transgene. Scale bar, 1 mm. **b,c,** Efficiency and specificity of astrocyte-specific
977 expression of the transgene. **(b)** Micrographic images of GFP (green) and anti-NeuN
978 immunostaining (blue) of the RVLM of SHRSPs analyzed in Fig. 3b. Scale bar, 50 μm. Images
979 are representative of three rats. **(c)** Quantification of the efficiency and specificity of transgene
980 expression. The relative populations (%) of GFP/ GFAP/ double positive ($GFP^+$ $GFAP^+$) or
981 GFP/ NeuN/ double positive ($GFP^+$ $NeuN^+$) cells were calculated by referring their numbers to
982 those of $GFP^+$, $GFAP^+$ or $NeuN^+$ cells ($P < 0.0001$ for column 1 vs. 2 and $P < 0.0001$ for
983 column 3 vs. 4. $n = 3$ rats for each group). **d,e,** Efficiency and specificity of neuron-specific
984 expression of the transgene. **(d)** Micrographic images of GFP (green) and anti-GFAP
985 immunostaining (blue) of the RVLM of SHRSPs analyzed in Fig. 3c. Scale bar, 50 μm. Images
986 are representative of three rats. **(e)** Efficiency and specificity quantified as in **(c)** ($P < 0.0001$for
987 column 1 vs. 2 and $P < 0.0001$ for column 3 vs. 4.). **f,** BP in SHRSPs injected with the control
988 vectors. BP was measured and MAP was quantified as in Fig. 1b ($P = 0.9918$ for blue vs.
989 orange, $P = 0.6465$ for blue vs. black, $P = 0.5966$ for orange vs. black. $n = 6$ rats for no AAV
990 injection; $n = 6$ rats for GFAP-control; $n = 7$ rats for NSE-control). The data for blue line are
991 identical to those demonstrated with blue line in Extended Data Fig. 1a. Data are presented as

992 mean ± s.e.m. ***$P < 0.001$; NS, not significant; unpaired two-tailed Student's *t*-test **(c,e)** or

993 two-way repeated measures ANOVA with Tukey's post hoc multiple comparisons test **(f)**.

Fig. 4

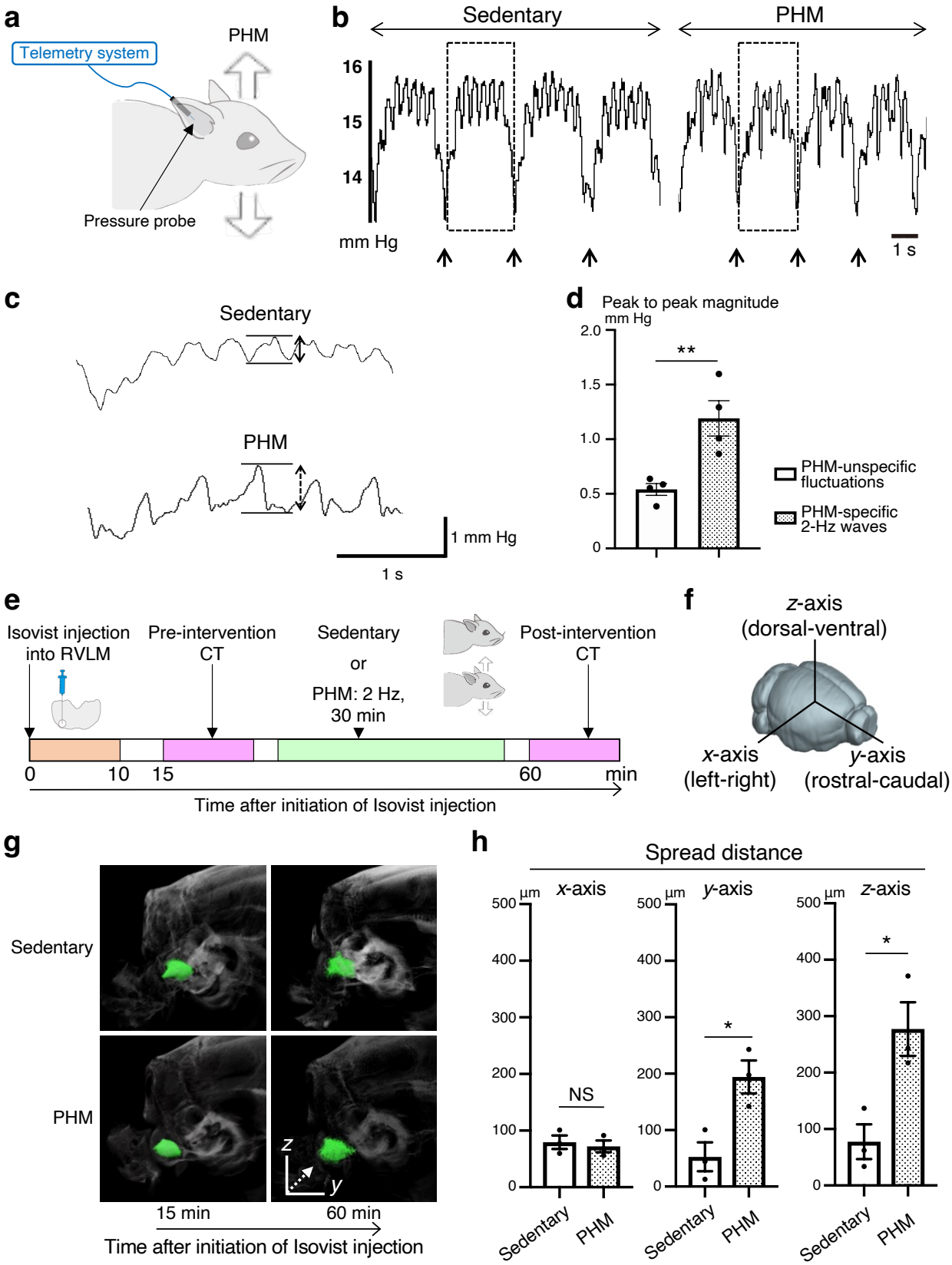


994

995 **Fig. 4 | PHM generates pressure waves of low amplitude, and facilitates interstitial fluid**

996 **movement (flow) in the rat RVLM. a,** Schematic representation of the pressure measurement
997 in the rat RVLM. **b,** Representative pressure waves recorded in the rat RVLM during the
998 sedentary condition and PHM. Arrows point to the time of transition from inhalation to
999 exhalation detected by simultaneous respiration monitoring. Scale bar, 1 s. Images are
1000 representative of four independent experiments with similar results. **c,** Respiration-
1001 unsynchronized pressure changes. Respiration-synchronized pressure waves indicated by dotted
1002 rectangles in **(b)** are presented with high magnification. Right-angled scale bar, 1 s / 1 mm Hg.
1003 Note that the 2-Hz pressure waves indicated by a two-headed dotted line arrow were specifically
1004 generated during PHM. **d,** Magnitude of PHM-specific and -unspecific pressure changes
1005 unsynchronized with respiration. The peak-to-peak magnitudes indicated by two-headed arrows
1006 in **(c)** were quantified ($P = 0.0089$. $n = 4$ rats for each group, 10 segments analyzed for each rat).
1007 **e,** Schematic representation of experimental protocol for the μCT analysis of Isovist injected
1008 into the rat RVLM. **f,** Definition of the *x*-(left-right), *y*-(rostral-caudal), and *z*-(dorsal-ventral)
1009 axes used in this study. **g,** Representative Isovist spread presented on X-ray images. Isovist
1010 clusters are indicated by green. Images are representative of three rats. A dotted line arrow
1011 indicates the main direction of spreading in this sample. **h,** Quantification of Isovist spread
1012 along each axis (left chart: $P = 0.6666$. middle chart: $P = 0.0218$. right chart: $P = 0.0244$. $n = 3$
1013 rats for each group). Data are presented as mean ± s.e.m. *$P < 0.05$; **$P < 0.01$; NS, not
1014 significant, unpaired two-tailed Student's *t*-test.

Extended Data Fig. 6

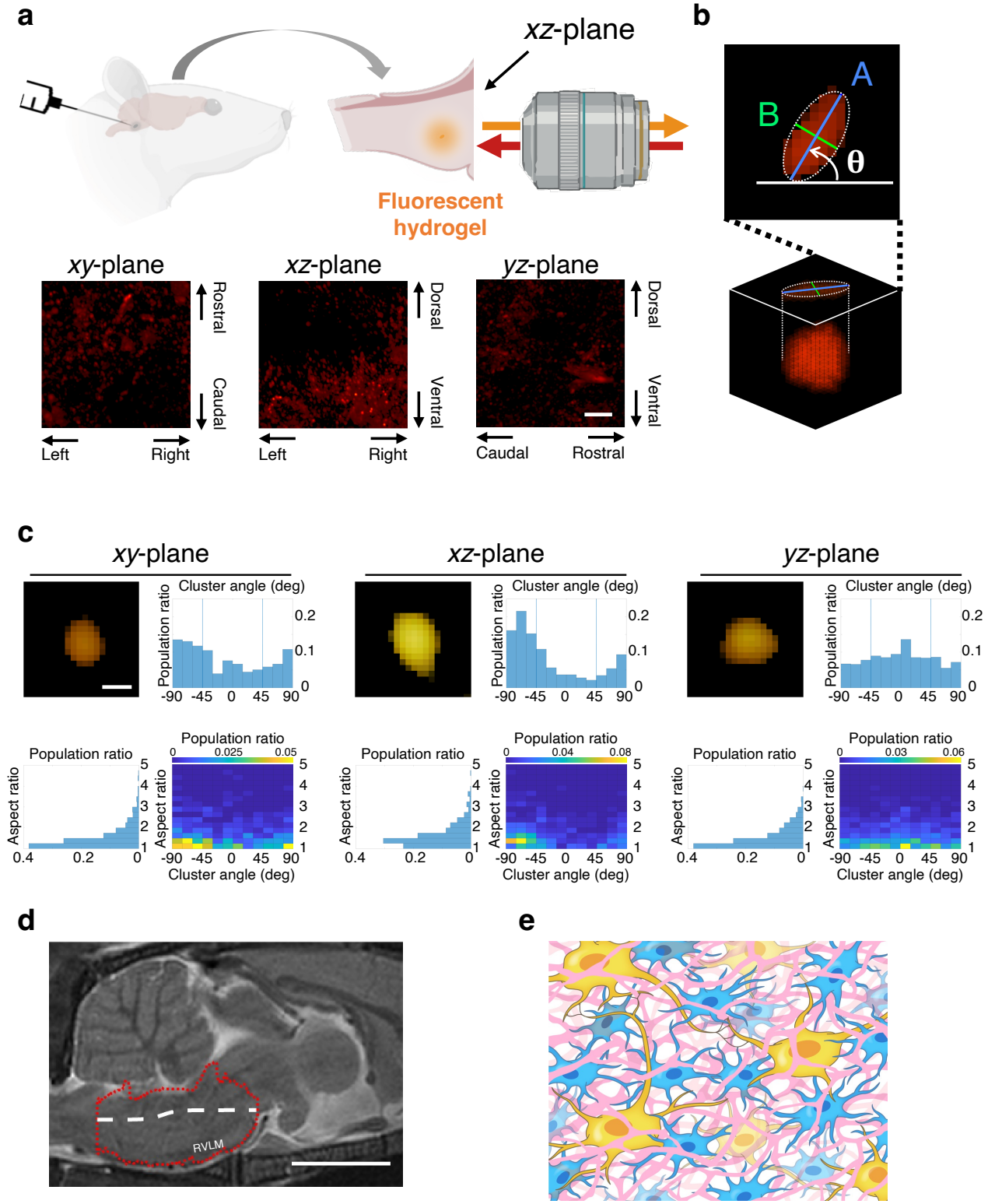


1015

1016 **Extended Data Fig. 6 | Structure and orientation of interstitial space in the rat RVLM. a,**

1017 Multiphoton microscopic imaging of fluorescent hydrogel-introduced rat RVLM in three

1018 mutually orthogonal planes. Top: schematic illustration of hydrogel introduction and *xz*-plane
1019 imaging. Bottom: processed volume images (see Methods) of interstitial space-representing
1020 fluorescence clusters projected onto the *xy*- (bottom left), *xz*- (bottom center), and *yz*- (bottom
1021 right) planes. Scale bar, 20 μm. **b,** Determination of the cluster angle and calculation of the
1022 aspect ratio. Interstitial space-representing fluorescence clusters were extracted, and their
1023 projection and elliptic fitting on the stacked plane were conducted as described in the Methods.
1024 The cluster angle (θ) in degrees was defined and analyzed as positive (counterclockwise; see arc
1025 arrow) or negative (clockwise) from the horizontal line in each plane. The aspect ratio was
1026 calculated as A/B. **c,** Distribution of the cluster angle and aspect ratio. Volume image of a cluster
1027 of typical shape and orientation (top left), histograms of the angle distribution (top right) and
1028 aspect ratio (bottom left), and 2-D histogram of the cluster orientation/aspect ratio (bottom right)
1029 are shown for the *xy*-, *xz*-, and *yz*-planes. From the location of seemingly unimodal peaks in the
1030 2-D histograms for the *xy*- and *xz*-planes, the *y*- and *z*-axes appear to be dominant over the *x*-axis
1031 concerning the cluster orientation. Furthermore, the *y*-axis appears slightly dominant over the *z*-
1032 axis (loose peak on the 0–15° block in the *yz*-plane). Collectively, the structure of the interstitial
1033 space-representing clusters seems loosely oriented in the direction close to the *y*-(rostral-caudal)
1034 axis with a slight counterclockwise (rostrally upward) inclination. Scale bar, 1 μm. **d,**
1035 Representative sagittal MR image of the rat brainstem (0.06 mm off the median plane). Red
1036 dotted line-indicated area and white broken line represent the lower brainstem and longest

1037 centroidal line of this part of the brain, respectively (see Methods). Note that the centroidal line

1038 is approximately along the *y*-axis with a slight rostrally upward inclination. Scale bar, 5 mm.

1039 Data shown in **(c,d)** represent at least three independent samples (rats) with similar results. **e,**

1040 Diagram of the mesoscale structure/orientation of interstitial space in the rat RVLM. The

1041 interstitial space (depicted in pink) is not randomly structured but oriented approximately along

1042 the direction of the centroidal line of this part of the brain with relatively minor lateral

1043 communications.

1044

Extended Data Fig. 7

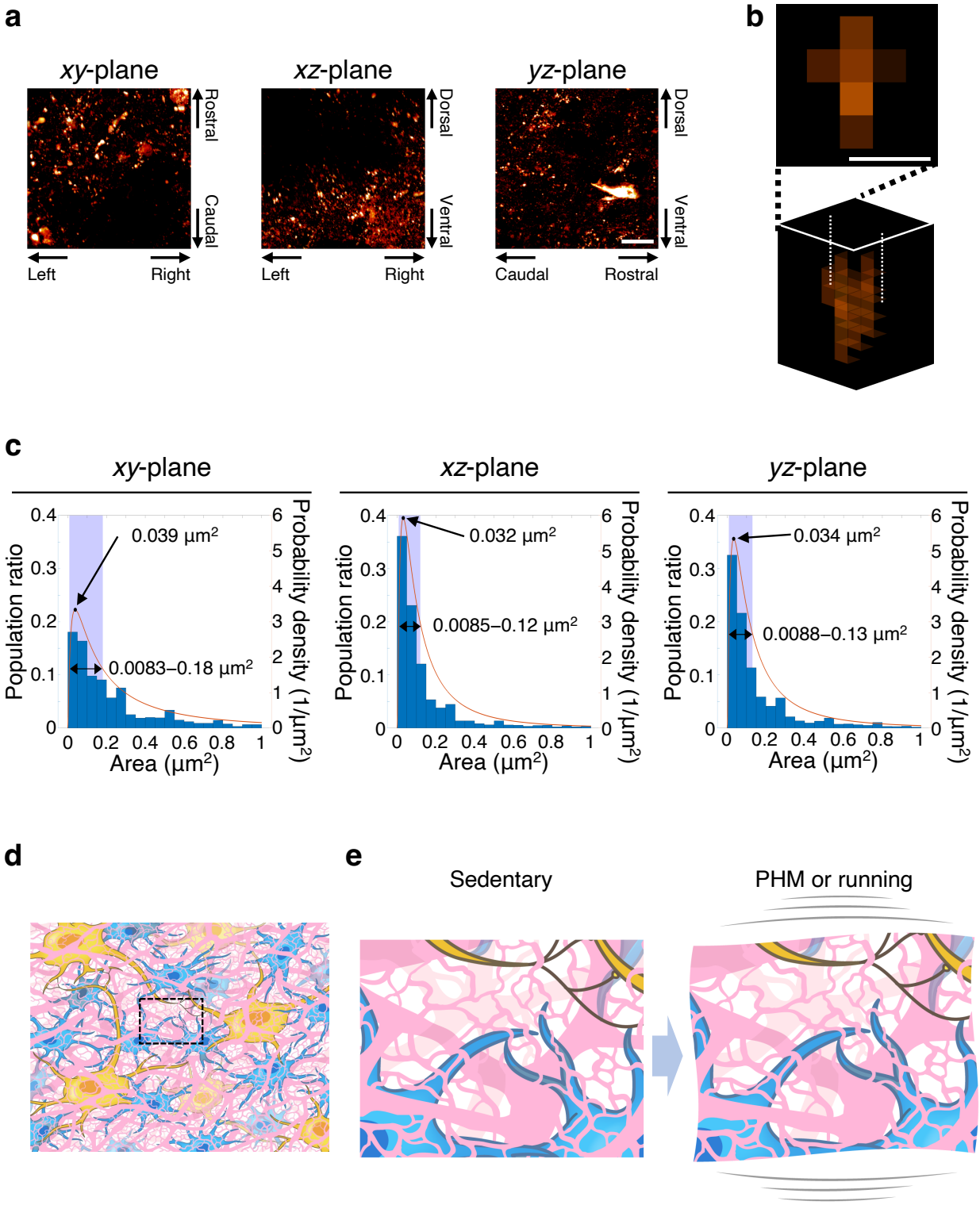


**Extended Data Fig. 7 | Dimension (cross-sectional area) of interstitial space in the rat RVLM. a,** Multiphoton microscopic images of interstitial space-representing fluorescence clusters projected onto *xy*- (left), *xz*- (center), and *yz*- (right) planes. Scale bar, 20 μm. **b,**

1049 Projection of 4-μm stack images of an individual cluster. Scale bar, 0.5 μm. **c,** Distribution of the
1050 cross-sectional areas of individual clusters. Red curves represent the probability densities
1051 revealed by fitting to log-normal distribution[77,78]. Black circles and two-way arrows indicate the
1052 mode and full width at half maximum (FWHM)[79], respectively. **d,** Diagram of the interstitial
1053 space in the rat RVLM. Dotted rectangle indicates the area illustrated in **(e)**. Because we
1054 analyzed the interstitial space with imaging experiments based on the spread of the injected
1055 gelatable fluorescent PEG solutions, we assumed the interstitial space to have a continuous
1056 structure. Nevertheless, we do not preclude the possible existence of dead ends of interstitial
1057 space. **e,** Illustration of cyclic microdeformation during PHM or treadmill running that generates
1058 small pressure changes in the rat RVLM, facilitating or promoting interstitial fluid movement in
1059 situ.
1060

Supplementary Table 1

**a**

| Property | Value |
|---|---|
| Porosity ($\varepsilon$) | 0.2 (20%) |
| Diameter of interstitial space ($D_p$; μm) | 0.10–0.48 |
| Kozeny constant ($k$) | 4.5–5.5 |
| Viscosity of interstitial fluid ($\mu$; mPa•s) | 0.72 |
| Velocity of interstitial fluid movement (flow) (μm/s) | 0.4–0.6 |

**b**

FSS ($\tau_x$) at the cell surface:

$$\tau = \frac{\mu u_\infty}{\sqrt{K_p}}$$

$$K_p = \frac{D_p^2 \varepsilon^3}{36k(1-\varepsilon)^2}$$

, where $K_p$ is the Darcy permeability in the brain (RVLM).

When the values listed in **a** are introduced in these equations, the Darcy permeability is calculated as **$6.63 \times 10^{-19} - 1.45 \times 10^{-17}$ m$^2$**, and the magnitude of FSS is estimated as **0.076–0.53 Pa**.

**Supplementary Table 1 | Calculation of the magnitude of PHM-generated FSS on rat RVLM cells. a,** Values referenced for calculation of the magnitude of FSS that PHM generated in the rat RVLM. Based on the estimated structure of the interstitial space in the rat RVLM (Extended Data Fig. 6e and Extended Data Fig. 7d), we referenced 4.5–5.5 as the Kozeny constant[80-82] to calculate the Darcy permeability (see Methods). Because the velocity of

1067 interstitial fluid movement has been reported to be ~0.2 μm/s in sedentary rats[37] and mice[38], we
1068 entered 0.4–0.6 μm/s as its value during PHM, based on our interpretation of the μCT study (i.e.,
1069 two- to three-fold increase in velocity; Fig. 4g,h). The property of the interstitial fluid in the
1070 brain, whose composition is similar to that of the cerebrospinal fluid (CSF)[35], was referenced
1071 from previous studies describing the viscosity of human CSF[83,84]. The diameter of the individual
1072 interstitial space was referenced from the values of the cross-sectional area of the interstitial
1073 space as shown in Extended Data Fig. 7c. **b,** Calculation of the magnitude of FSS generated by
1074 PHM. The Darcy permeability ($K_p$) is calculated as $6.63 \times 10^{-19} - 1.45 \times 10^{-17}$ $m^2$. Following the
1075 calculation reported previously[85], the magnitude of FSS (τ) at the cell surface is estimated as
1076 0.076–0.53 Pa.
1077

**Extended Data Fig. 8**

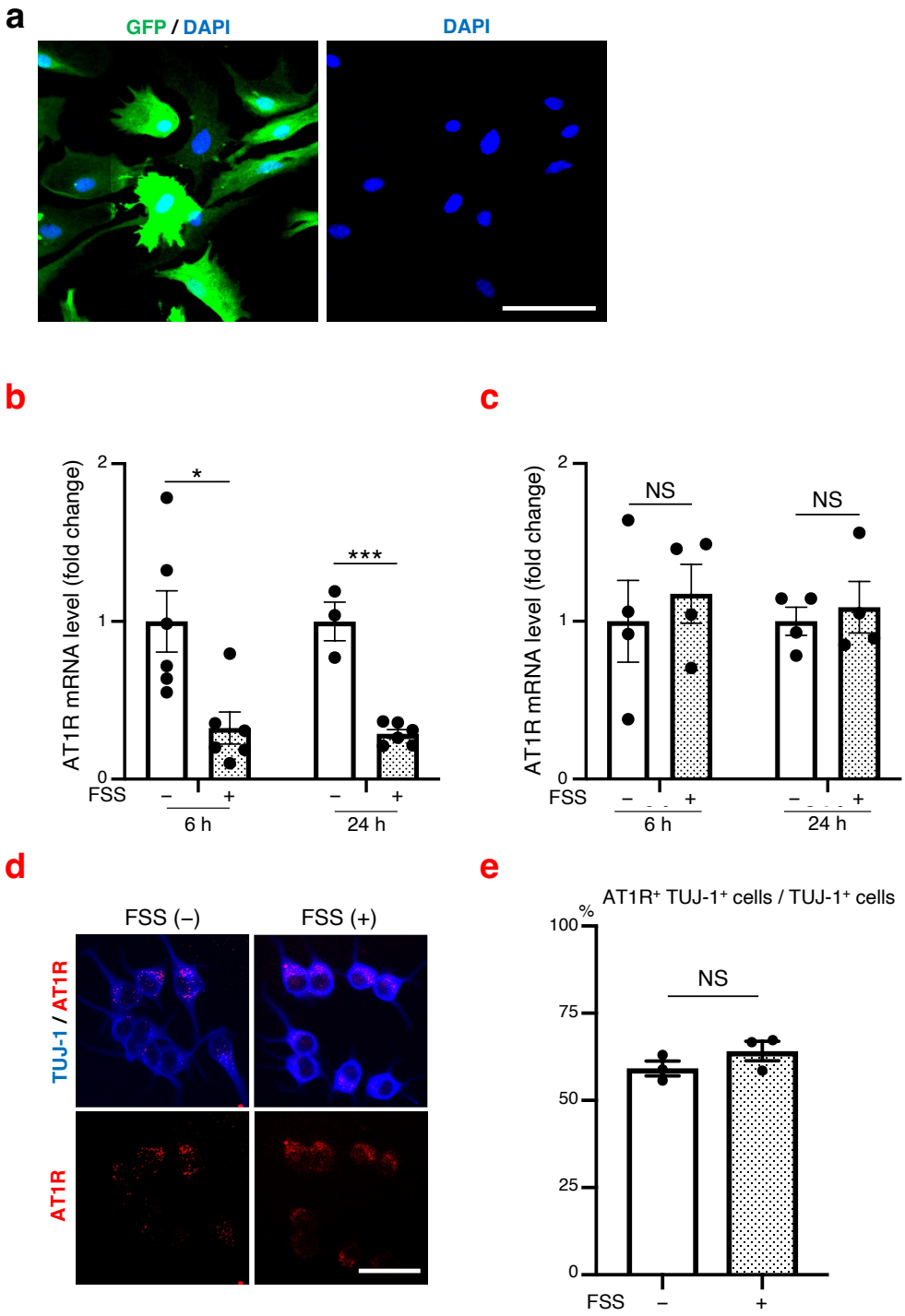


1078

1079 **Extended Data Fig. 8 | Preparation of astrocyte-enriched primary culture, and lack of**

1080 **decreasing effect of FSS on AT1R expression in cultured neuronal cells. a,** Representative

1081 micrographic image of anti-GFP immunostaining (green) and DAPI staining (blue) of astrocyte-

1082 enriched culture prepared from the astrocyte-GFP mice. Scale bar, 50 μm. Note that most of the

1083 cells are GFP-positive. **b**,**c,** Effects of FSS on the AT1R mRNA expression in astrocytes and

1084 Neuro2A cells. AT1R mRNA expression in cultured astrocytes **(b)** and Neuro2A cells **(c)** 6 or 24

1085 h after 30-min FSS application (0.7 Pa, 0.5 Hz) was analyzed as in Fig. 5a [**b**: $P = 0.0116$ for 6

1086 h, $P < 0.0001$ for 24 h. $n = 6$ for 6 h; $n = 3$ for 24 h/FSS (−); $n = 6$ for 24 h/FSS (+). **c**: $P =$

1087 0.6065 for 6 h, $P = 0.6490$ for 24 h. $n = 4$ for each group]. **d,** Microscopic images of anti-AT1R

1088 (red) and anti-TUJ-1 (blue) immunostaining of Neuro2A cells, either left unexposed or exposed

1089 to pulsatile FSS (0.7 Pa, 0.5 Hz, 30 min), and fixed 24 h after the intervention. Images are

1090 representative of three independent experiments with similar results. Scale bar, 50 μm. **e,**

1091 Relative population of AT1R/TUJ-1/ double positive ($AT1R^+$ $TUJ\text{-}1^+$) cells quantified as a ratio

1092 to total TUJ-1-positive ($TUJ\text{-}1^+$) cells in each sample ($P = 0.2308$. More than 100 TUJ-1-

1093 positive cells were analyzed in each sample. $n = 3$). Data are presented as mean ± s.e.m. *$P <$

1094 0.05; ***$P < 0.001$; NS, not significant; unpaired two-tailed Student's *t*-test **(b,c,e)**.

Fig. 5

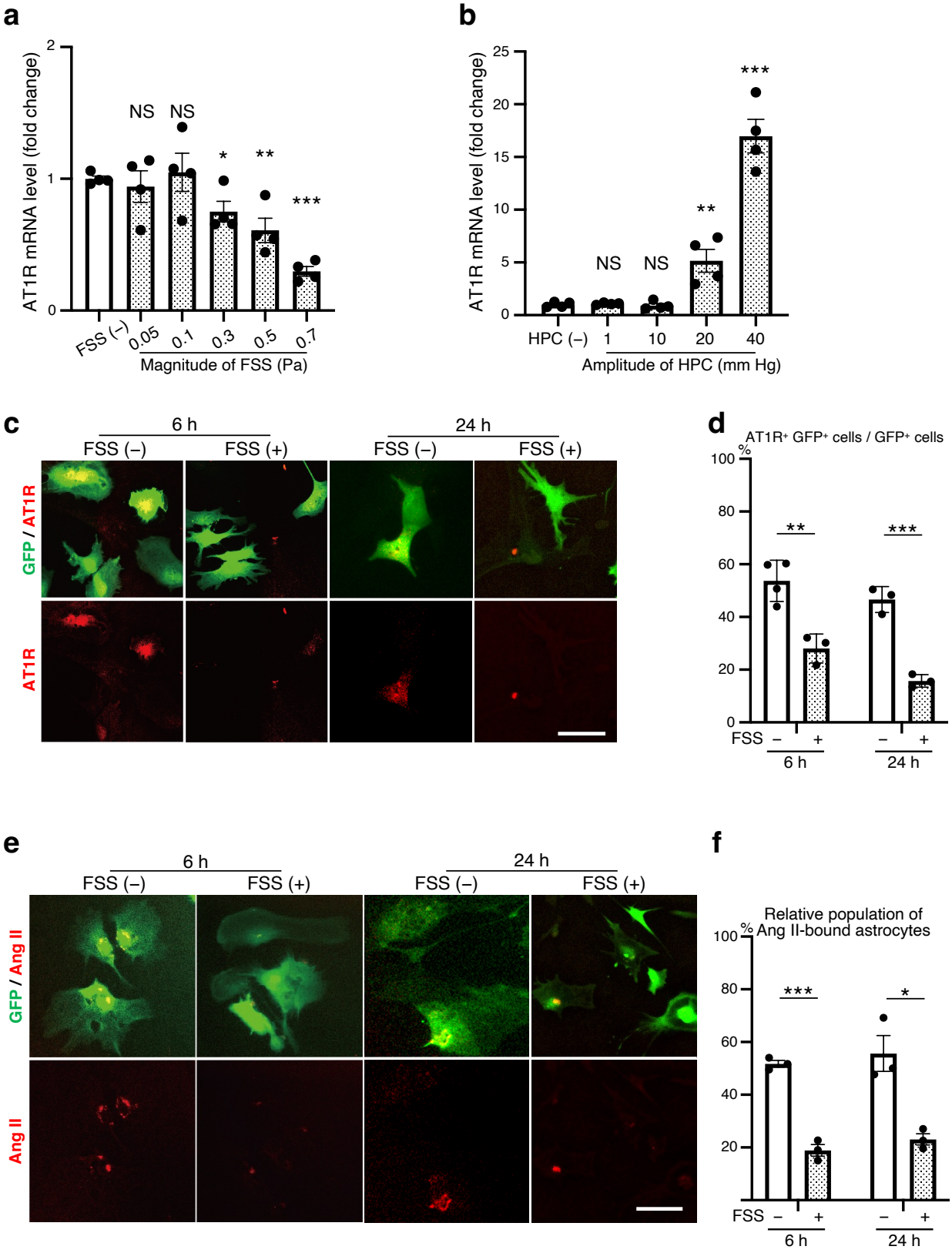


**Fig. 5 | FSS on cultured astrocytes decreases their AT1R expression and Ang II-binding potential in vitro. a–d,** AT1R expression in cultured astrocytes with or without exposure to FSS

1098 or HPC. Astrocytes prepared from the astrocyte-GFP mice, either left unexposed or exposed to
1099 pulsatile FSS (average 0.05−0.7 Pa, 0.5 Hz, 30 min) **(a)** or cyclical HPC (1−40 mm Hg, 0.5 Hz,
1100 30 min) **(b)** were solubilized 24 h after the termination of intervention, and subjected to qPCR
1101 analysis. AT1R mRNA expression levels were normalized against GAPDH expression and
1102 scaled as the mean value from control samples (cells left unexposed to FSS or HPC) set as 1 (**a**:
1103 $P = 0.6453$ for 0.05 Pa, $P = 0.7517$ for 0.1 Pa, $P = 0.0226$ for 0.3 Pa, $P = 0.0064$ for 0.5 Pa, $P <$
1104 0.0001 for 0.7 Pa. $n = 4$. **b**: $P = 0.5592$ for 1 mm Hg, $P = 0.7113$ for 10 mm Hg, $P = 0.0088$ for
1105 20 mm Hg, $P < 0.0001$ for 40 mm Hg. $n = 4$). **(c)** Microscopic images of anti-AT1R (red) and
1106 anti-GFP (green) immunostaining of cultured astrocytes, either left unexposed or exposed to
1107 pulsatile FSS (0.7 Pa, 0.5 Hz, 30 min) and fixed 6 or 24 h after the intervention. Images are
1108 representative of three or four independent experiments with similar results. Scale bar, 50 μm.
1109 **(d)** Relative population of AT1R/GFP/ double positive ($AT1R^+$ $GFP^+$) cells were quantified as a
1110 ratio to total GFP-positive ($GFP^+$) cells in each sample [$P = 0.0049$ for 6 h, $P = 0.0006$ for 24 h.
1111 More than 100 GFP-positive cells were analyzed in each sample. $n = 4$ for 6 h FSS (−); $n = 3$ for
1112 the other groups]. **e,f,** Effect of FSS on astrocytes' Ang II-binding potential. Cultured astrocytes
1113 were either left unexposed or exposed to FSS as in **(a,c−d)**. Six or twenty-four hours after the
1114 cessation of 30-min FSS application (0.7 Pa, 0.5 Hz), cells were subjected to fluorescent Ang II
1115 binding assay. **(e)** Microscopic images representative of three independent experiments with
1116 similar results. Scale bar, 50 μm. **(f)** GFP-positive cells with punctate red fluorescence

1117 (TAMRA-Ang II-bound astrocytes) were quantified as a ratio (%) to total GFP-positive cells in

1118 each sample ($P = 0.0002$ for 6 h, $P = 0.0104$ for 24 h. One-hundred GFP-positive cells were

1119 analyzed in each sample. $n = 3$ for each group). Data are presented as mean ± s.e.m. *$P < 0.05$,

1120 **$P < 0.01$, ***$P < 0.001$; NS, not significant; unpaired two-tailed Student's *t*-test.

1121

**Extended Data Fig. 9**

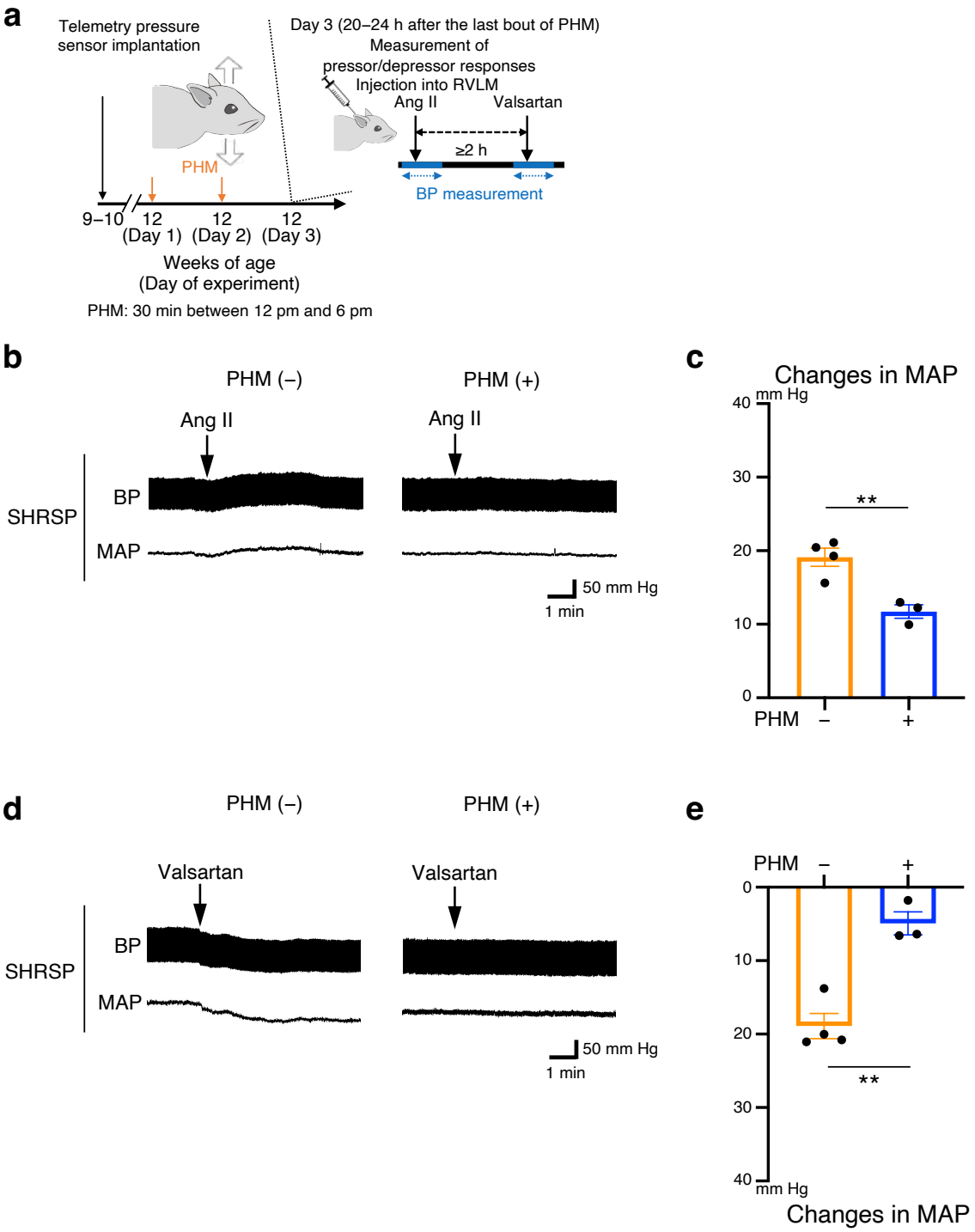


**Extended Data Fig. 9 | Two-day PHM alleviates the sensitivity of RVLM in SHRSPs to Ang II or valsartan. a,** Schematic representation of the experimental protocol. Pressor and depressor responses were analyzed as in Fig. 2. **b–e,** Pressor **(b,c)** and depressor **(d,e)** responses in

1126 SHRSPs with and without 2-day PHM. **(b,d)** Representative trajectories of the BP (top in each

1127 panel) and MAP (bottom in each panel). Arrows point to the time of the initiation of RVLM

1128 injection of Ang II **(b)** or valsartan **(d)**. Right-angled scale bars, 1 min / 50 mm Hg. **(c,e)** MAP

1129 change caused by Ang II **(c)** or valsartan **(e)** injection [**c**: $P = 0.0064$. **e**: $P = 0.0022$. $n = 4$ rats

1130 for PHM (–); $n = 3$ rats for PHM (+)]. Data are presented as mean ± s.e.m. $^{**}P < 0.01$; unpaired

1131 two-tailed Student's *t*-test.

**Extended Data Fig. 10**

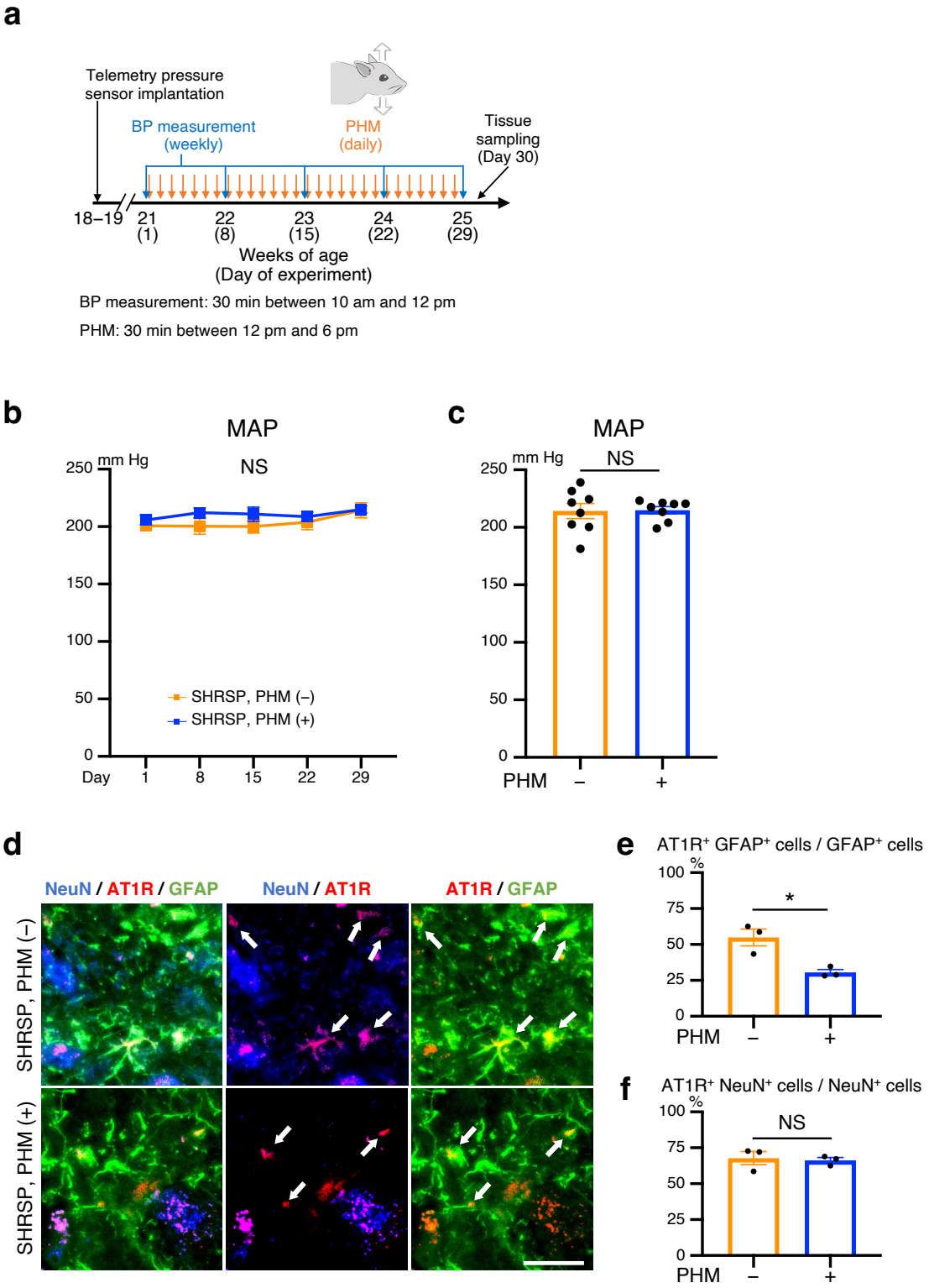


**Extended Data Fig. 10 | PHM does not lower the BP in SHRSPs, but decreases the AT1R expression in their RVLM astrocytes during the plateau phase of hypertension**

1135 **development. a,** Schematic representation of the experimental protocol to analyze the effects of

1136 PHM. **b,c,** Time courses **(b)** and values on Day 29 **(c)** of the MAP of SHRSPs, subjected to

1137 either daily PHM or anesthesia only (**b**: $P > 0.9999$ for Day 15, Day 22, and Day 29. **c**: $P =$

1138 $0.9167$. $n = 8$ rats for each group). **d,** Micrographic images of anti-GFAP (green), anti-AT1R

1139 (red), and anti-NeuN (blue) immunostaining of the RVLM of SHRSPs, either left sedentary

1140 (top) or subjected to PHM (bottom) under anesthesia (30 min/day, 28 days). Arrows point to

1141 anti-AT1R immunosignals that overlap with anti-GFAP, but not anti-NeuN, immunosignals in

1142 merged images. Scale bars, 50 μm. Images are representative of three rats. **e,f,** Quantification of

1143 AT1R-positive astrocytes **(e)** and neurons **(f)** in the RVLM of SHRSPs, either left sedentary or

1144 subjected to PHM. One-hundred GFAP-positive ($GFAP^+$) cells **(e)** and 50 NeuN-positive

1145 ($NeuN^+$) cells **(f)** were analyzed for each rat (**e**: $P = 0.0173$. **f**: $P = 0.7812$. $n = 3$ rats for each

1146 group). Data are presented as mean ± s.e.m. *$P < 0.05$; NS, not significant; two-way repeated

1147 measures ANOVA with Bonferroni's post hoc multiple comparisons test **(b)** or unpaired two-

1148 tailed Student's *t*-test **(c,e,f)**.

Fig. 6

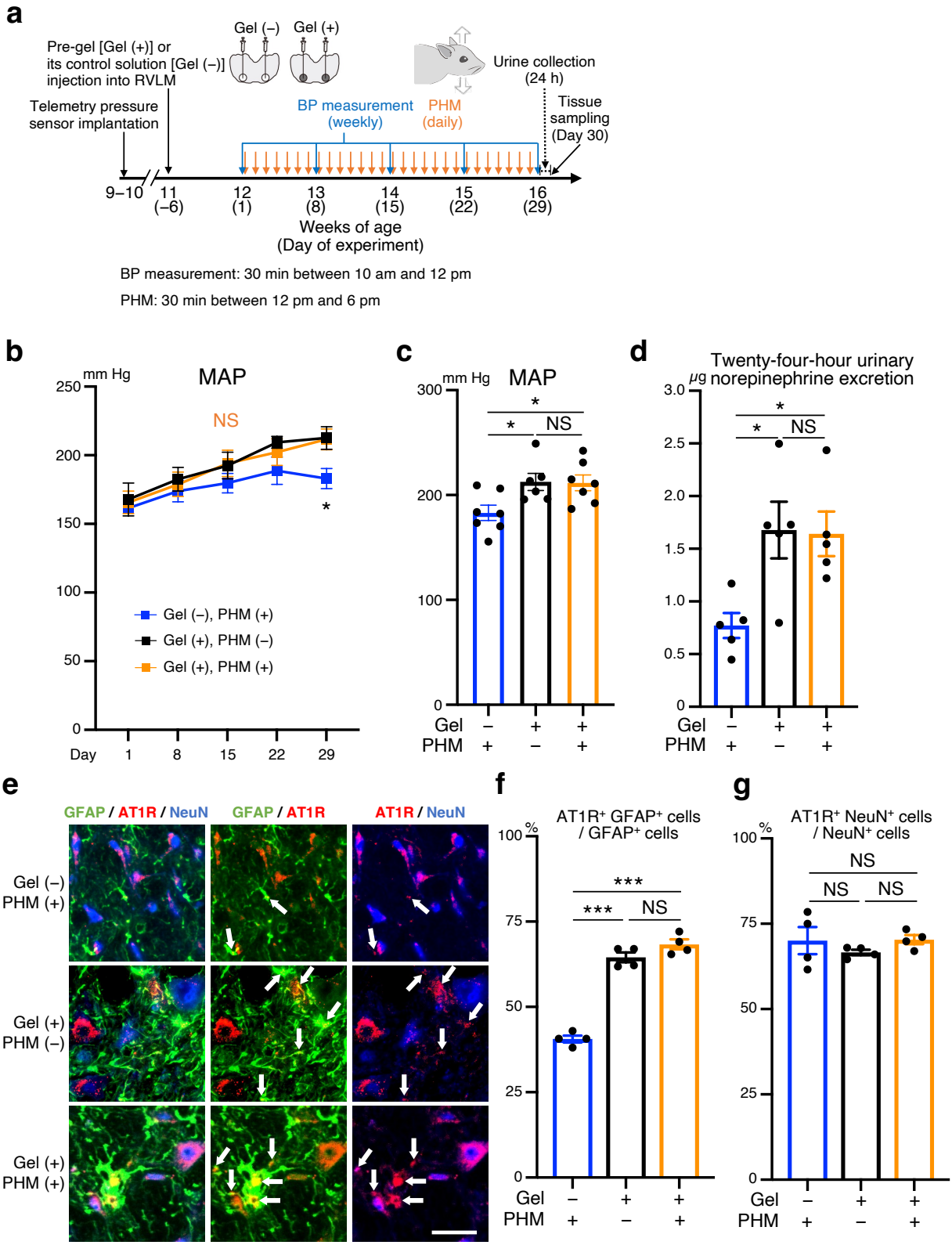


**Fig. 6 | Hydrogel introduction eliminates the decreasing effects of PHM on BP and AT1R expression in the RVLM astrocytes in SHRSPs. a,** Schematic representation of the

1152 experimental protocol to analyze the effects of PHM with and without PEG hydrogel

1153 introduction in the bilateral RVLMs of SHRSPs. PHM was applied daily for consecutive 28

1154 days. **b−d,** Time courses **(b)** and values on Day 29 **(c)** of MAP, and 24-h urinary norepinephrine

1155 excretion **(d)** of SHRSPs, subjected to various combinations of daily PHM application and

1156 hydrogel introduction in the bilateral RVLMs. Note the absence of significant difference in the

1157 BP **(b,c)** and urinary norepinephrine excretion **(d)** of SHRSPs with hydrogel introduced RVLMs

1158 [Gel (+)] between with and without PHM [**b**, blue vs. orange: $P = 0.4314$ for Day 15, $P =$

1159 $0.4685$ for Day 22, $P = 0.0389$ for Day 29; blue vs. black: $P = 0.5372$ for Day 15, $P = 0.2000$

1160 for Day 22, $P = 0.0406$ for Day 29; black vs. orange: $P = 0.9911$ for Day 15, $P = 0.8222$ for Day

1161 22, $P = 0.9965$ for Day 29. **c**: $P = 0.0387$ for column 1 vs. 2, $P = 0.0372$ for column 1 vs. 3, $P =$

1162 $0.9959$ for column 2 vs. 3. $n = 7$ rats for Gel (−), PHM (+) and Gel (+), PHM (+); $n = 6$ rats for

1163 Gel (+), PHM (−); **d**: $P = 0.0247$ for column 1 vs. 2, $P = 0.0307$ for column 1 vs. 3, $P = 0.9920$

1164 for column 2 vs. 3. $n = 5$ rats for each group]. **e**, Micrographic images of anti-GFAP (green),

1165 anti-AT1R (red), and anti-NeuN (blue) immunostaining of the RVLM in SHRSPs subjected to

1166 various combinations of hydrogel introduction in the bilateral RVLMs and 4-week PHM

1167 application. Arrows point to anti-AT1R immunosignals that overlap with anti-GFAP, but not

1168 anti-NeuN, immunosignals in merged images. Scale bar, 50 μm. Images are representative of

1169 four rats. **f,g,** Quantification of AT1R-positive astrocytes **(f)** and neurons **(g)** in the RVLM. Note

1170 the absence of significant difference in the ratio of AT1R-positive astrocytes of SHRSPs with

1171 hydrogel introduced RVLMs [Gel (+)] between with and without PHM (**f**, columns 2 and 3).

1172 Fifty $NeuN^+$ cells and 100 $GFAP^+$ cells were analyzed for each rat (**f**: $P < 0.0001$ for column 1

1173 vs. 2 and column 1 vs. 3, $P = 0.1597$ for column 2 vs. 3. **g**: $P = 0.6029$ for column 1 vs. 2, $P =$

1174 $0.9963$ for column 1 vs. 3, $P = 0.5552$ for column 2 vs. 3. $n = 4$ rats for each group). Data are

1175 presented as mean ± s.e.m. *$P < 0.05$; ***$P < 0.001$; NS, not significant; two-way repeated

1176 measures ANOVA **(b)** or one-way ANOVA **(c,d,f,g)** with Tukey's post hoc multiple comparisons

1177 test.

**Extended Data Fig. 11**

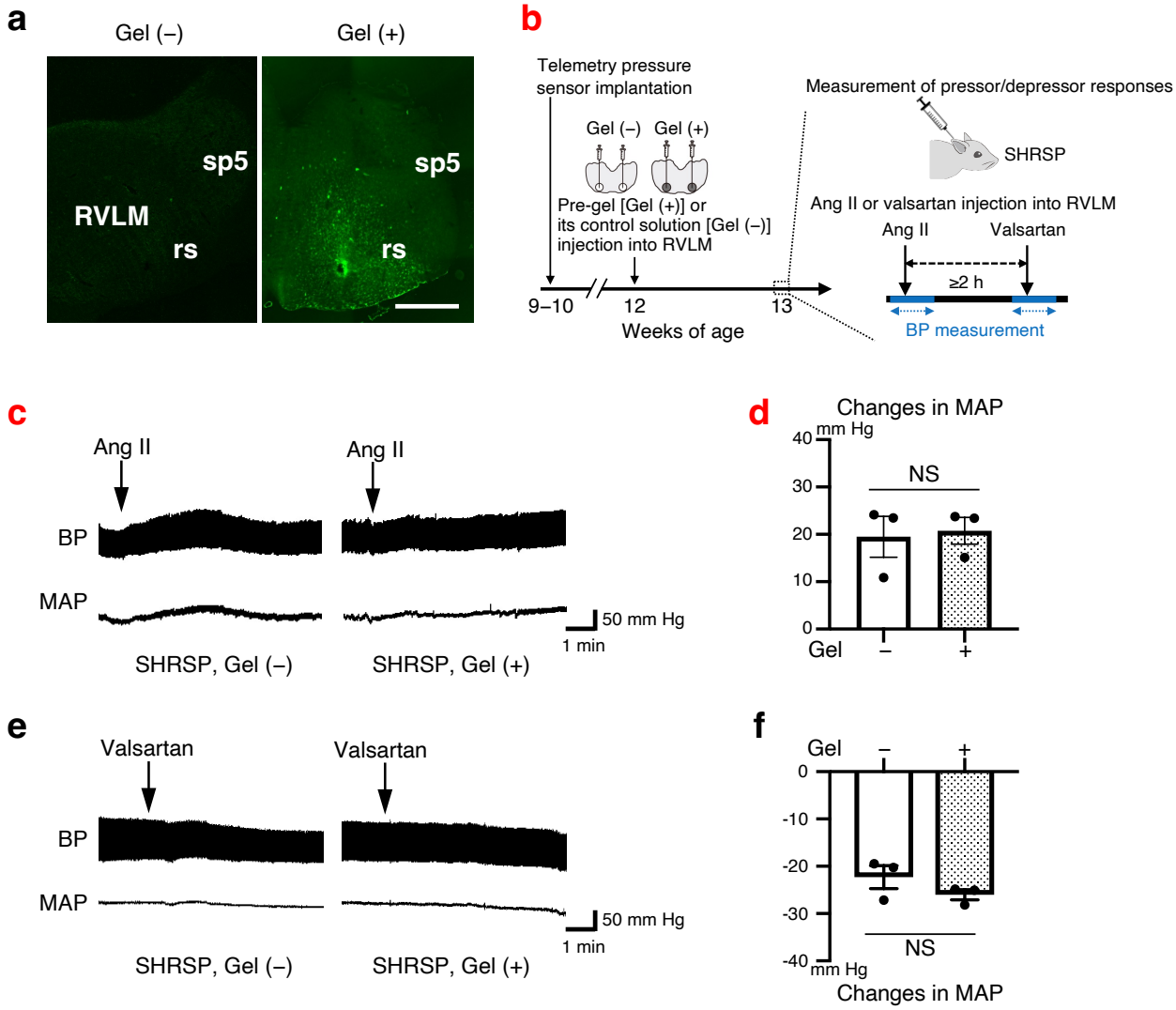


**Extended Data Fig. 11 | Hydrogel introduction in the RVLM does not affect the pressor and depressor responses to AngII and valsartan, respectively, in SHRSPs. a,** Introduction of the PEG hydrogel in the rat RVLM. Twenty-four hours after the injection of control ungelatable fluorescent PEG solution (left) or one week after the injection of pre-gel fluorescent PEG solution (right), brainstem samples were prepared. Coronal-section images representative of three rats with similar results are shown. Scale bar, 1 mm. **b–f,** Pressor and depressor responses analyzed one week after the injection of pre-gel PEG solution or its ungelatable control. **(b)**

1186 Schematic representation of the experimental protocol. Pressor and depressor responses were

1187 analyzed as in Fig. 2. **(c–f)** Representative trajectories **(c,e)** and quantification **(d,f)** of the BP

1188 ascent upon AngII injection **(c,d)** and descent upon valsartan injection **(e,f)** to the RVLM of

1189 SHRSPs with or without the hydrogel introduction (**d**: $P = 0.8226$. **f**: $P = 0.2342$. $n = 3$ rats for

1190 each group). Right-angled scale bars, 1 min / 50 mm Hg. Data are presented as mean ± s.e.m.

1191 NS, not significant; unpaired two-tailed Student's *t*-test.

Extended Data Fig. 12

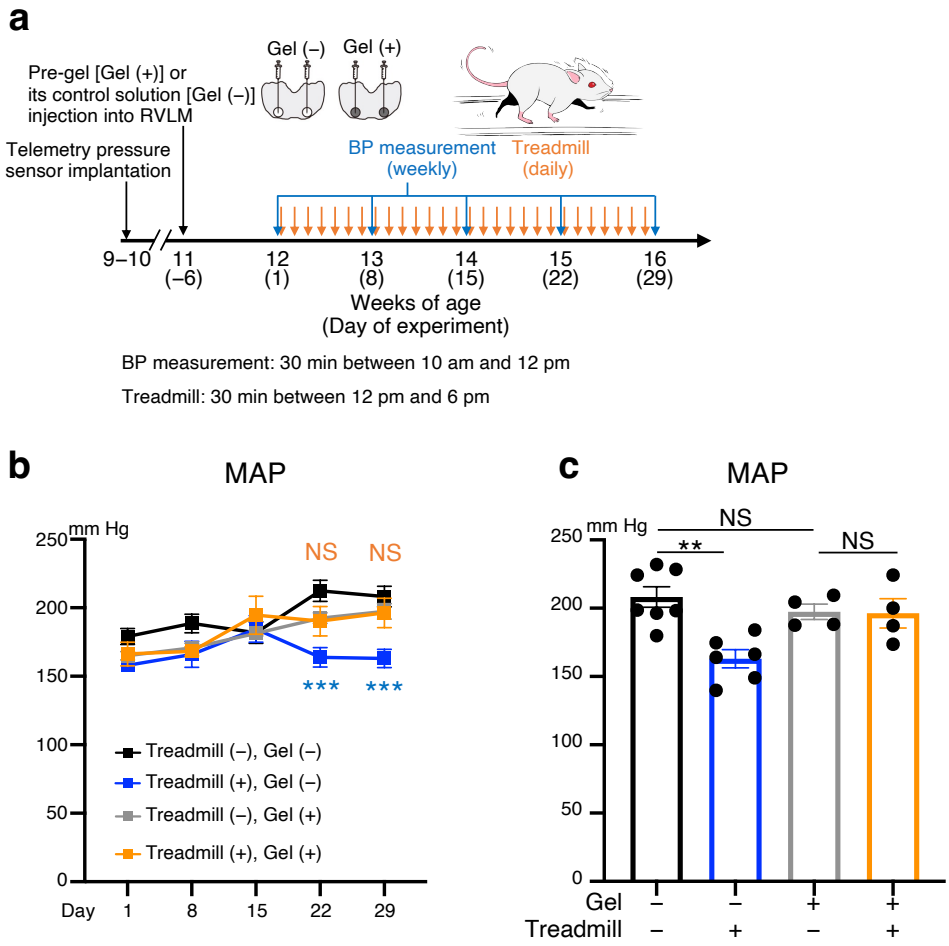


**Extended Data Fig. 12 | Hydrogel introduction to the RVLM eliminates the antihypertensive effect of treadmill running in SHRSPs. a,** Schematic representation of the experimental protocol to analyze the effects of treadmill running on the BP in SHRSPs. **b,c,** Time courses **(b)** and values on Day 29 **(c)** of the MAP of SHRSPs with (**b**: gray and orange lines, **c**: columns 3 and 4) and without (**b**: black and blue lines, **c**: columns 1 and 2) the hydrogel introduction, subjected to either daily treadmill running (30 min/day, 28 days; **b**: blue and orange lines, **c**: columns 2 and 4) or its control (placing on the belt without turning on the treadmilling; **b**: black and gray lines, **c**: columns 1 and 3) [**b**, black vs. blue: $P > 0.9999$ for Day 15, $P = 0.0001$ for Day 22, $P = 0.0004$ for Day 29; gray vs. orange: $P > 0.9999$ for Day 15, Day

1202 22, and Day 29. **c**: $P = 0.0015$ for column 1 vs. 2, $P = 0.9997$ for column 3 vs. 4, $P = 0.7751$ for

1203 column 1 vs. 3. $n = 7$ rats for treadmill (–)/Gel (–); $n = 6$ rats for treadmill (+)/Gel (–); $n = 4$ rats

1204 for each group of Gel (+)]. Data are presented as mean ± s.e.m. $^{**}P < 0.01$, $^{***}P < 0.001$; NS,

1205 not significant; two-way repeated measures ANOVA with Bonferroni's post hoc comparisons

1206 test **(b)** or one-way ANOVA with Tukey's post hoc multiple comparisons test **(c)**.

**Extended Data Fig. 13**

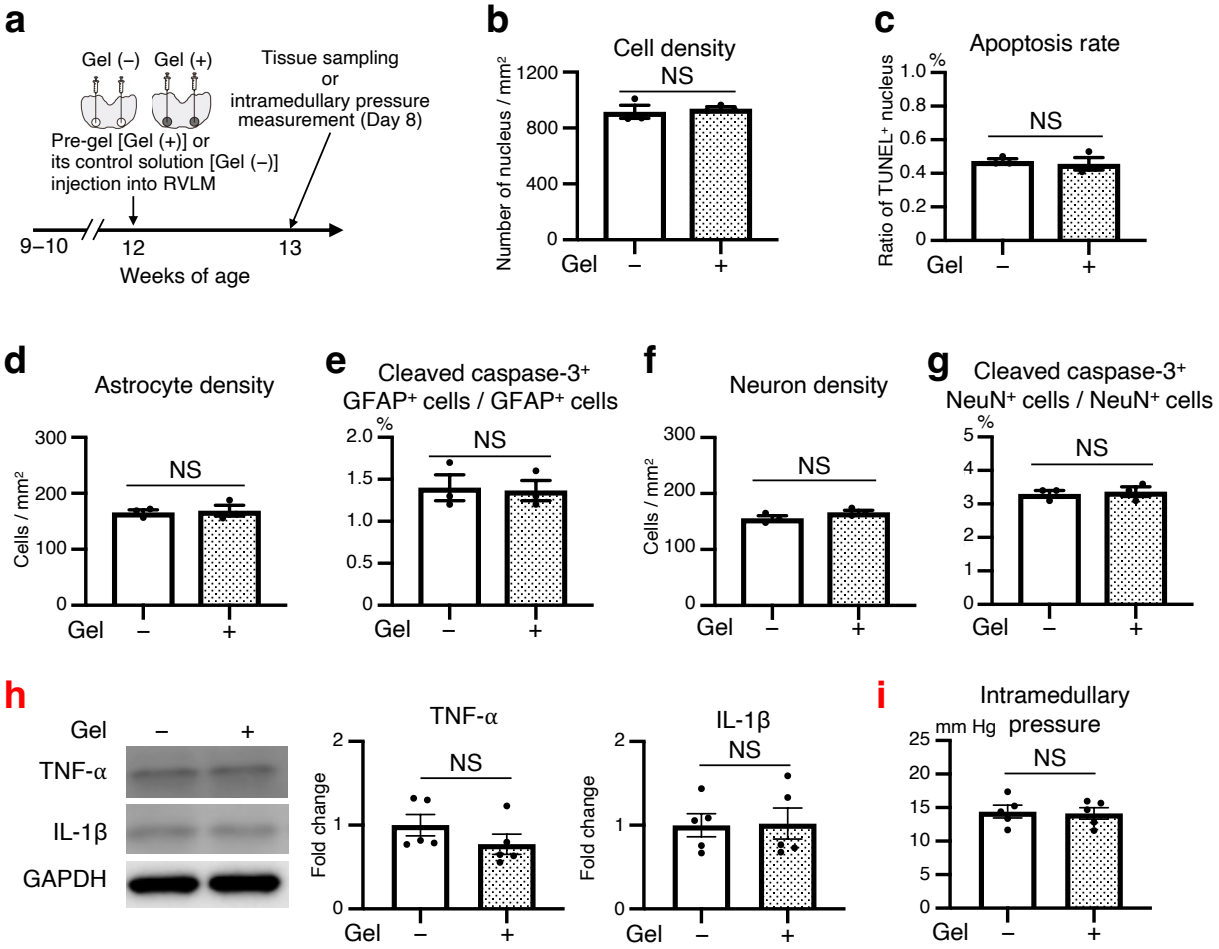


**Extended Data Fig. 13 | Hydrogel introduction does not affect the cell number/apoptosis, the expression of pro-inflammatory cytokines, and the pressure in the RVLM of SHRSPs.** **a,** Schematic representation of the experimental protocol to analyze the hydrogel-introduced RVLM in SHRSPs. **b–g,** Effects of hydrogel introduction on the survival/apoptosis of RVLM cells in SHRSPs. Fixed rat RVLM sections were subjected to TUNEL assay **(b,c)**, or combinations of anti-GFAP, anti-NeuN and anti-cleaved caspase-3 immunostaining **(e–g)**. DAPI-positive nuclei **(b)**, GFAP- **(d)** or NeuN- **(f)** positive cells were counted, and the relative populations of cells doubly positive for indicated combinations of TUNEL **(c)** and cleaved caspase-3 **(e,g)** were quantified. Each value in **(b–g)** represents an average from five images of

1217 1 x 1-mm area analyzed for each rat. **h,** Expression of TNF-α and IL-1β in SHRSPs' RVLM

1218 with and without the hydrogel introduction. Anti-TNF-α, anti-IL-1β, and anti-GAPDH

1219 immunoblots (left). Expressions of TNF-α and IL-1β were normalized against GAPDH

1220 expression, and scaled with the mean values of the control samples [Gel (−)] set as 1. **i,**

1221 Intramedullary pressure of SHRSPs with and without the hydrogel introduction in their RVLM.

1222 The intramedullary pressure was measured as in Fig. 4a−d, and the mean value was obtained

1223 from 30-s steady-state continuous measurement for each rat (**b**: $P = 0.6518$. **c**: $P = 0.6943$. **d**: $P$

1224 $= 0.7938$. **e**: $P = 0.8722$. **f**: $P = 0.1679$. **g**: $P = 0.7247$. **h**: $P = 0.2312$ for TNF-α, $P = 0.9342$ for

1225 IL-1β. **i**: $P = 0.8433$. **b-g**: $n = 3$ rats for each group. **h,i**: $n = 5$ rats for each group). Data are

1226 presented as mean ± s.e.m. NS, not significant; unpaired two-tailed Student's *t*-test **(b-i)**.

Extended Data Fig. 14

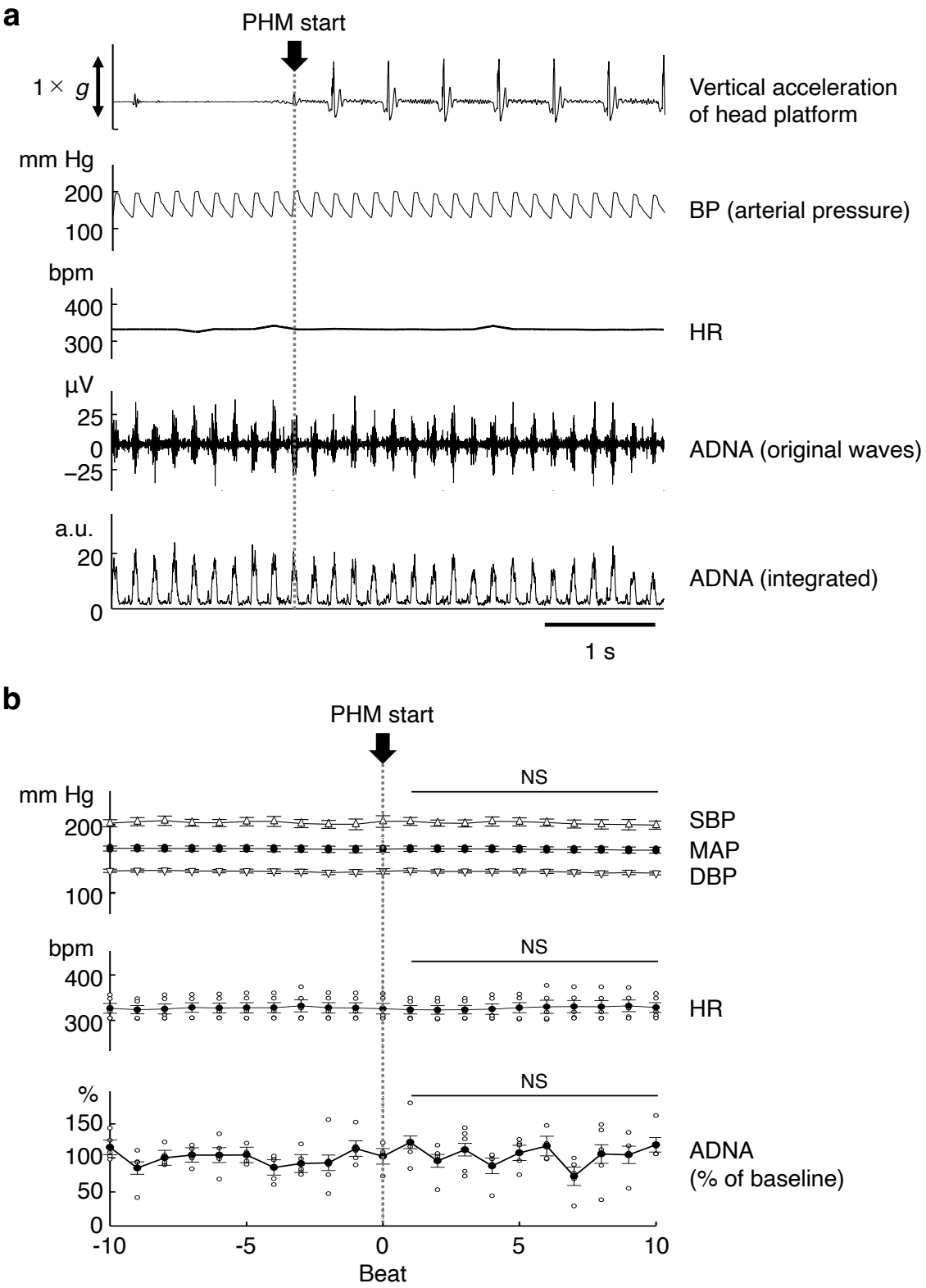


**Extended Data Fig. 14 | BP, HR, and aortic depressor nerve activity (ADNA) remain unchanged during the transition from before to after the initiation of PHM in SHRSPs. a,**

1230 BP, HR, and ADNA in a 16-week-old male SHRSP monitored and recorded simultaneously with
1231 vertical accelerations of the oscillating PHM platform. Integrated ADNA was normalized in
1232 each rat and is presented in arbitrary units (a.u.) (see Methods). Data shown represent five
1233 independent experiments using five different SHRSPs with similar results. **b,** Beat-by-beat BP
1234 (SBP, MAP, and DBP), HR, and ADNA. The beat that elicited SBP immediately before the
1235 PHM initiation was defined as "beat 0". Statistical analysis was conducted against the mean
1236 values of beat –9 to beat 0 (SBP; $P = 0.5829$ for beat 1, $P = 0.9994$ for beat 2, $P = 0.9627$ for
1237 beat 3, $P = 0.4169$ for beat 4, $P = 0.6948$ for beat 5, $P = 0.9999$ for beat 6, $P = 0.8152$ for beat 7,
1238 $P = 0.1381$ for beat 8, $P = 0.3191$ for beat 9, and $P = 0.5286$ for beat 10. MAP; $P = 0.9906$ for
1239 beat 1, $P > 0.9999$ for beat 2, $P = 0.9997$ for beat 3, $P = 0.9997$ for beat 4, $P = 0.9349$ for beat 5,
1240 $P = 0.3562$ for beat 6, $P = 0.2239$ for beat 7, $P = 0.1599$ for beat 8, $P = 0.3001$ for beat 9, and $P$
1241 $= 0.2596$ for beat 10. DBP; $P = 0.9810$ for beat 1, $P > 0.9999$ for beat 2, $P > 0.9999$ for beat 3,
1242 $P > 0.9999$ for beat 4, $P = 0.9996$ for beat 5, $P = 0.9997$ for beat 6, $P = 0.9421$ for beat 7, $P =$
1243 $0.5327$ for beat 8, $P = 0.4949$ for beat 9, and $P = 0.5215$ for beat 10. HR; $P = 0.8547$ for beat 1,
1244 $P = 0.7825$ for beat 2, $P =0.8267$ for beat 3, $P = 0.6800$ for beat 4, $P = 0.9996$ for beat 5, $P =$
1245 $0.9834$ for beat 6, $P = 0.8658$ for beat 7, $P = 0.9460$ for beat 8, $P = 0.4602$ for beat 9, and $P$
1246 $=0.8992$ for beat 10. ADNA; $P = 0.6663$ for beat 1, $P = 0.9996$ for beat 2, $P = 0.9258$ for beat 3,
1247 $P = 0.8960$ for beat 4, $P = 0.9211$ for beat 5, $P = 0.4492$ for beat 6, $P = 0.3520$ for beat 7, $P$
1248 $=0.9995$ for beat 8, $P =0.9979$ for beat 9, and $P = 0.5181$ for beat 10. $n = 5$ rats). Data are

1249 presented as mean ± s.e.m. NS, not significant; one-way repeated measures ANOVA with

1250 Dunnett's multiple comparisons test. Arrows and dotted lines in (**a,b**) indicate the time point of

1251 PHM initiation.

**Extended Data Fig. 15**

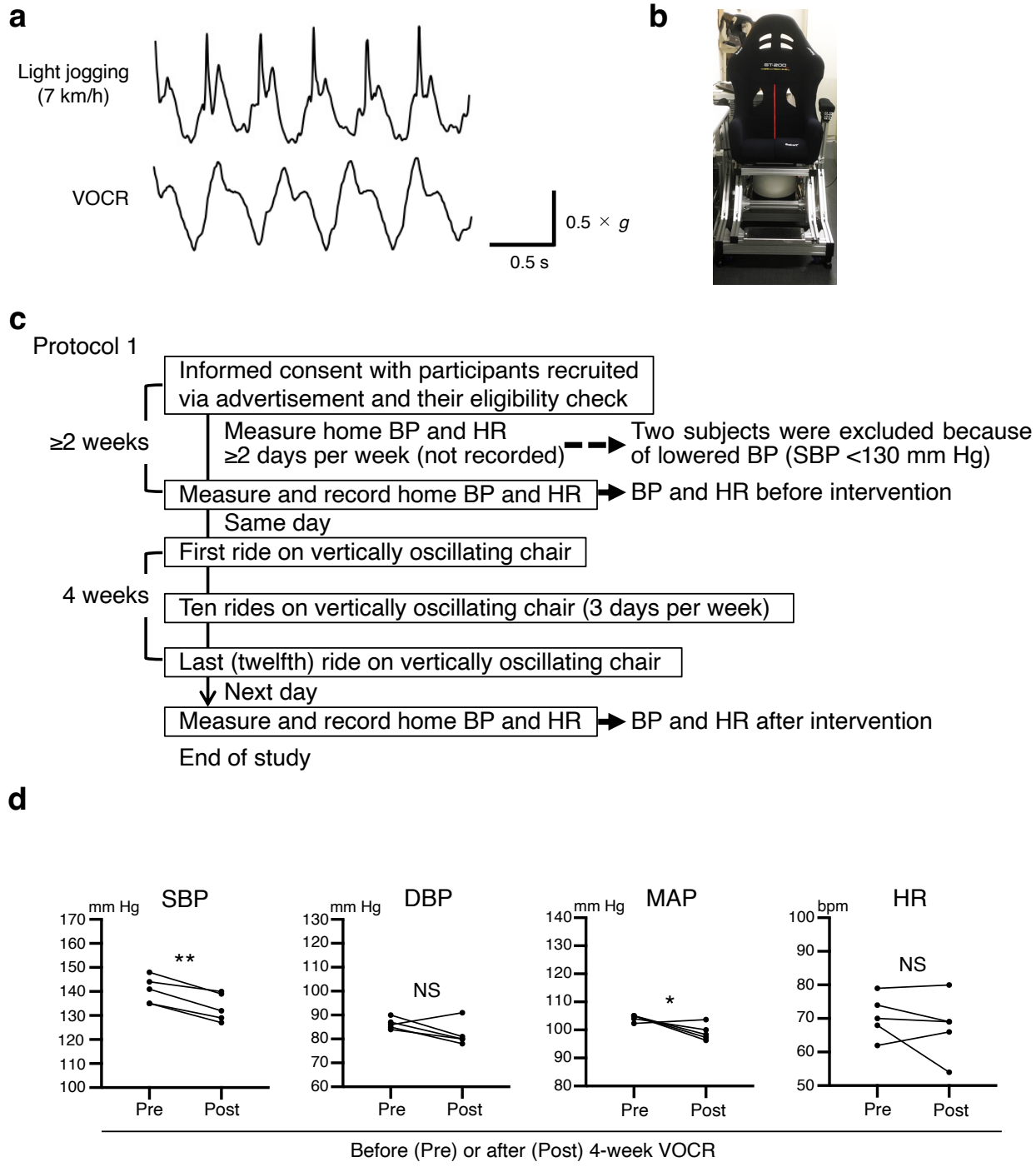


**Extended Data Fig. 15 | Vertically oscillating chair that reproduces the mechanical accelerations in the head during light jogging, and the design and results of protocol 1 as a pilot study to examine antihypertensive effect of VOCR in hypertensive adult humans. a,** Vertical accelerations generated at adult human head during light jogging on a treadmill machine

1257 (velocity: 7 km/h) and VOCR (frequency: 2 Hz). The VOCR system was adjusted to produce

1258 ~1.0 × *g* vertical acceleration peaks. Right-angled scale bar, 0.5 s / 0.5 × *g*. Images are

1259 representative of three independent experiments with similar results. **b**, Photograph of the chair.

1260 **c,** Schematic representation of protocol 1. **d,** BP and HR "value of the day"s immediately before

1261 and after 4-week VOCR in the study of protocol 1 (SBP: $P = 0.0018$. DBP: $P = 0.1509$. MAP: $P$

1262 $= 0.0459$. HR: $P = 0.3900$. $n = 5$). *$P < 0.05$; **$P < 0.01$; NS, not significant; paired two-tailed

1263 Student's *t*-test.

1264

**Extended Data Fig. 16**

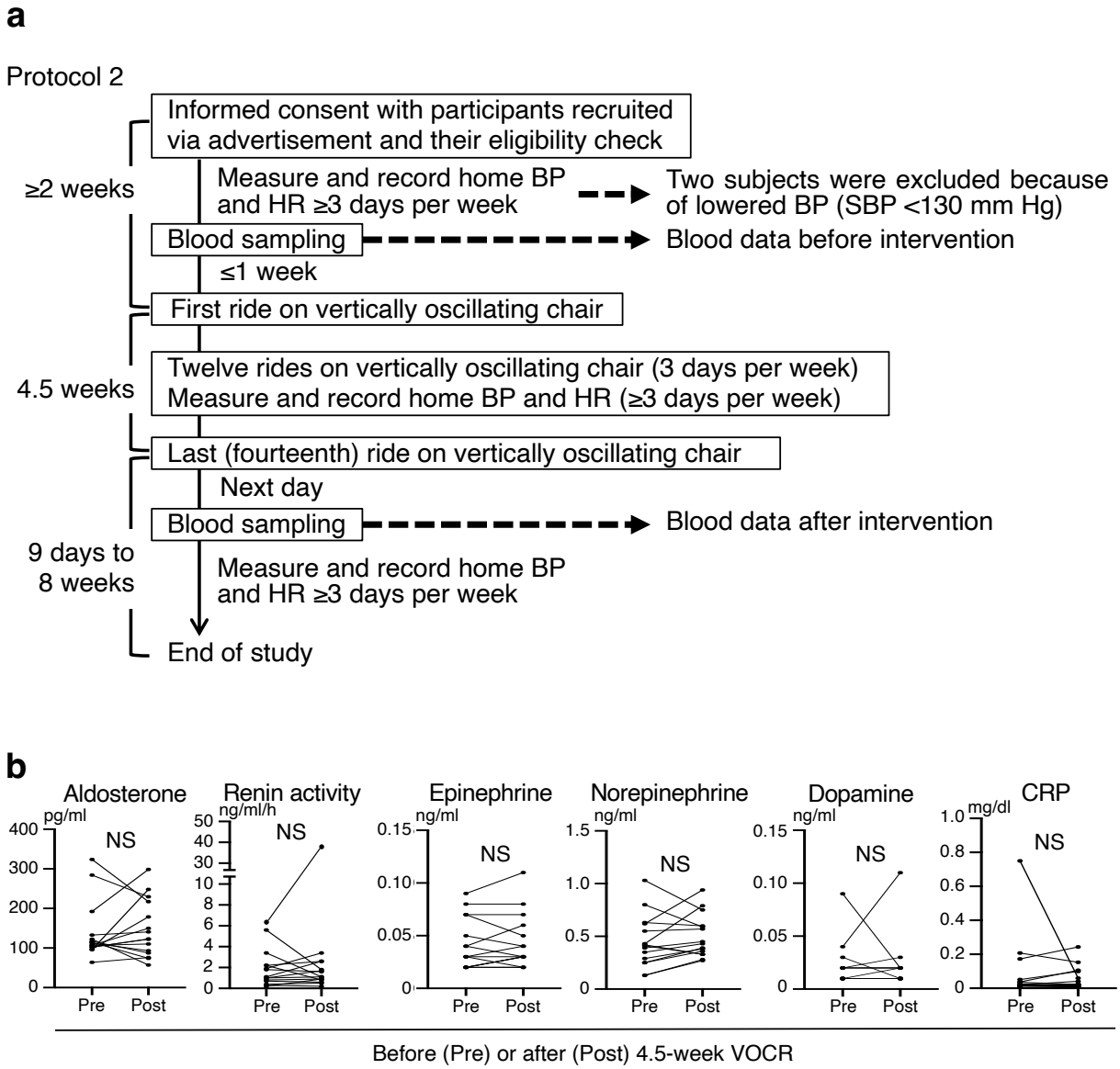


**Extended Data Fig. 16 | Design and blood test results of the human study of protocol 2. a,** Schematic representation of protocol 2. **b,** Blood test values before and after the intervention period. Significant change was not observed in any of tested parameters. NS, not significant; paired two-tailed Student's *t*-test. (Aldosterone: $P = 0.6265$. Renin activity: $P = 0.3794$. Epinephrine: $P = 0.5103$. Norepinephrine: $P = 0.2653$. Dopamine: $P > 0.9999$. CRP: $P = 0.4412$. $n = 15$. A participant (subject #18) showed a large increase in plasma renin activity after

1272 VOCR. We advised him to consult his primary care physician, who ruled out the disqualifying

1273 conditions for this study (e.g., severe renal disease; see Methods) based on comprehensive

1274 evaluation. Therefore, we did not exclude subject #18 from our statistical analysis of BP and

1275 HR.

1276

Fig. 7

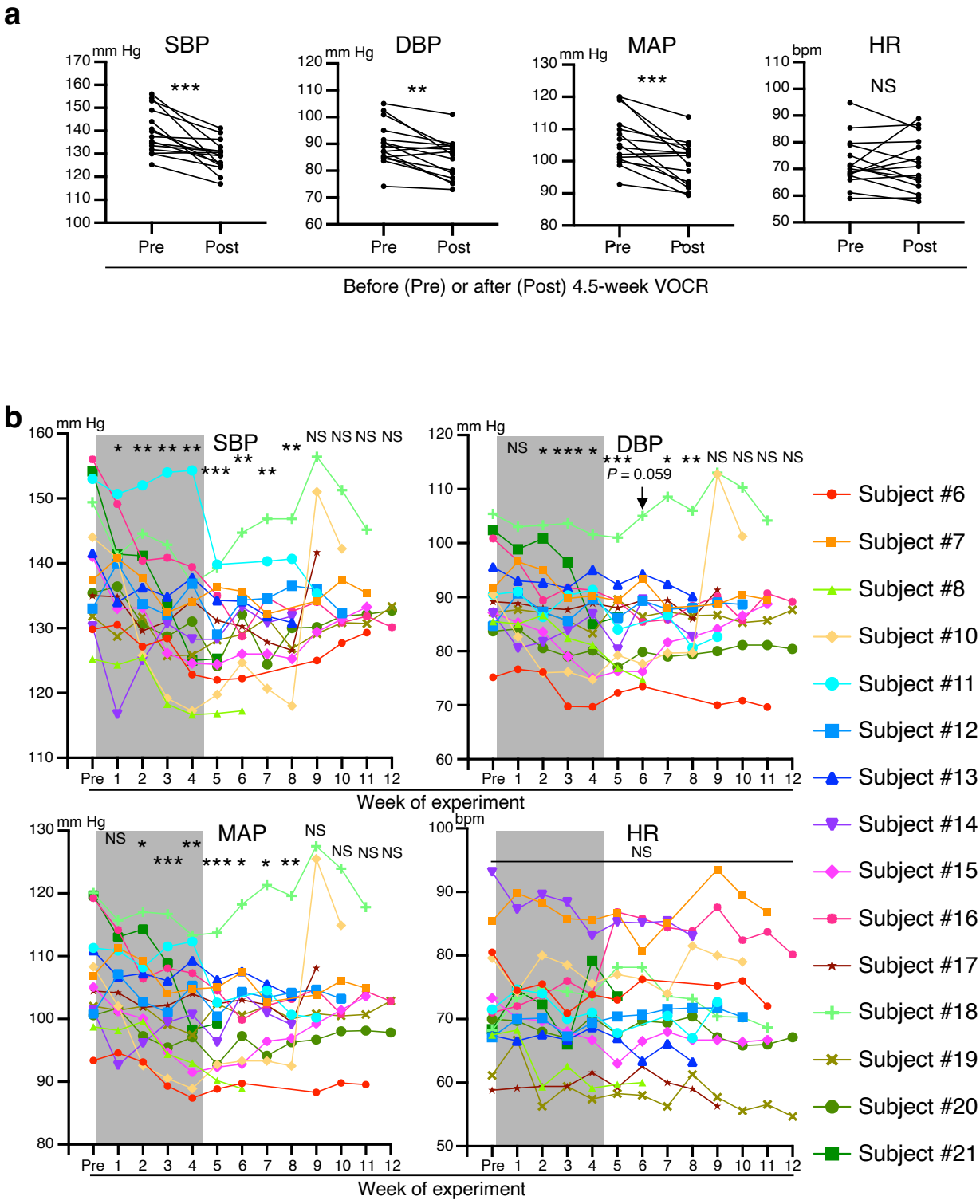


**Fig. 7 | VOCR has an antihypertensive effect on hypertensive adult humans. a,** BP and HR "value of the week"s immediately before and after 4.5-week VOCR in the study of protocol 2 (SBP: $P = 0.0005$. DBP: $P = 0.0011$. MAP: $P = 0.0008$. HR: $P = 0.7845$. $n = 15$). **b,** Subject

1281 number-corresponding trajectories and statistical analysis of BP and HR in the study of protocol
1282 2. Gray-shaded rectangles indicate the VOCR intervention periods (4.5 weeks). The colors and
1283 symbols of individual lines correspond to those of individual subject numbers listed on the right,
1284 excluding subject 9 (see Supplementary Table 2). Each "value of the week" was statistically
1285 compared with that of the week immediately before the initiation of VOCR intervention (SBP: $P$
1286 = 0.0293 for Pre vs. Week 1, $P$ = 0.0028 for Pre vs. Week 2, $P$ = 0.0013 for Pre vs. Week 3, $P$ =
1287 0.0035 for Pre vs. Week 4, $P$ = 0.0002 for Pre vs. Week 5, $P$ = 0.0078 for Pre vs. Week 6, $P$ =
1288 0.0035 for Pre vs. Week 7, $P$ = 0.0075 for Pre vs. Week 8, $P$ = 0.2132 for Pre vs. Week 9, $P$ =
1289 0.1314 for Pre vs. Week 10, $P$ = 0.0973 for Pre vs. Week 11, $P$ = 0.3993 for Pre vs. Week 12.
1290 DBP: $P$ = 0.3022 for Pre vs. Week 1, $P$ = 0.0436 for Pre vs. Week 2, $P$ = 0.0010 for Pre vs.
1291 Week 3, $P$ = 0.0100 for Pre vs. Week 4, $P$ = 0.0006 for Pre vs. Week 5, $P$ = 0.0599 for Pre vs.
1292 Week 6, $P$ = 0.0488 for Pre vs. Week 7, $P$ = 0.0096 for Pre vs. Week 8, $P$ = 0.9346 for Pre vs.
1293 Week 9, $P$ = 0.7850 for Pre vs. Week 10, $P$ = 0.0769 for Pre vs. Week 11, and $P$ = 0.3137 for Pre
1294 vs. Week 12. MAP: $P$ = 0.1075 for Pre vs. Week 1, $P$ = 0.0132 for Pre vs. Week 2, $P$ = 0.0008
1295 for Pre vs. Week 3, $P$ = 0.0063 for Pre vs. Week 4, $P$ = 0.0003 for Pre vs. Week 5, $P$ = 0.0251
1296 for Pre vs. Week 6, $P$ = 0.0136 for Pre vs. Week 7, $P$ = 0.0071 for Pre vs. Week 8, $P$ = 0.6795
1297 for Pre vs. Week 9, $P$ = 0.4295 for Pre vs. Week 10, $P$ = 0.0704 for Pre vs. Week 11, $P$ = 0.3662
1298 for Pre vs. Week 12. HR: $P$ = 0.6287 for Pre vs. Week 1, $P$ = 0.7840 for Pre vs. Week 2, $P$ =
1299 0.1573 for Pre vs. Week 3, $P$ = 0.5380 for Pre vs. Week 4, $P$ = 0.7331 for Pre vs. Week 5, $P$ =

0.6995 for Pre vs. Week 6, $P = 0.9110$ for Pre vs. Week 7, $P = 0.9875$ for Pre vs. Week 8, $P = 0.5866$ for Pre vs. Week 9, $P = 0.9566$ for Pre vs. Week 10, $P = 0.6487$ for Pre vs. Week 11, $P = 0.9905$ for Pre vs. Week 12. $n = 15$ for Pre and Weeks 1 to 5; $n = 13$ for Week 6; $n = 12$ for Week 7; $n = 11$ for Weeks 8 and 9; $n = 9$ for Week 10; $n = 7$ for Week 11; $n = 3$ for Week 12). *$P < 0.05$; **$P < 0.01$; ***$P < 0.001$; NS, not significant; paired two-tailed Student's *t*-test.

**Supplementary Table 2**

| Subject # | Sex<br>Age (years)<br>Body weight (kg)<br>Height (cm)<br>BMI | Period since diagnosis or self-recognition as hypertension<br>Declared health problems and diseases other than hypertension | Smoking<br>Alcohol (if yes, how often) | Current medication (dose per day) | Habitual exercise (times per week) | SBP/DBP (mm Hg) and HR (bpm) just before (left) and after (right) VOCR period (month of first - last bout of VOCR) | |
|---|---|---|---|---|---|---|---|
| 1 | Male<br>60<br>73<br>165.2<br>27.2 | 13 years<br>Hyperuricemia | No<br>Almost every day | Azilsartan ・Amlodin (20 mg • 5 mg)<br>Febuxostat (10 mg)<br>Bisoprolol fumarate (5 mg) | Walking<br>90 min<br>(3 or 4 times) | 148/85<br>62<br>February - March | 139/78<br>66 |
| 2 | Female<br>53<br>50<br>159<br>19.8 | 14 years<br>None | No<br>Almost every day | None | Sit-ups 2 x 30 times<br>(every day) | 135/90<br>70<br>March | 127/81<br>69 |
| 3 | Male<br>37<br>113<br>186<br>32.7 | 19 years<br>None | No<br>Occasionally | None | Judo<br>(once) | 135/86<br>68<br>March | 129/91<br>54 |
| 4 | Female<br>60<br>73<br>156<br>30 | 6 years<br>None | No<br>Occasionally | None | None | 141/87<br>79<br>April - May | 132/80<br>80 |
| 5 | Female<br>52<br>50<br>148<br>22.8 | 1 year<br>None | No<br>Occasionally | Azilsartan (20 mg)<br>Amlodin (2.5 mg) | None | 144/84<br>74<br>April - May | 140/80<br>69 |
| 6 | Female<br>57<br>68<br>164<br>25.3 | 10 years<br>None | No<br>Occasionally | None | None | 130/74<br>79<br>November - December | 124/73<br>72 |
| 7 | Male<br>61<br>67<br>168<br>23.7 | Uncertain (<1 year)<br>Diabetes mellitus<br>Hyperlipidemia | No<br>No | Metformin hydrochloride (1000 mg)<br>Rosuvastatin calcium (5 mg)<br>Sitagliptin phosphate hydrate (50 mg) | Walking<br>120 min<br>(once) | 137/92<br>85<br>November - December | 136/89<br>87 |
| 8 | Male<br>46<br>72<br>178<br>22.7 | 3 months<br>Allergic rhinitis | Yes<br>Occasionally | Montelukast sodium (10 mg)<br>Ebastine (10 mg) | Walking<br>60 min<br>(once)<br>Stretching<br>30 min<br>(once) | 125/86<br>68<br>November - December | 117/76<br>60 |
| 9 | Male<br>55<br>87<br>173<br>29.1 | 7 months<br>Diabetes mellitus | No<br>No | None | Karate<br>(2 or 3 times) | 150/85<br>72<br>November - December | 146/87<br>71 |
| 10 | Male<br>70<br>62<br>166<br>22.5 | 6 months<br>None | No<br>Occasionally | None | Walking<br>40 min<br>(4 times) | 144/91<br>80<br>November - December | 120/79<br>80 |
| 11 | Female<br>60<br>45<br>157<br>18.3 | Uncertain (>1year)<br>Breast cancer<br>(post-surgery) | No<br>Almost every day | Tamoxifen citrate (20 mg) | None | 153/91<br>72<br>November - December | 141/84<br>64 |
| 12 | Male<br>68<br>72<br>171<br>24.6 | Uncertain (<1 year)<br>None | No<br>No | None | None | 134/85<br>69<br>January - February | 131/87<br>71 |
| 13 | Female<br>56<br>58<br>160<br>22.7 | 7 years<br>None | No<br>No | Telmisartan • Amlodipine<br>(40 mg • 5 mg) | None | 140/95<br>66<br>January - February | 129/90<br>68 |
| 14 | Male<br>49<br>69<br>168<br>24.5 | Uncertain (<1 year)<br>Diabetes mellitus | No<br>No | Sitagliptin phosphate hydrate (50 mg)<br>Acetazolamide (250 mg) | None | 130/85<br>95<br>January - February | 131/80<br>85 |

1306

**Supplementary Table 2 (continued)**

| Subject # | Sex<br>Age (years)<br>Body weight (kg)<br>Height (cm)<br>BMI | Period since diagnosis or self-recognition as hypertension<br>Declared health problems and diseases other than hypertension | Smoking<br>Alcohol (if yes, how often) | Current medication (dose per day) | Habitual exercise (times per week) | SBP/DBP (mm Hg) and HR (bpm) just before (left) and after (right) VOCR period (month of first - last bout of VOCR) | |
|---|---|---|---|---|---|---|---|
| 15 | Male<br>43<br>69<br>165<br>25.3 | Uncertain (<1 year)<br>None | No<br>Occasionally | None | None | 141/87<br>75<br>August - September | 125/75<br>64 |
| 16 | Female<br>48<br>45.3<br>157.2<br>18.3 | 15 years<br>None | No<br>Occasionally | None | Walking<br>60 min<br>(6 times) | 156/101<br>71<br>October - November | 133/89<br>89 |
| 17 | Male<br>65<br>60.1<br>167.1<br>21.5 | 8 years<br>None | Yes<br>Almost every day | None | None | 135/89<br>59<br>October | 131/88<br>59 |
| 18 | Male<br>55<br>93.4<br>168.1<br>33.1 | 8 years<br>Reflex esophagitis<br>Hyperlipidemia | No<br>Almost every day | Azilsartan (20 mg)<br>Lansoprazole (15 mg)<br>Atorvastatin calcium hydrate (10 mg)<br>Benidipine hydrochloride (4 mg) | None | 149/105<br>68<br>November - December | 139/101<br>78 |
| 19 | Male<br>41<br>92.3<br>183.2<br>27.5 | 2 years<br>None | No<br>Almost every day | None | Walking<br>60 min<br>(3 times) | 132/87<br>61<br>January - February | 129/89<br>58 |
| 20 | Female<br>65<br>48.7<br>158.6<br>19.4 | 1 year<br>Hyperlipidemia<br>Lumbar spinal canal stenosis (post-surgery) | No<br>Almost every day | Amlodipine besilate (5 mg)<br>Atorvastatin calcium hydrate (10 mg)<br>Limaprost alfadex (15 μg)<br>Loxoprofen sodium hydrate (120 mg)<br>Rebamipide (200 mg) | Swimming<br>40 min<br>(5 times) | 135/84<br>70<br>January - February | 126/77<br>67 |
| 21 | Male<br>32<br>65.1<br>168.9<br>22.8 | 2 years<br>None | No<br>Almost every day | None | None | 154/102<br>68<br>January - February | 125/86<br>74 |

**Supplementary Table 2 | Information of subjects who participated in the human studies of protocol 1 and 2.** SBP/DBP (mm Hg) and HR (bpm) just before and after VOCR are "value of the day"s in subjects #1−#5 (protocol 1) and "value of the week"s in subjects #6−#21 (protocol 2). Subject 9 was excluded from our statistical analysis because of the high serum CRP value before VOCR (2.85 mg/dL), which made it difficult to rule out acute infection, a possible disqualifier, at the time of the initiation of VOCR, albeit the lack of specific complaint or local symptom related to acute physical problem(s). His serum CRP after the VOCR period was within the normal range (0.12 mg/dL).

Extended Data Fig. 17

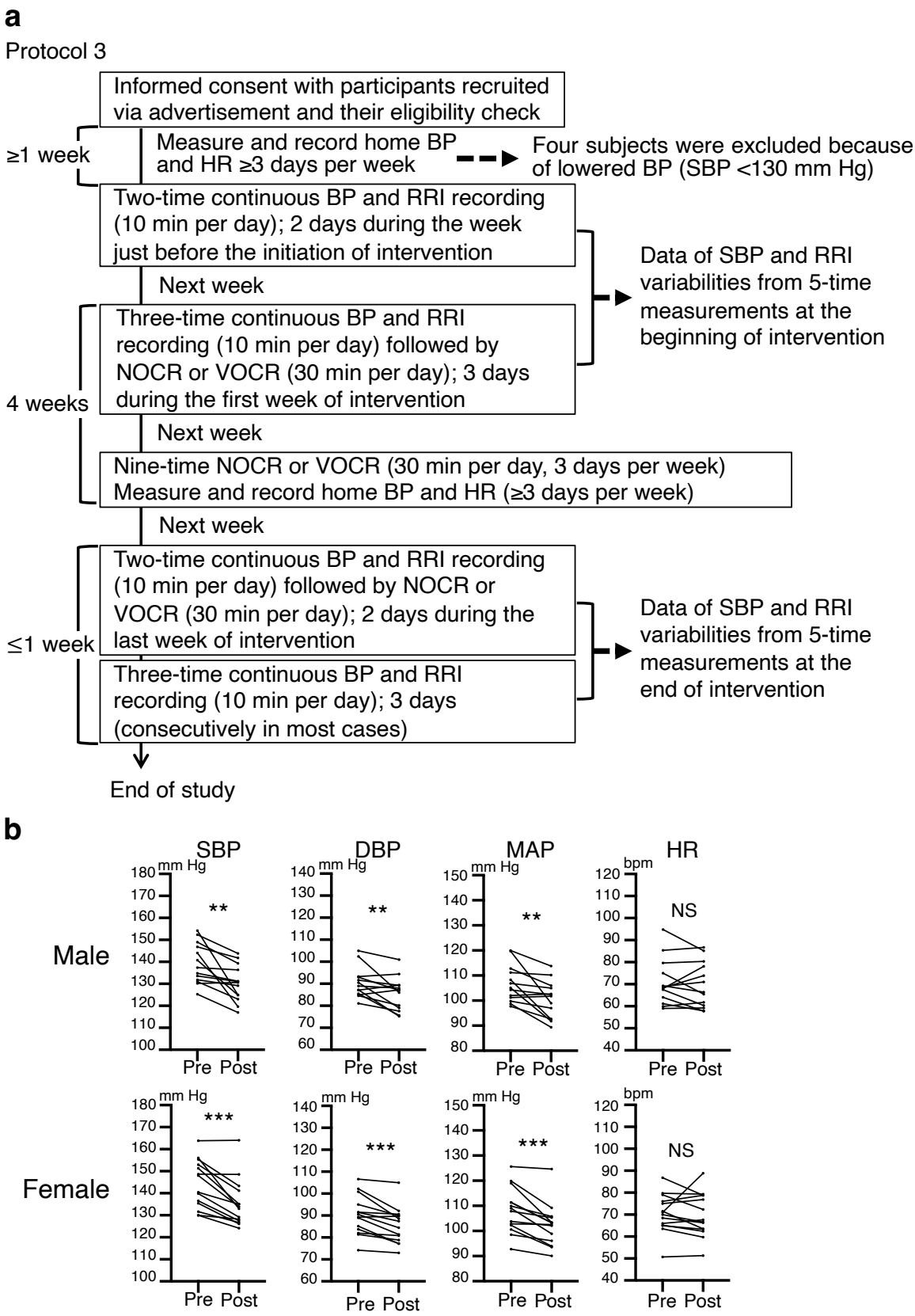


**Extended Data Fig. 17 | Design of the human study of protocol 3, and sex-segregated**

1318 **analysis of BP and HR in protocols 2 and 3**. **a,** Schematic representation of protocol 3. **b,** BP

1319 and HR "value of the week"s immediately before and after 4.5-week VOCR in the study of

1320 protocols 2 and 3. To avoid duplicate inputs, the VOCR data from subjects #22 and #31 in

1321 protocol 3, who were subjects #15 and #7 in protocol 2 (see Supplementary Table 3), were

1322 excluded from this analysis (male, SBP: $P = 0.0033$. DBP: $P = 0.0094$. MAP: $P = 0.0046$. HR:

1323 $P = 0.4373$. $n = 13$; female, SBP: $P = 0.0002$. DBP: $P = 0.0005$. MAP: $P = 0.0003$. HR: $P =$

1324 $0.6257$. $n = 14$). $^{**}P < 0.01$; $^{***}P < 0.001$; NS, not significant; paired two-tailed Student's *t*-

1325 test.

Fig. 8

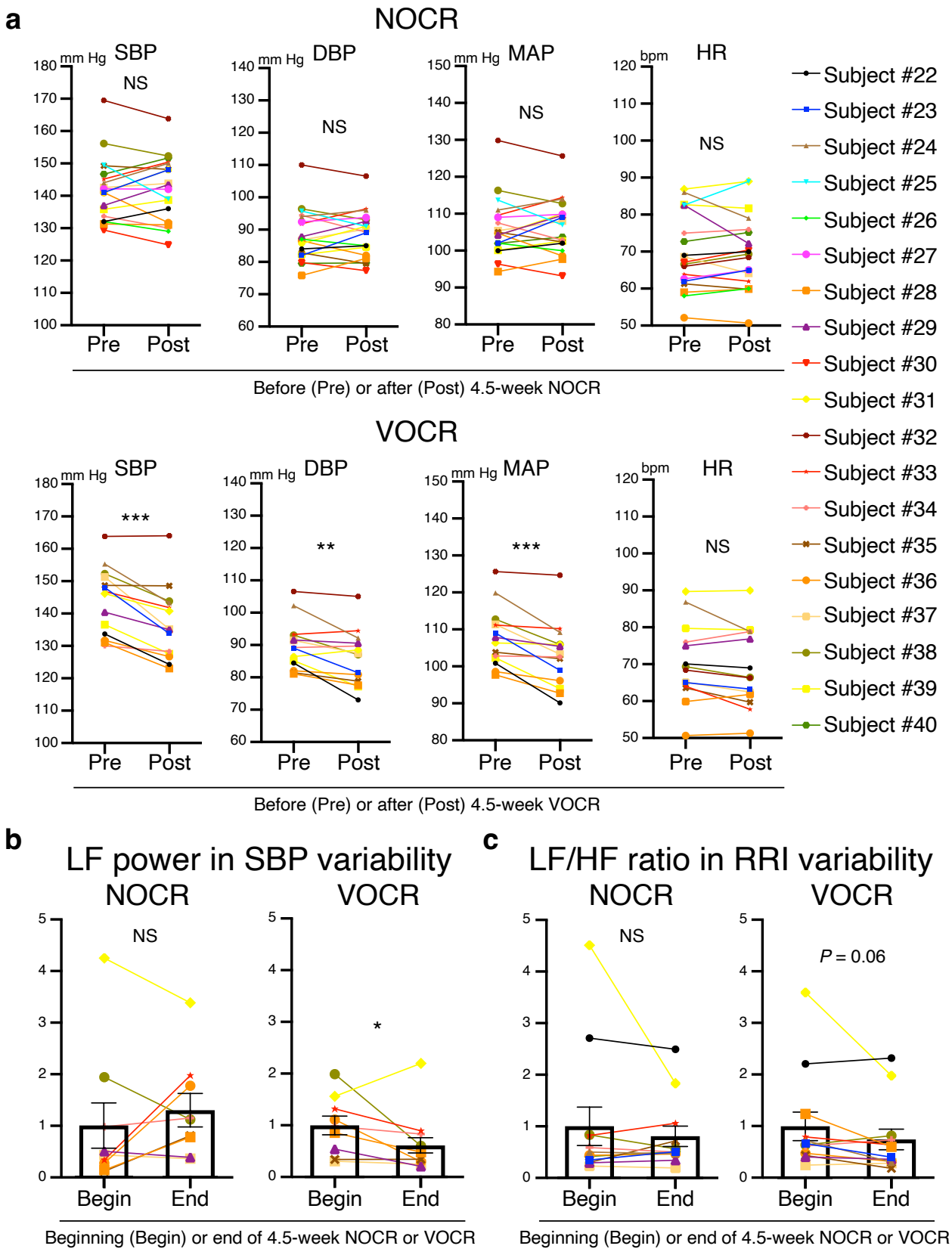
a
NOCR
SBP
mm Hg
NS
DBP
mm Hg
NS
MAP
mm Hg
NS
HR
bpm
NS
Pre
Post
Before (Pre) or after (Post) 4.5-week NOCR
VOCR
SBP
mm Hg
***
DBP
mm Hg
**
MAP
mm Hg
***
HR
bpm
NS
Before (Pre) or after (Post) 4.5-week VOCR
Subject #22
Subject #23
Subject #24
Subject #25
Subject #26
Subject #27
Subject #28
Subject #29
Subject #30
Subject #31
Subject #32
Subject #33
Subject #34
Subject #35
Subject #36
Subject #37
Subject #38
Subject #39
Subject #40
b
LF power in SBP variability
NOCR
VOCR
NS
*
Begin
End
Beginning (Begin) or end of 4.5-week NOCR or VOCR
c
LF/HF ratio in RRI variability
NOCR
VOCR
NS
P = 0.06
Begin
End
Beginning (Begin) or end of 4.5-week NOCR or VOCR

1326

1327 **Fig. 8 | VOCR, but not NOCR, has an antihypertensive and sympathoinhibitory effect in**

1328 **hypertensive adult humans. a,** BP and HR "value of the week"s immediately before and after

1329 4.5-week NOCR (top) and VOCR (bottom) in the study of protocol 3 (NOCR, SBP: $P = 0.9148$.

1330 DBP: $P = 0.6597$. MAP: $P = 0.7502$. HR: $P = 0.9002$. $n = 19$; VOCR, SBP: $P = 0.0001$. DBP: $P$

1331 $= 0.0051$. MAP: $P = 0.0006$. HR: $P = 0.0867$. $n = 14$). **b,c,** LF power in SBP variability **(b)** and

1332 LF/HF ratio in RRI variability **(c)** at the beginning (Begin) and ending (End) periods of

1333 intervention (NOCR and VOCR) scaled as the mean value from "Begin" (left column in each

1334 graph) set as 1 (**b**, NOCR: $P = 0.492$, $n = 10$; VOCR: $P = 0.016$, $n = 12$. **c**, NOCR: $P = 0.969$, $n$

1335 $= 12$; VOCR: $P = 0.063$, $n = 12$). Data are presented as mean ± s.e.m. *$P < 0.05$; **$P < 0.01$;

1336 ***$P < 0.001$; NS, not significant; paired two-tailed Student's *t*-test (**a**) or Wilcoxon signed-rank

1337 test (**b,c**).

## Supplementary Table 3

| Subject # | Sex<br>Age (years)<br>Body weight (kg)<br>Height (cm)<br>BMI | Period since diagnosis or self-recognition as hypertension<br>Declared health problems and diseases other than hypertension | Smoking<br>Alcohol (if yes, how often) | Current medication (dose per day) | Habitual exercise (times per week) | SBP/DBP (mm Hg) and HR (bpm) just before (left) and after (right) NOCR period (month of first - last bout of NOCR) | SBP/DBP (mm Hg) and HR (bpm) just before (left) and after (right) VOCR period (month of first - last bout of VOCR) |
|---|---|---|---|---|---|---|---|
| 22<br>(15) | Male<br>44<br>69<br>165<br>25.3 | Uncertain (>1 year)<br>None | No<br>Occasionally | None | None | 132/84 136/85<br>69 70<br>September - October | 134/84 124/73<br>70 69<br>March - April |
| 23 | Female<br>69<br>38<br>152<br>16.5 | 3 years<br>Lumbar spinal canal stenosis | No<br>No | Mecobalamin (1.5 mg) | Walking 30 min (2 or 3 times) | 141/82 148/89<br>62 65<br>October - November | 148/89 134/81<br>65 63<br>November - December |
| 24 | Female<br>45<br>49<br>157<br>19.9 | None | No<br>Almost every day | None | Walking 30 min (once or twice) | 144/94 150/96<br>86 79<br>October - November | 155/102 143/92<br>87 79<br>March - April |
| 25<br>(11) | Female<br>61<br>45<br>157<br>18.3 | Uncertain (>1 year)<br>Breast cancer (post-surgery) | No<br>Almost every day | Tamoxifen citrate (20 mg) | None | 150/96 139/91<br>83 89<br>October - November | ND ND<br>ND |
| 26<br>(17) | Male<br>66<br>60.1<br>167.1<br>21.5 | 8 years<br>None | Yes<br>Almost every day | None | None | 132/87 129/85<br>58 60<br>October - December | ND ND<br>ND |
| 27 | Male<br>37<br>82<br>178<br>25.9 | This study (<1 month)<br>None | No<br>Occasionally | None | None | 142/92 142/94<br>63 65<br>October - November | ND ND<br>ND |
| 28 | Male<br>23<br>125<br>178<br>39.5 | This study (<1 month)<br>None | No<br>Occasionally | None | Resistance training (3 times) | 131/76 131/81<br>59 60<br>November - December | 131/81 123/78<br>60 62<br>December - January |
| 29 | Female<br>59<br>77.5<br>160<br>30.3 | 14 years<br>Hyperlipidemia | No<br>No | Amlodin • Atorvastatin (5 mg • 5 mg)<br>Telmisartan (40 mg)<br>Vonoprazan (10 mg) | None | 137/88 143/93<br>83 72<br>November - December | 140/92 135/91<br>75 77<br>January - February |
| 30<br>(20) | Female<br>66<br>48.7<br>158.6<br>19.4 | 2 years<br>Hyperlipidemia<br>Lumbar spinal canal stenosis (post-surgery) | No<br>Almost every day | Amlodipine besilate (5 mg)<br>Atorvastatin calcium hydrate (10 mg)<br>Limaprost alfadex (15 μg)<br>Loxoprofen sodium hydrate (120 mg)<br>Rebamipide (200 mg) | Swimming 40 min (5 times) | 129/80 125/77<br>67 70<br>November - December | ND ND<br>ND |
| 31<br>(7) | Male<br>62<br>67<br>168<br>23.7 | Uncertain (>1 year)<br>Diabetes mellitus<br>Hyperlipidemia | No<br>No | Metformin hydrochloride (1000 mg)<br>Rosuvastatin calcium (5 mg)<br>Sitagliptin phosphate hydrate (50 mg) | Walking 120 min (once) | 141/86 148/91<br>87 89<br>November - December | 146/86 141/89<br>90 90<br>January - February |
| 32 | Female<br>75<br>62<br>157<br>25.2 | Uncertain (>1year)<br>Atrial fibrillation<br>Hyperuricemia | No<br>Almost every day | Irbesartan (50 mg)<br>Warfarin potassium (1 mg)<br>Bisoprolol fumarate (5 mg)<br>Lansoprazole (15 mg)<br>Cilnidipine (5 mg)<br>Topiroxostat (20 mg)<br>Ramelteon (8 mg) | None | 170/110 164/107<br>66 68<br>February - March | 164/107 164/105<br>68 66<br>March - April |
| 33 | Male<br>71<br>62<br>165<br>22.8 | 7 year<br>Prostate cancer (post-radiation therapy) | No<br>Almost every day | None | Squash 120 min (4 times) | 145/92 150/96<br>64 62<br>February - March | 147/93 142/94<br>64 58<br>March - April |
| 34 | Female<br>46<br>65<br>167<br>23.3 | This study (<1 month)<br>None | No<br>No | None | None | 134/94 130/89<br>75 76<br>February - March | 130/89 128/90<br>76 79<br>March - April |
| 35 | Female<br>69<br>65<br>148<br>29.7 | 19 years<br>Hyperlipidemia | No<br>Almost every day | None | None | 149/83 148/80<br>61 60<br>February - March | 149/81 149/79<br>64 60<br>March - April |

1338

**Supplementary Table 3 (continued)**

| Subject # | Sex<br>Age (years)<br>Body weight (kg)<br>Height (cm)<br>BMI | Period since diagnosis or self-recognition as hypertension<br>Declared health problems and diseases other than hypertension | Smoking<br>Alcohol (if yes, how often) | Current medication (dose per day) | Habitual exercise (times per week) | SBP/DBP (mm Hg) and HR (bpm) just before (left) and after (right) NOCR period (month of first - last bout of NOCR) | SBP/DBP (mm Hg) and HR (bpm) just before (left) and after (right) VOCR period (month of first - last bout of VOCR) |
|---|---|---|---|---|---|---|---|
| 36 | Female<br>64<br>54<br>148<br>24.7 | 3 years<br>None | No<br>No | None | Walking 60 min (5 times) | 141/87 132/82<br>52 51<br>February - March | 132/82 127/81<br>51 51<br>March - April |
| 37 | Female<br>80<br>54<br>148<br>24.7 | 1 year<br>None | No<br>No | None | None | 143/87 144/90<br>69 64<br>March - April | 151/91 135/87<br>65 62<br>May - June |
| 38 | Male<br>56<br>77<br>170<br>26.6 | 2 years<br>None | Yes<br>No | None | None | 156/96 152/93<br>67 69<br>March - April | 152/93 144/87<br>69 66<br>May - June |
| 39 | Female<br>85<br>50.2<br>148<br>22.9 | 29 years<br>Atrial fibrillation<br>Diabetes mellitus | No<br>Occasionally | Candesartan cilexetil • Amlodipine (8 mg • 5mg)<br>Rivaroxaban (10 mg)<br>Rosuvastatin (5 mg)<br>Carvedilol (5 mg)<br>Metformin hydrochloride (500 mg)<br>Esomeprazole (20 mg)<br>Sennoside (60 mg) | None | 136/82 139/85<br>83 82<br>August - October | 137/85 128/77<br>80 79<br>May - June |
| 40 | Male<br>62<br>84<br>172<br>28.4 | 13 years<br>Diabetes mellitus | No<br>Occasionally | Valsartan • Amlodipine (80 mg • 5 mg)<br>Atorvastatin (10 mg)<br>Benzbromarone (25 mg)<br>Canagliflozin (100 mg)<br>Metformin hydrochloride (1000 mg)<br>Bisoprolol fumarate (5 mg) | None | 147/80 152/80<br>73 75<br>July - August | ND ND<br>ND |

**Supplementary Table 3 | Information of subjects who participated in the study of protocol 3.** SBP/DBP (mm Hg) and HR (bpm) just before and after NOCR or VOCR are "value of the week"s. Five of 19 subjects in protocol 3 were participants in protocol 2. The parenthesized subject numbers indicate their subject numbers in protocol 2 (see Supplementary Table 2). They participated in protocol 3 upon their eligibility check at least nine months after the last bout of VOCR in protocol 2.

**Extended Data Fig. 18**

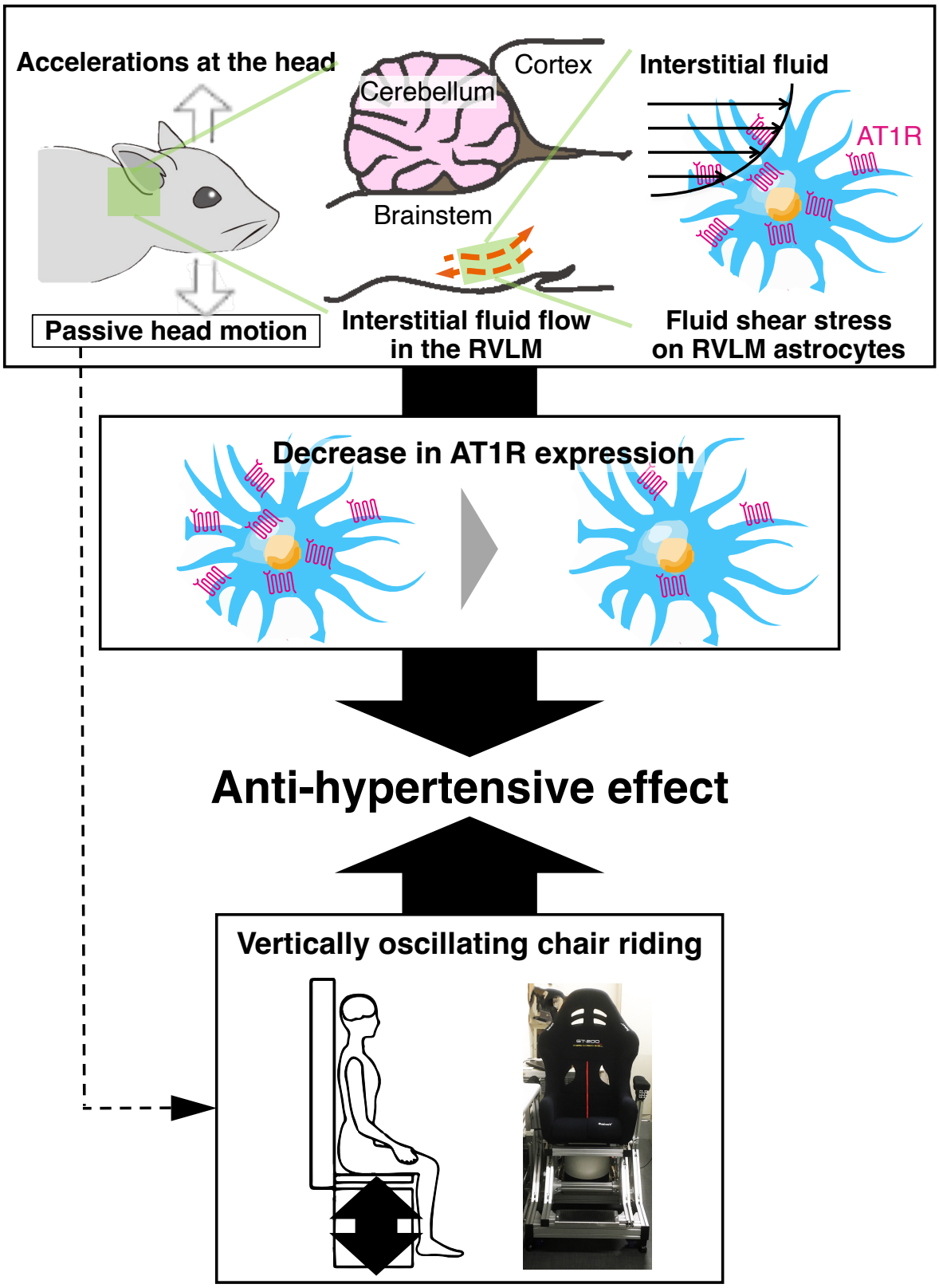


1346

1347 **Extended Data Fig. 18 | Schematic representation of the antihypertensive effects observed**

1348 **in PHM of hypertensive rats and VOCR of hypertensive humans.** The results from our

1349 animal experiments indicate that cyclical application of mechanical intervention to the head

1350 generates interstitial fluid movement in the RVLM, leading to FSS-induced decrease in the

1351 AT1R expression in astrocytes in situ, and thereby ameliorates hypertension. Our studies also

1352 show that the VOCR of hypertensive adult humans, which produces vertical accelerations at

1353 their heads, lowers their BP.

1354 **Methods**

1355 **Animal experiments and human studies.** Animals were housed under a 12/12 h light-dark
1356 cycle with controlled temperature (23−25°C), and treated with humane care under approval
1357 from the Animal Care and Use Committee of National Rehabilitation Center for Persons with
1358 Disabilities (approval number: 30-07). Male SHRSP/Izm and WKY/Izm rats were provided
1359 from the Disease Model Cooperative Association (Kyoto, Japan) and astrocyte-GFP mice
1360 (Aldh1L1-GFP mice)[40] were obtained from GENSAT (New York, NY), acclimated to the
1361 laboratory environments for at least 1 week, randomly divided into experimental groups, and
1362 used for experiments.

1363 All participants in our human studies provided written informed consent. The studies
1364 were approved by the Ethics Committees of the Iwai Medical Foundation and the National
1365 Rehabilitation Center for Persons with Disabilities (approval number: 30-01).

1366

1367 **Chemicals and antibodies.** All the chemicals were purchased from Sigma-Aldrich unless noted
1368 otherwise. Primary antibodies and their dilution rates used for immunostaining in this study are
1369 as follows: mouse monoclonal anti-GFAP (MAB360; Millipore, Billerica, MA) at 1:1,000;
1370 rabbit polyclonal anti-GFAP (Z0334; Dako, Glostrup, Denmark) at 1:1,000; chicken polyclonal
1371 anti-GFAP (ab4674; Abcam, Cambridge, UK) at 1:2,000; rabbit polyclonal anti-cleaved caspase-
1372 3 (9661; Cell Signaling Technology, Danvers, MA) at 1:1,000; mouse monoclonal anti-NeuN

1373 (MAB377; Millipore) at 1:200; rabbit polyclonal anti-NeuN (ABN78; Millipore) at 1:1,000,
1374 rabbit polyclonal anti-AT1R (HPA003596; Sigma-Aldrich, St. Louis, MO) at 1:200; rabbit
1375 polyclonal anti-AGTRAP (HPA044120; Sigma-Aldrich) at 1:1,000; rabbit polyclonal anti-GFP
1376 (598; MBL, Nagoya, Japan) at 1:2,000; chicken polyclonal anti-GFP (ab13970; Abcam) at
1377 1:2,000; mouse monoclonal anti-TUJ-1 (ab78078; Abcam) at 1:1,000. Secondary antibodies
1378 conjugated with Alexa Fluor 350, 488, 568, 633, and 647 (Thermo Fisher Scientific, Waltham,
1379 MA) were used at a dilution rate of 1:400. Cell nuclei were stained with DAPI (D9542; Sigma-
1380 Aldrich). Primary antibodies and their dilution rates used for immunoblot analysis are as
1381 follows: rabbit polyclonal anti-TNF-α (ab66579; Abcam) at 1:250; rabbit polyclonal anti-IL-1β
1382 (ab9722; Abcam) at 1:250; rabbit polyclonal anti-GAPDH (5174; Cell Signaling Technology) at
1383 1:10,000. Horseradish peroxidase-conjugated anti-rabbit IgG (H + L) secondary antibody
1384 (W401B; Promega, Madison, WI) was used at a dilution rate of 1:5,000 for anti-TNF-α or -IL-
1385 1β blotting, and 1:10,000 for anti-GAPDH blotting.
1386
1387 **PHM application to rats.** Rats were subjected to PHM in a prone position using a platform that
1388 we developed to move their heads up and down[24] (schematically represented in Fig. 1a). During
1389 PHM, animals were kept anesthetized with 1.5% isoflurane except for the μCT study, in which
1390 we used intraperitoneal injection of 2 mg/kg of midazolam (Sandoz, Basel, Switzerland), 2.5
1391 mg/kg of butorphanol (Meiji Seika, Tokyo, Japan) and 0.15 mg/kg of medetomidine (Kyoritsu

1392 Seiyaku, Tokyo, Japan) for anesthesia. Body temperature of tested animals was maintained
1393 using a light heater. The PHM system was set up to reproduce the head motion (5 mm, 2 Hz) of
1394 treadmill running (20 m/min) which made 1.0 × *g* vertical acceleration peaks in the head of rats
1395 examined[24]. The control rats in PHM experiments were anesthetized likewise, and placed in a
1396 prone position with their heads on the platform that was left static.
1397
1398 **Treadmill running of rats.** Rats were subjected to compulsive running using a belt drive
1399 treadmill equipped with an electrical shock system (MK-680S; Muromachi, Tokyo, Japan). We
1400 habituated the rats to the treadmill system by placing them in the machine several times without
1401 turning on the treadmill belt during the acclimation period. The electrical stimulation was turned
1402 on only once or twice during the first 5 min of the 30-min treadmill running on the first day of
1403 the 4-week treadmill running period. Thereafter, we did not need to turn on the electrical shock
1404 system to have the animals keep running, perhaps because the velocities we employed (20
1405 m/min) were moderate. The control rats in treadmill running experiments were placed on the
1406 belt daily for 30 min without turning on the treadmilling.
1407
1408 **Measurement of BP and HR of rats by radio-telemetry.** A telemetry pressure probe equipped
1409 with a micro electro mechanical systems (MEMS)-based 2.0-mm-long 0.47-mm-wide 0.60-mm
1410 thick sensor (Millar, Houston, TX) was implanted in the abdominal aorta of a rat at 9−10 weeks

1411 of age, following the surgical procedure described previously[86]. Rats were allowed to recover
1412 for at least 14 days before the initiation of experimental interventions or analyses. During the
1413 periods of experimentation that involved repeated BP and HR measurements over multiple
1414 weeks, BP and HR were monitored and recorded for continuous 30 min every 7 days between
1415 10:00 AM and 12:00 PM (noon) by a multichannel amplifier and signal converter (LabChart 8;
1416 ADInstruments, Bella Vista, Australia).
1417
1418 **Measurement of urinary norepinephrine excretion of rats.** Urine excreted during the
1419 indicated 24-h period was collected under an acidic condition using a metabolic cage (KN-646;
1420 Natsume Seisakusho, Tokyo, Japan) connected to a glass flask containing 10 mL of 6 N HCl,
1421 and stored at −80˚C until assayed. Excretion of urinary norepinephrine was calculated by
1422 multiplying its concentration measured using an enzyme-linked immunosorbent assay (ELISA)
1423 kit (KA1891; Abnova, Taipei, Taiwan) with the urine volume.
1424
1425 **Tissue preparation and immunostaining (immunohistochemical or immunocytochemical**
1426 **analysis).** Rats were anesthetized with intraperitoneal injection of midazolam, butorphanol, and
1427 medetomidine, and perfused transcardially with 4% paraformaldehyde (PFA; TAAB
1428 Laboratories Equipment, Aldermaston, UK) in phosphate-buffered saline [PBS (137 mM NaCl,
1429 10 mM $Na_2HPO_4$, 2.7 mM KCl, 1.5 mM $KH_2PO_4$)]. The brainstems were excised and post-fixed

1430 with 4% PFA in PBS overnight at 4°C. The tissues were cryoprotected by soaking in 20%
1431 sucrose/PBS for 24 h and in 30% sucrose/PBS for additional 24 h at 4°C. Fixed brainstems were
1432 frozen in optimal cutting temperature compound (Sakura Finetek, Tokyo, Japan) and cut into 16
1433 μm-thick coronal sections using a cryostat (CM3050S; Leica Microsystems, Wetzlar, Germany).
1434 Sliced sections were permeabilized and blocked with 0.1% Tween-20 and 4% donkey serum
1435 (Merck Millipore, Burlington, MA) in Tris-buffered saline, blocked with, and stained by
1436 incubating with primary antibodies at appropriate dilutions followed by their species-matched
1437 secondary antibodies. Cell nuclei were stained with DAPI (Sigma-Aldrich). The slides were
1438 mounted with ProLong Gold Antifade Reagent (Thermo Fisher Scientific) and images were
1439 captured with a BZ-9000 digital microscope system (Keyence, Osaka, Japan). Quantitative
1440 immunohistochemical analysis (i.e., cell counting) of the RVLM was performed in the
1441 approximately same relative section for each rat (11.3–12.3 mm caudal to the bregma, 1.5–2.5
1442 mm lateral to the midline, 0–1 mm dorsal to the ventral surface of the medulla).
1443 For immunocytochemistry, cultured cells were fixed with 4% PFA in PBS for 20 min at
1444 room temperature (RT) and permeabilized and blocked with 0.1% Triton X-100 and 10% fetal
1445 bovine (FBS; GE Healthcare Life Science, Marlborough, MA) in PBS for 30 min at RT. The
1446 cells were then incubated with primary antibodies for 2 h and then with secondary antibodies for
1447 1 h at RT.
1448

1449 **Microinjection into the rat RVLM.** Rats were anesthetized with intraperitoneal injection of
1450 midazolam, butorphanol, and medetomidine except for Ang II or valsartan injection studies, in
1451 which we used 1.2−1.4 g/kg of urethane (Sigma-Aldrich), and subjected to microinjection as
1452 described previously[87]. In brief, a 25s-G microsyringe (Hamilton, Bonaduz, Switzerland) was
1453 stereotaxically positioned on anesthetized rats after exposure of dorsal surface of medulla. The
1454 needle placement was defined according to an atlas of the rat with stereotaxic coordinates[88 63];
1455 anteroposterior angle: 18˚, 1.8 mm lateral to the calamus scriptorius, 3.5 mm ventral to the
1456 dorsal surface of the medulla. The placement of the needle tip in RVLM was confirmed by
1457 ensuring the pressure response to a test-dose injection of L-glutamate[12,89] (100 nL of 1 mmol/L
1458 in PBS). Microinjection of various compounds or mediums was made through a needle
1459 reinserted at the same coordinates with fixed infusion rates using a microsyringe pump
1460 instrument (KD scientific, Holliston, MA). Except for the experiments to analyze the pressor or
1461 depressor responses, we held the syringe for 5 min after the injection to avoid reflux, pulled out
1462 the needle carefully, and sutured the skin. The volumes and rates of microinjection were as
1463 follows; Ang II (Auspep, Tullamarine, Australia) and valsartan (Tocris Bioscience, Bristol, UK):
1464 100 nL of 1 mmol/L in PBS at 0.1 μL/min, AAV solutions: 300 nL at 0.03 μL/min, PEG
1465 solutions: 1 μL at 0.1 μL/min, Isovist: 1 μL at 0.2 μL/min.
1466
1467 **Analysis of pressor/depressor responses.** Rats implanted with a telemetry pressure probe were

1468 anesthetized with urethane, and subjected to the analysis of pressor/depressor responses.

1469 Monitoring the BP, we injected Ang II or valsartan (100 pmol) stereotaxically into the unilateral

1470 RVLM following the microinjection procedures described above. The injection side (right or

1471 left) was chosen randomly. When both pressor and depressor responses were analyzed, at least 2

1472 h elapsed between the injections of Ang II and valsartan (Fig. 2a). The maximal MAP change

1473 elicited from the baseline was statistically analyzed[60].

1474

1475 **Production of AAV vectors.** To obtain astrocyte- and neuron-specific transduction, we used

1476 AAV9 vectors that expressed a transgene under the control of mouse GFAP and rat NSE

1477 promoters, respectively. The astrocyte-specific GFAP promoter consists of 0.6-kb hybrid

1478 fragments containing ABC1D genomic regions upstream of the mouse *GFAP* gene[90]. The

1479 neuron-specific NSE promoter is composed of the 1.2-kb genomic region upstream of the rat

1480 *NSE* gene[91]. Full-length rat AGTRAP cDNA was synthesized (Eurofins Genomics, Tokyo,

1481 Japan) and inserted into plasmid pAAV-GFAP-GFP-P2A-Cre-woodchuck hepatitis virus post-

1482 transcriptional regulatory element (WPRE)-simian virus 40 polyadenylation signal (SV40pA)

1483 and pAAV-NSE-GFP-P2A-Cre-WPRE-SV40pA to generate pAAV-GFAP-GFP-P2A-AGTRAP-

1484 WPRE-SV40pA and pAAV-NSE-GFP-P2A-AGTRAP-WPRE-SV40pA. pAAV-GFAP-GFP-

1485 WPRE-SV40pA and pAAV-NSE-GFP-WPRE-SV40pA were used for experimental controls.

1486 Recombinant single-strand AAV2/9 vectors were produced by transfection of HEK293T cells

1487 (Thermo Fisher Scientific) with the respective pAAV expression plasmid, pAAV2/9 and a helper
1488 plasmid (Stratagene, La Jolla, CA) as previously described[92]. After harvesting conditioned
1489 medium, the viral particles were precipitated using polyethylene glycol 8000 and iodixanol
1490 continuous gradient centrifugation as previously described[93]. The genomic titer of purified
1491 AAV9 vectors was determined by qPCR that targeted the WPRE sequence.
1492
1493 **Measurement of pressure in the rat medulla.** Intramedullary pressure was measured using a
1494 blood pressure telemeter following the procedure we previously reported[24,94]. To place the
1495 pressure sensor in the rat medulla, we made a ~1-mm sized hole in the occipital bone (2 mm
1496 lateral to the midline, 2 mm rostral to the caudal margin of occipital bone) using a dental
1497 handpiece (Osada Electric, Tokyo, Japan), stereotaxically inserted a 20-G needle (Terumo,
1498 Tokyo, Japan) as a guide sheath (4 mm in depth from the occipital bone surface) at an
1499 anteroposterior angle of 20˚, and sealed it airtightly using dental cement (GC, Tokyo, Japan) to
1500 avoid pressure escape. We macroscopically observed that the needle tip was placed in the rat
1501 RVLM after these procedures in our pilot experiments. However, for this pressure measurement,
1502 we did not strictly confirm the placement of the needle tip in the RVLM using the
1503 aforementioned test-dose injection of L-glutamate. Therefore, we designate this experiment as
1504 an “intramedullary” pressure measurement. During the pressure measurement, respiration was
1505 monitored using a pulse transducer (TN1012/ST; ADInstruments) attached to the tested rats.

1506 Low-pass (50 Hz) filtered intramedullary pressure waves were analyzed using LabChart 8

1507 software.

1508

1509 **In vivo analysis of the distribution dynamics of interstitial fluid in the rat RVLM using**

1510 **μCT.** Isovist (Bayer, Berlin, Germany) was stereotaxically microinjected into the RVLM of

1511 anesthetized 12-week-old male WKY rats following the procedure described above, and

1512 visualized using μCT (inspeXio SMX-100CT; Shimadzu, Kyoto, Japan). After Isovist injection,

1513 rats were subjected to two serial brain μCT scans between which PHM was either applied or left

1514 unapplied (kept sedentary) for 30 min (Fig. 4e). μCT images were analyzed using software for

1515 3-D morphometry (TRI/3D-BON-FCS64; RATOC System, Tokyo, Japan). Voxels with ≥1.02

1516 times signal intensity as compared with that of air was defined as Isovist cluster in the rat

1517 RVLM.

1518

1519 **Hydrogel introduction in the rat RVLM.** Just before use, a pre-mixture of PEG with

1520 functional groups (25 g/L in PBS) was prepared from tetra-armed thiol-terminal (TetraPEG-SH)

1521 (Yuka-Sangyo, Tokyo, Japan) and acrylate-terminal (Tetra-PEG-ACR) (JenKem Technology,

1522 TX, USA) PEG solutions as we previously described[24]. Tetra-armed polyethylene glycol without

1523 functional groups (25 g/L in PBS) was used as an ungelatable control. For the analysis of

1524 hydrogel distribution in rat RVLM, we used Tetra-PEG-SH fluorescently labeled with a thiol-

1525 reactive probe (Thermo Fisher Scientific or Merck KGaA, Darmstadt, Germany). Microinjection
1526 of PEG solutions into rat RVLM was conducted as described above.
1527 To specifically analyze the consequences of PHM and hydrogel introduction by
1528 minimizing possible invasive influences of microinjection itself, we gave 1-week recovery time
1529 before the first BP measurement, and then applied PHM to the rats (daily 30 min, 14 or 28
1530 days). Immediately subsequent to post-PHM 24-h urine collection (Fig. 6a), rats were sacrificed
1531 by transcardial infusion of PFA and subjected to histological analysis.
1532
1533 **Multiphoton microscopic imaging and analysis of the interstitial space**
1534 **structure/orientation and dimension in the rat RVLM.** We prepared PFA-fixed lower
1535 brainstem tissue samples from 12-week-old WKY rats 24 h after introducing fluorescently
1536 labeled hydrogel conjugated with Alexa Fluor 594 C5 maleimide (A10256, Thermo Fisher
1537 Scientific) to their RVLM as described above. We used a multiphoton microscope (FVMPE-RS-
1538 UPSP2; Olympus, Tokyo, Japan), which is suitable for viewing a deep part of a relatively large
1539 sample. This was because we wanted to minimize the possible influence of plastic
1540 deformation/distortion or disruption of hydrogels (and tissues) that might occur during the
1541 experimental procedures (e.g., sample sectioning) particularly in the vicinity of the cut section.
1542 The sample was partially embedded in 2% (w/v) agarose (A9414; Sigma-Aldrich) and immersed
1543 in PBS. An excitation laser (Mai Tai DeepSee; Spectra-Physics, Milpitas, CA) was tuned at 800

1544 nm, and the beam was focused with an objective lens (XLPLN25XWMP2; Olympus). The
1545 fluorescence was collected with the same objective lens, and detected using a GaAsP detector
1546 after passing through a red band pass filter (BA575-645; Olympus). Considering the relative
1547 extension of multiphoton excitation in the incident direction of excitation laser beam[95], which is
1548 parallel to the optical axis of objective lens, we acquired and analyzed images of the three
1549 mutually orthogonal planes (*xy*-, *xz*-, and *yz*-planes; Extended Data Fig. 6a-c and Extended Data
1550 Fig. 7a-c).

1551 Image analysis to determine the structure/orientation of the interstitial space was
1552 conducted as follows. Approximately 20-μm stacked long-rectangular voxel images (20 voxels
1553 of 1-μm length) were resampled to 100 cubic voxels (0.2072 μm on each side), and smoothed to
1554 a width of 5 voxels (~1 μm). Following the previous reports on the occupancy of interstitial
1555 space in the brain[74,96], we extracted the top 20% high-fluorescence voxel population as clusters
1556 representing the interstitial space (Extended Data Fig. 6a, bottom). For huge clusters (>5,000
1557 voxels), the bottom 50% population of low-fluorescence voxels in them were removed to reduce
1558 their size. These procedures, together with a clearance of clusters of <50 voxels enabled us to
1559 apply elliptic fitting to determine the major and minor axes of each processed cluster on the
1560 stacked plane (Extended Data Fig. 6b). For each sample, we analyzed 100 slices, focusing on the
1561 plane with the highest mean fluorescence intensity along the stack direction.

1562 To quantitatively analyze the cross-sectional area of the interstitial space, we resampled

1563 ~4-μm stacked long-rectangular voxel images to 20 cubic voxels (Extended Data Fig. 7a).
1564 Based on the voxel number of each individual cluster (Extended Data Fig. 7b), we drew the
1565 distribution of its cross-sectional area (Extended Data Fig. 7c). Analyzing the probability density
1566 by fitting to the log-normal distribution[77,78], we determined the mode and full width at half
1567 maximum (FWHM)[79] of the cross-sectional areas of the individual interstitial spaces (Extended
1568 Data Fig. 7c). We used MATLAB software (version 2021a; Math Works, Natick, MA) for these
1569 image analyses.
1570
1571 **MRI scanning and orientation analysis of the rat lower brainstem.** Twelve-week-old male
1572 WKY rats were scanned in a 7.0-Tesla MRI system (Biospec 70/30-USR; Bruker BioSpin,
1573 Ettlingen, Germany) using a 2-D-rapid acquisition with relaxation enhancement (RARE).
1574 Parameters for the sagittal $T_2$-RARE sequence were as follows: echo time (TE), 33 ms;
1575 repetition time (TR), 3600 ms; slice thickness (SL), 0.75 mm; field of view (FOV), 38.4 × 38.4
1576 mm; voxel, 0.15 × 0.15 × 0.75 mm; RARE factor, 8; number of averages, 4. We analyzed the
1577 MR images using SPM12 on MATLAB
1578 (https://www.fil.ion.ucl.ac.uk/spm/software/spm12/). Each image was smoothed with 0.24-mm
1579 FWHM, and registered to the template atlas of the Fischer 344 rat brain[97] (An MRI-Derived
1580 Neuroanatomical Atlas of the Fischer 344 Rat Brain (Version v4) [Data set]. Zenodo.
1581 https://doi.org/10.5281/zenodo.3900544). Assuming an equivalent weight for each voxel, we

1582 determined the center of mass of the lower brainstem in each image in a particular plane (*xy*-,
1583 *xz*- or *yz*-plane) and drew its centroidal line by combining the least squares and sigmoid fitting.
1584 Because the *y*-axis was actually the direction of the maximum diameter of this part of the brain,
1585 the longest centroidal line was drawn by fitting to the mass centers determined in the *xz*-plane
1586 images (Extended Data Fig. 6d).
1587
1588 **Calculation of the magnitude of FSS on the cells in the rat RVLM during PHM.** We
1589 calculated the interstitial fluid flow-derived FSS imposed on cells in the rat RVLM during PHM
1590 by referring to the findings from our μCT analysis (Fig. 4g,h) and multiphoton microscopy
1591 analyses (Extended Data Fig. 6 and 7) according to Henry Darcy's law, which defines the flux
1592 density of penetrating fluid per unit time[98]. Based on the PHM-induced enhancement of Isovist
1593 spread (Fig. 4g,h), we estimated the velocity of the interstitial fluid flow ($u$) during PHM as
1594 0.4−0.6 μm/s, two- to three-times that in the brain of sedentary rodents, which is reported to be
1595 0.2 μm/s[37,38]. We then calculated the Darcy permeability ($K_p$), which relates to the flow or
1596 pressure drop of liquid across a porous structure[99], in the rat RVLM tissue. The Kozeny–Carman
1597 equation allows us to calculate permeability given pore-size/sphericity data[80,81], where a value of
1598 4.5–5.5 was considered the Kozeny constant[80-82] (Supplementary Table 1a) based on the
1599 apparent structure/orientation of the interstitial space in the rat RVLM (Extended Data Fig. 6e
1600 and Extended Data Fig. 7d). We referenced the interstitial space dimension (cross-sectional area

1601 or diameter) estimated by analyzing the microscopic images (Extended Data Fig. 7c). FSS (τ) at

1602 the interstitial cell surface was calculated as described in Supplementary Table 1[85].

1603

1604 **Cell culture.** Primary cultures of astrocytes were prepared from the cortex of neonatal (one day

1605 old) mouse pups as described previously[100,101] with some modifications. The brains were excised

1606 from astrocyte-GFP mice[40] immediately after euthanasia by $CO_2$ inhalation (typically 4–5 pups

1607 at one time), and the cortices were dissected to small pieces in DMEM (FUJIFILM Wako Pure

1608 Chemical, Osaka, Japan) using forceps under a stereomicroscope (SV-11; Zeiss, Oberkochen,

1609 Germany). The dissected pieces of cortex tissue were collected by 190-×-*g* centrifugation for 3

1610 min, suspended, and incubated in an isotonic solution (124 mM NaCl, 5 mM KCl, 3.2 mM

1611 $MgCl_2$, 0.1 mM $CaCl_2$, 26 mM $NaHCO_3$, 10 mM D-glucose, 100 I.U./mL penicillin, 100 μg/ml

1612 streptomycin) containing 0.1% trypsin, 0.67 mg/ml hyaluronidase, and 0.1 mg/ml

1613 deoxyribonuclease I at 37°C for 10 min to dissociate cells. Subsequently, an equal volume of

1614 DMEM/F12 (Thermo Fisher Scientific) containing 10% FBS, 100 I.U./mL penicillin, and 100

1615 μg/mL streptomycin was added to neutralize trypsin. After multiple pipetting for further

1616 homogenization with a 10-mL serological pipet, the cell suspension was cleared of tissue debris

1617 using a 70-μm nylon-mesh strainer (Corning Life Sciences, Corning, NY). Cells were then

1618 washed twice with DMEM/F12 containing 10% FBS, 100 I.U./mL penicillin, and 100 μg/mL

1619 streptomycin, plated on a poly-D-lysine-coated T75 flask (Corning Life Sciences, Corning, NY),

1620 and kept in a humidified incubator (5% $CO_2$, 95% air, 37°C). The culture medium was replaced
1621 with fresh one every 3 days, and it typically took 7−10 days for the cells to become confluent in
1622 the flask. Then, astrocyte-enriched cell population was obtained by physically detaching the
1623 other types of cells, such as microglia and oligodendrocytes. After shaking the flask overnight
1624 using an orbital shaker (200 rpm with BR-40LF; TAITEC, Koshigaya, Japan), detached cells
1625 were removed together with the medium. Cells remained attached to the flask were replated on
1626 poly-D-lysine-coated 10-cm dishes (Corning Life Sciences) at a ratio of 1:3 regarding the
1627 density (typically 3−4 dishes). The medium was replaced with fresh one every 3 days until the
1628 cells reached 80−90% confluence and were used for experiments. We confirmed that >95% of
1629 the cells were GFP-positive (Extended Data Fig. 8a), indicating a high degree of astrocyte
1630 purity.

1631 Mouse neuroblastoma-derived Neuro2A cells (provided from Dr. Yokota, Tokyo
1632 Medical and Dental University, Japan), which exhibit neuronal phenotypes and morphology[41,42],
1633 were cultured in DMEM supplemented with 10% FBS, 100 I.U./mL penicillin and 100 μg/mL
1634 streptomycin in a humidified incubator (5% $CO_2$, 95% air, 37°C).

1635

1636 **Application of FSS to astrocytes or Neuro2A cells in culture.** Astrocytes or Neuro2A cells
1637 grown in a poly-D-lysine-coated 35-mm culture dish (Corning Life Sciences, Corning, NY)
1638 were exposed to pulsatile FSS (average 0.7 Pa) for 30 min. As we previously reported[23,24,34], a

1639 parallel plate flow-chamber and a roller pump (Masterflex; Cole-Parmer, Vernon Hills, IL) were
1640 used to apply FSS. The flow-chamber, which was composed of a cell culture dish, a
1641 polycarbonate I/O unit, and a silicone gasket, generated a 23-mm-long 10-mm-wide 0.5-mm-
1642 high flow channel. Astrocytes or Neuro2A cells were seeded at a density of $8 \times 10^5$ cells/8.0
1643 $cm^2$. To maintain pH and temperature of culture medium, we used a 5% $CO_2$-containing
1644 reservoir and a temperature-controlled bath.
1645
1646 **Application of HPC to astrocytes in culture.** Astrocytes seeded at a density of $8 \times 10^5$
1647 cells/8.0 $cm^2$ were exposed to cyclical HPC with various amplitudes at a frequency of 0.5 Hz for
1648 30 min using a custom-made pressure system described previously[34]. The system consists of a
1649 cell culture dish, a polycarbonate pressure chamber, a silicone gasket, an O-ring, a quartz glass,
1650 two holding jigs, a thermostatic chamber, and a syringe pump. The system was completely
1651 airtight, enabling precise and strict pressure control with the syringe pump. To maintain the
1652 temperature of culture medium, the entire system was placed in a 37ºC incubator during HPC
1653 application. In both FSS and HPC experiments, cell adhesion and morphology were observed
1654 using a light microscope (DM IRE2; Leica Microsystems, Wetzlar, Germany).
1655
1656 **Quantitative PCR Analysis (reverse transcription and real-time PCR).** 500 ng of total RNA
1657 extracted from cell culture were subjected to reverse transcription, using ISOGEN II (NIPPON

1658 GENE, Tokyo, Japan) and PrimeScript RT reagent Kit (TaKaRa, Kusatsu, Japan). The resulting
1659 cDNA was subjected to real-time PCR analysis using glyceraldehyde-3-phosphate
1660 dehydrogenase (GAPDH) as an internal control in Applied Biosystems 7500 Real Time PCR
1661 System with Power SYBR Green PCR Master Mix (Thermo Fisher Scientific).
1662 The primers (sense and antisense, respectively) were as follows: mouse *Agtr1a* (AT1R-encoding
1663 gene); 5'-AAAGGCCAAGTCGCACTCAAG-3'
1664 and 5'-TCCACCTCAGAACAAGACGCA-3',
1665 mouse *Gapdh* (GAPDH-encoding gene); 5'-GCAAAGTGGAGATTGTTGCCAT-3' and
1666 5'-CCTTGACTGTGCCGTTGAATTT-3', WPRE (for genomic titration of purified AAV9
1667 vectors); 5'-CTGTTGGGCACTGACAATTC-3' and 5'-GAAGGGACGTAGCAGAAGGA-3'.
1668
1669 **Fluorescent Ang II binding assay.** Six or twenty-four hours after the termination of FSS
1670 application, cultured astrocytes were incubated with Ang II type 2 receptor inhibitor, PD123319
1671 ($10^{-6}$ mol/L in PBS; ab144564, Abcam), for 20 min, and then with tetramethylrhodamine
1672 (TAMRA)-labeled Ang II ($10^{-8}$ mol/L in PBS; AS-61181, AnaSpec, Fremont, CA) for 30 min.
1673 After 3 times wash with PBS, samples were fixed and subjected to anti-GFP immunostaining to
1674 strengthen the GFP-derived green fluorescence signals and corroborate our analysis on
1675 astrocytes prepared from astrocyte-GFP mice as well as to secure the binding of fluorescent Ang
1676 II. Green and red fluorescence was viewed with a fluorescence microscope (BZ-9000 HS;

1677 Keyence). Samples from astrocytes left unexposed to FSS were prepared and viewed likewise,
1678 and provided an experimental control.
1679
1680 **Terminal deoxynucleotidyl transferase-mediated dUTP nick-end labeling (TUNEL) assay.**
1681 Rat RVLM sections were stained using a TUNEL kit (Biotium, Fremont, CA) according to the
1682 manufacturer's protocols, counterstained with DAPI, and then viewed using a 20× objective with
1683 a fluorescence microscope (BZ-9000 HS; Keyence). The nuclei of apoptotic cells were
1684 determined by the existence of green fluorescent patches, and cell apoptosis was quantified by
1685 referring their counts to total numbers of nuclei defined by DAPI staining.
1686
1687 **Immunoblot analysis.** Rat RVLM tissue was excised immediately after cervical dislocation,
1688 mechanically homogenized, solubilized with RIPA buffer (25 mM Tris•HCl pH 7.6, 150 mM
1689 NaCl, 1% NP-40, 1% sodium deoxycholate, 0.1% SDS) with protease and phosphatase
1690 inhibitors (78440; Thermo Fisher Scientific), and subjected to SDS-PAGE followed by anti-
1691 TNF-α, anti-IL-1β, and anti-GADPH immunoblotting. Specific signals were visualized and
1692 quantified using Odyssey infrared imaging system (LI-COR Biosciences, Lincoln, NE) and
1693 ImageJ software (NIH, Bethesda, MD).
1694
1695 **Analysis of rat ADNA and BP during the transition from before to after the initiation of**

1696 **PHM.** ADNA recording was conducted in isoflurane (2%)-anesthetized 12−16-week-old male
1697 SHRSPs as described previously[102] with some modifications. Briefly, using a stereomicroscope
1698 (M80; Leica, Heerbrugg, Switzerland), we surgically exposed and isolated the left aortic
1699 depressor nerve through an anterior neck approach. We then placed a bipolar cuff electrode
1700 below the nerve bundle and embedded the nerve-electrode contacting complex in a two-
1701 component silicone gel (932; Wacker Chemie, Munich, Germany). Multifiber ADNA was
1702 50−10,000-Hz band-pass filtered and amplified with a differential preamplifier (MEG-5200;
1703 Nihon Kohden, Tokyo, Japan). The ADNA was identified using its unique spontaneous activity
1704 synchronous with the arterial systolic cycle as an indicator. BP was monitored with a pressure
1705 transducer (DX-360; Nihon Kohden, Tokyo, Japan)/polygraph system (UBS-100-6; Unique
1706 Medical, Tokyo, Japan) connected to a catheter inserted in the right femoral artery. The PHM
1707 cycle was also monitored using a piezoelectric pulse transducer (MLT1010; ADInstruments).
1708 ADNA, BP, and PHM cycle were digitized using Power1401 mkII and Spike2 software
1709 (Cambridge Electronic Design, Cambridge, UK) at a 3-kHz sampling frequency. The recorded
1710 ADNA was then subjected to DC offset removal, rectified, integrated and smoothed with a time
1711 constant of 3 ms by Spike2. The integrated value of ADNA measured after euthanasia by
1712 isoflurane overdose was considered background noise and subtracted from the entire data
1713 collected. ADNA was then normalized in each rat (presented in a.u. in Extended Data Fig. 14a).
1714 The relative ADNA value (%) averaged for each heartbeat was scaled with the mean of 10

1715 heartbeats immediately before the PHM initiation set as a baseline (100%) (Extended Data Fig.
1716 14b). The SBP, DBP, MAP, and HR were determined using Spike2.
1717
1718 **Measurement of accelerations in the human head.** To measure the accelerations at the human
1719 head during treadmill running or VOCR, we fixed an accelerometer (NinjaScan-Light;
1720 Switchscience, Tokyo, Japan) on foreheads with a surgical tape. Vertical acceleration was
1721 evaluated using the software application provided from the manufacture.
1722
1723 **Design and participants of clinical study on antihypertensive effects of vertically oscillating**
1724 **chair riding.** We conducted single-arm (protocol 1 and 2) and non-randomized controlled
1725 (protocol 3) clinical studies. The study of protocol 1 (Extended Data Fig. 15c) was carried out at
1726 the affiliated health services facility of Iwai Medical Foundation (Iwai Keiaien, Tokyo, Japan).
1727 The studies of protocol 2 (Extended Data Fig. 16a) and 3 (Extended Data Fig. 17a) were carried
1728 out at the National Rehabilitation Center for Persons with Disabilities Hospital. In protocol 3,
1729 participants were assigned to either NOCR or VOCR, depending on their intention and choice,
1730 whereas 14 individuals underwent both NOCR and VOCR after we obtained their consent
1731 (Supplementary Table 3). In principle for the "NOCR and VOCR" participants, NOCR
1732 intervention was administered prior to VOCR considering the antihypertensive effect of VOCR
1733 remaining for a while after its termination (Fig. 7b). In only one participant (#39), VOCR

1734 intervention was performed prior to NOCR. She first participated in the VOCR study upon her
1735 agreement and choice, and then agreed to the NOCR study after the completion of the VOCR
1736 intervention. We confirmed that her BP had stably returned to the pre-VOCR level before
1737 starting the NOCR intervention; her NOCR was initiated 10 weeks after the last bout of VOCR.
1738 Continuous beat-by-beat recording of BP and RRI was conducted for the participants who
1739 agreed to these measurements in protocol 3. Because the system for continuous BP recording
1740 became available after we started the protocol 3 study, two participants in the NOCR group (#22
1741 and #23) were subjected to continuous RRI recording alone (i.e., void of continuous BP
1742 recording). Subjects #32 and #39 were excluded from continuous BP and RRI recording, despite
1743 agreeing to these measurements, because arrhythmia was revealed on electrocardiography (the
1744 first RRI recording) and confirmed to be atrial fibrillation by their primary care physicians
1745 (Supplementary Table 3).

1746 Subjects were considered eligible if they were 20−75 (protocols 1 and 2) or ≥20
1747 (protocol 3) years old of age and confirmed to have 130−160 mm Hg of SBP at the time of
1748 interview for informed consent and eligibility check. Subjects with mental or psychological
1749 illnesses, history or presence of cardiovascular events, history or presence of severe
1750 dysfunction/disorder of liver, kidney, lung, gastrointestinal tract, and spine, or presence of acute
1751 injuries/diseases (e.g., recent traumas and infectious diseases) were excluded with the exception
1752 of those who were given permission for participating in this study from their primary care

1753 physicians. Whereas antihypertensive medication did not disqualify the subjects (Supplementary
1754 Table 2 and 3), they were advised not to change their medication from at least one month prior
1755 to the first bout of NOCR or VOCR through the study period (i.e., up to 8 weeks after the last
1756 bout of NOCR or VOCR). At a certain (approximately fixed) time point in the morning
1757 (typically just before breakfast), they conducted 3 consecutive measurements of BP (mm Hg)
1758 and HR (bpm) using an automated upper arm-cuff sphygmomanometer, and recorded the values
1759 from all those measurements. These procedures of BP measurement and recording accord with
1760 the Japanese Society of Hypertension Guidelines for the management of hypertension
1761 (JSH2019)[103]. Subjects were directed to start periodical (≥3 days per week) BP/HR
1762 measurements at least 2 weeks (protocols 1 and 2) or 1 week (protocol 3) before the initiation of
1763 the intervention (i.e., NOCR or VOCR) and continue to measure BP/HR throughout the study
1764 period using the same sphygmomanometers. Particularly at the studies of protocol 2 and 3 (i.e.,
1765 the studies at the National Rehabilitation Center for Persons with Disabilities), participants were
1766 advised to record all the data of those measurements. Those whose BP lowered below the
1767 eligibility requirement of the study (≥130 mm Hg of SBP) prior to the initiation of intervention
1768 (NOCR or VOCR) were eliminated from the study. Participants were directed to be rested and
1769 keep calm for at least 1 min before starting to measure BP/HR. The mean BP/HR value from 3-
1770 time measurements was defined as "value of the day", and used for statistical analysis. When BP
1771 and HR were measured and recorded on ≥3 days during a particular week in the studies of

1772 protocol 2 and 3, the mean of all the "value of the day"s through the week was defined as "value
1773 of the week". For the participants who agreed, periodical BP/HR measurement and recording
1774 (≥3 days per week) was extended up to 8 weeks after the last bout of VOCR (protocol 2 and 3).
1775 MAP was calculated with a standard formula as follows: MAP = DBP + 1/3 (SBP – DBP).
1776
1777 **Blood sampling and measurement of parameters in plasma and serum of humans.** Blood
1778 sampling in the human study of protocol 2 was conducted between 12 PM and 3 PM.
1779 Participants were rested in a sitting position for at least 10 min before starting the sampling
1780 procedures. After plasma (for catecholamines and renin activity) and serum (for aldosterone and
1781 CRP) separation by centrifugation, we outsourced the measurement of parameters be tested
1782 (BML, Kawagoe, Japan).
1783
1784 **Continuous beat-by-beat BP and RRI recording to evaluate vascular sympathetic nerve**
1785 **activity and balance of cardiac sympathetic/parasympathetic nerve activity, respectively.** In
1786 the study of protocol 3, we evaluated the vascular sympathetic nerve activity and the balance
1787 between the cardiac sympathetic and parasympathetic nerve activities (i.e., sympatho-vagal
1788 balance) in the participants who agreed to these measurements. We analyzed the LF (0.04–0.15
1789 Hz) power of the power spectrum density (PSD) of SBP variability[52,53] and the LF/HF (0.15–0.4
1790 Hz) ratio of the PSD of RRI variability[52,54], respectively, at the beginning and ending periods of

1791 the intervention (NOCR and VOCR) (Extended Data Fig. 17a). The PSDs of the SBP and RRI
1792 variability signals were calculated by applying a Fourier transform with Hanning window[104].
1793 Continuous BP recording was performed using a continuous non-invasive arterial pressure
1794 system that measures BP via an automated inflatable cuff wrapped around the proximal phalanx
1795 of index or middle finger (LiDCOrapid V3; Merit Medical Japan, Tokyo, Japan)[105]. Continuous
1796 RRI recording was conducted using a wearable electrocardiography system (myBeat; Union
1797 Tool, Tokyo, Japan)[106]. Whilst we monitored BP and RRI continuously for 10 min at each
1798 recording, we analyzed the data from the central 256 s (4.27 min) of the last 5 min. It took us ~5
1799 min to prepare for continuous BP and RRI monitoring and confirm the proper system operation
1800 before starting BP and RRI recording. Therefore, the analyzed data were from the subjects who
1801 had rested on the chair for at least 10 min. The average values from five-time (i.e., 5-day)
1802 measurements at the beginning and ending periods of intervention (NOCR or VOCR) were
1803 statistically analyzed. In case the BP was not determined or SBP was recorded as <50 mm Hg,
1804 the measurement was considered a failure. For RRI analysis, we first removed RRIs of <0.5 s
1805 and >1.5 s as erroneous values. RRI values outside the range of 0.6- to 1.4-times the average of
1806 the 10 immediately preceding ones were also removed because of a lack of reliability. In case
1807 the sum of time for BP recording failures exceeded 4% or that for RRI value removal exceeded
1808 10% during the last 5 min of recording, the continuous BP or RRI measurement on that
1809 particular day was deemed unsuccessful and excluded from the statistical analysis. Nevertheless,

1810 all statistically analyzed data were the mean values from at least four measurements except for

1811 the "End" RRI variability for subject #31's NOCR, which was from three measurements

1812 because of two failures in recording.

1813

1814 **Statistical analysis.** All the quantitative data are presented as mean ± s.e.m. Parametric

1815 statistical analyses were conducted by paired or unpaired two-tailed Student's *t*-test for two-

1816 group comparison except for SBP and RRI variabilities, using Prism software (Version 8;

1817 GraphPad Software, San Diego, CA). SBP and RRI variabilities were analyzed by Wilcoxon

1818 signed-rank test, using R software (https://www.r-project.org/) in the human study of protocol 3.

1819 One-way ANOVA and one- or two-way repeated measures ANOVA with Tukey's, Dunnett 's, or

1820 Bonferroni's post hoc test were conducted for multiple (≥3) group comparison, using Prism.

1821 Differences were considered as significant at *P* values below 0.05.